UNIVERSITÀ DI PARMA

DOTTORATO DI RICERCA IN "SCIENZE DEL FARMACO, DELLE BIOMOLECOLE E DEI PRODOTTI PER LA SALUTE"

CICLO XXX

MEDICAZIONI AVANZATE PER IL RILASCIO DI ANTIOSSIDANTI E PROBIOTICI PER LA RIPARAZIONE TISSUTALE.

ADVANCED MEDICATIONS FOR DELIVERY OF ANTIOXIDANTS AND PROBIOTICS FOR TISSUE REPAIR.

Coordinatore:
Chiar.mo Prof. Marco Mor

Tutore:
Chiar.ma Prof.ssa Carla Marcella Caramella

Dottorando: Alessandro Invernizzi

Anni 2014/2017

Index

List of Abbreviations

AMC	Amphiphilic modified chitosan
BrdU	Bromodeoxyuridine
DoE	Design of Experiment
ECM	Extracellular Matrix
GG	Guar Gum
Gly	Glycine
MMP	Matrix Metalloproteinase
MTT	[3- (4,5-dimethyl-2-thiazolyl) -2,5-diphenyl-2H-tetrazolium bromide]
NE	Nanoemulsion
PCNA	Proliferating Cell Nuclear Antigen
PVA	Polyvinyl Alcohol
RNS	Reactive Nitrogen Species
ROS	Reactive Oxygen Species
TBARS	Thiobarbituric Acid-Reactive Species
TIMPS	Tissue inhibitors of metalloproteinase
TNF-α	Tumor Necrosis Factor α
XG	Xanthan Gum
α-Thp	α-tocopherol

List of Figures

List of Tables

1. INTRODUCTION

1.1 Wound healing

Skin structure

Skin is the largest organ of the human body and acts as protective barrier against the environment. It protects the body from mechanical injuries, chemical and bacteriological intrusion; it prevents dehydration by water loss and helps thermoregulation; nevertheless it mediates the sense of touch, contributes to immune surveillance and hormone production (Rittié and Fisher, 2015).

Skin presents two main layers: the external one is the epidermis and it is mainly composed by keratinocytes; the dermis, below, consists of collagen, elastin, and glycosaminoglycans, that forms the extracellular matrix (ECM), produced by the small portions of dermis cells, the fibroblasts. This layer provides the physical strength and flexibility of the skin, the support for epidermis, vasculature, lymphatic system, and nerve bundles (Zhong et al. 2010). The deepest layer is the hypodermis that consists mainly of adipose tissue (Oktay Arda et al. 2014).

A skin injury leads to a loss of its barrier function. The consequent loss of fluids, proteins, and electrolytes, vital for our body, can cause serious pathologies, major disability or even death. (Singer A.J. et Clark R., 1999).

Wound healing definition

Wound Healing Society defines a wound as the result of "*disruption of normal anatomic structure and function of the skin*".

A wound can be described as a defect or a break in the skin, caused by physical or thermal injury or as a result of the presence of an underlying medical or physiological condition. Wounds could be classified in acute or chronic wounds, depending on the wound healing process.

Acute wounds are usually caused by traumas (that would result in abrasions, avulsions, incisions, contusions and lacerations) and typically tends to heal completely in 8–12 weeks. Other causes of acute wounds include burns and chemical injuries.

Wound healing is a dynamic interactive process that includes parenchymal cells, blood cells, ECM and soluble mediators. It includes different overlapping stages: after formation of the clot, hemostasis occurs then followed by inflammation, migration, proliferation and remodeling phases, including angiogenesis and maturation and ending in tissue reconstitution (Fig. 1).

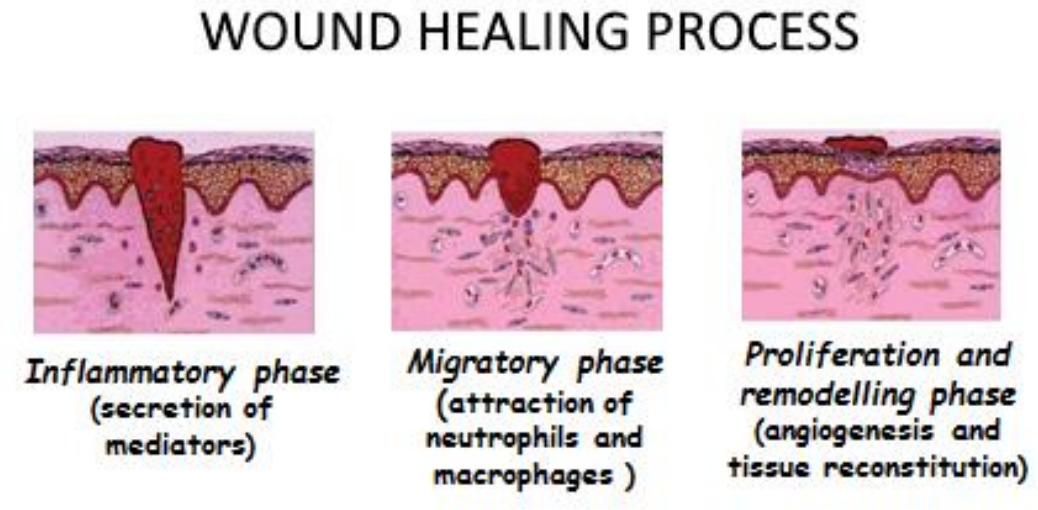

Fig. 1 Schematic representation of wound healing phases. (modified from Boateng J.S. et al., Journal of Pharmaceutical Sciences 97 2892–2923 2008)

Haemostasis

Usually, after a skin injury, bleeding occurs that flushes out bacteria and antigens from the wound and activates haemostasis. The clotting mechanism stimulated by fibrinogen and the formation of a fibrin network resulting in a clot that ends the bleeding (Boateng J.S. et al., 2007). The blood clot offers a provisional support for cell migration (Singer A.J. et Clark R., 1999). The wound causes damage of blood vessels and extravasation of blood constituents such as the platelets that allow the formation of a hemostatic plug and secrete a number of biological mediators.

Inflammation

During the inflammatory phase occur activation of complement, improved vessel permeability. However, the polymorphonuclear leukocytes and macrophages move to the wounded area. These cells provide the phagocitation of bacteria and foreign particles, release proteases (essential to degrade ECM damaged macromolecules) and provide the secretion of a number of growth factors (Tab. 1). The cytokines are molecules capable of stimulation, inhibition and actions on inflammatory cells controlling the inflammation processes. Cytokines stimulate the migration of fibroblasts, epithelial cells, and vascular endothelial cells form granulation tissue into the wounded area and regulate the activities of fibroblasts and other cells. In particular, chemokines (chemo-attractive cytokine) represent a group of proteins that affect wound healing regulating the migration of leukocyte. (Schultz G.S., 2003; Boateng J.S. et al., 2007)

Migration

During the migration phase epithelial cells and fibroblasts move to the wounded area to replace the injured tissue. The fibroblasts, endothelial cells, and keratinocytes start the synthesis of growth factor

as the inflammatory cells amount decrease in the injured tissue. These cells migrate from the wound edge and grow under the clot.

Proliferation

During the proliferative phase the development of granulation tissue takes place. This phase occurs at the same time or follows the migration phase and continues for up to 2 weeks.

Some days after the injury, fibroblasts migrate into the wound area and proliferate, stimulated by platelets, macrophages growth factors and chemotactic factors (Tab. 1). These cells produce new collagen, elastin and proteoglycan molecules, and secrete lysyl oxidase, an enzyme which provide the cross-links of collagen in the ECM. In addition, the re-epithelialization process begins several hours after injury.

Later, the fibroblasts change from a migratory phenotype to a myofibroblast phenotype, showing features common to both fibroblasts and smooth muscle cells. They produce the granulation tissue that consist of a moveable and provisory ECM mainly composed of fibronectin and hyaluronic acid. In the next few days, the composition of the granulation tissue changes because the collagen will represent the main component. The action of myofibroblasts in the matrix contraction helps an organized deposition of collagen fibers. A high metabolic rate takes place to sustain cell proliferation and synthesis of new ECM, which required a significant increase in vascularity in the granulation tissue. (Farrar D., 2011, Schultz G.S. et al., 2003)

Angiogenesis

The induction of angiogenesis depends on many mechanisms that includes macromolecules like vascular endothelial growth factors (VEGF), low oxygen tension, lactic acid and proteases. An appropriate extracellular matrix and endothelial receptors also play a key role in angiogenesis. The stimulation of macrophages and endothelial cells lead to a release of basic fibroblast growth factor and vascular endothelial growth factor. Basic fibroblast growth factor appears crucial for the beginning of angiogenesis during the first three days after the injury, while vascular endothelial-cell growth factor is essential for angiogenesis during the formation of granulation tissue.

Angiogenesis concludes as the granulation tissue occupied wound. Subsequently many of the new blood vessels undergo apoptosis. (Singer A.J. et Clark R., 1999)

Main wound healing cytokines		
Cytokines	Cells	Effects
Epidermal growth factor (EGF)	Platelets	Mesenchymal cells regeneration. Keratinocyte Proliferation and motility. ECM deposition.
Transforming growth factor α (TGF α)	Macrophage, Epithelial cells	
Heparin-binding EGF-like growth factor (HB-EGF)	Macrophage	
Basic-Fibroblast growth factor (bFGF)	Macrophage, endothelial cells	Angiogenesis. Fibroblasts proliferation. Endothelial cells activation, keratinocyte proliferation and migration. ECM deposition
Acid-Fibroblast growth factor (aFGF)	Macrophage, cells endothelial	
keratinocyte growth factor (KGF)	Fibroblasts	Epidermis cells Proliferation and motility
Transforming growth factor β1 e β2 (FGF-β1, FGF-β2)	Platelets, macrophage, fibroblasts	Epidermis cells, motility, macrophage and fibroblasts chemotaxis, ECM synthesis and remodeling
Transforming growth factor β3 (FGF-β3)	Macrophage	Fibrosis, keloid prevention
Platelet derived growth factor (PDGF-AA, PDGF-BB)	Platelets, macrophage, keratinocyte e fibroblasts	Fibroblasts proliferation and chemoattraction, macrophage chemoattraction and activation. Increase of collagen synthesis and ECM deposition, increase TIMP expression, decrease MMP expression. Angiogenesis.
Vascular Endothelial growth factor (VEGF)	Macrophage, Epithelial cells	Angiogenesis and increase vascular permeability.
Tumor necrosis factor α (TNF-α)	Neutrophils	Pleiotropic expression of growth factors
Interleukin 1 (IL-1)	Neutrophils	Pleiotropic expression of growth factors, fibroblasts and keratinocyte chemotaxis. Collagens synthesis.
Insulin-like growth factor (ILGF)	Fibroblasts, neutrophils, macrophage, hepatic cells, Skeletal muscle cells	Collagens synthesis and granulation tissue formation. Keratinocyte and fibroblasts proliferation. Endothelial cells activation. Re-epithelization.
Colony stimulating factor 1 (SCF-1)	Different cells type	Macrophage activation and granulation tissue formation.
Connective tissue growth factor (CTGF)	Fibroblasts, endothelial cells and Epithelial cells	TGF-β mediated effect on collagens synthesis.

Tab. 1 Main cytokines involved in skin wound healing. (Adapted from Singer A.J. and Clark A.F., New England Journal of Medicine. 1999; Schultz G.S. et al., Wound repair and regeneration. 2003)

Maturation phase

The maturation phase occurs usually 2–3 weeks after the injury. In this final phase of tissue repair, the collagen content in the wound bed decrease due to collagenase enzymes that balance the amount of collagen produced and degraded. A remodeling and re-aligning of collagen fibers arise to increase the strength of the tissue. The final morphology and aspect of the scar may develop in over 1 year. (Greenhalgh D.G. et al., 1998; Boateng J.S. et al., 2007)

1.1.1 Impaired wound healing

A chronic wound consists in a wound that fails to heal or needs a prolonged healing time. Typically, it requires more than 12 weeks to heal and often reoccur. Repeated tissue injuries or underlying physiological conditions, such as diabetes and infections, cause a fail in the sequence of events during the wound healing process. Chronic wounds are classified into vascular ulcers, pressure ulcers and diabetic ulcers (Boateng J.S. et al., 2007; Mayet M et al. 2014).

In addition to the financial cost, chronic wounds cause handicap and pain in the patients, reducing the quality of life. (Phillips *et al*. 1994; Krasner 1998; Persoon *et al*. 2004). Only in the USA, the management and care of non-healing ulcers result in an annual cost over 20 billion USD. (Jarbrink et al. 2017; Han 2017). During the Congress of World Union of Wound Healing Societies in Florence in 2016, the management costs of chronic ulcer in Italy was estimated in over 1 billion Euros.

Vascular ulcers

Venous ulcers imply ineffectiveness of valvular activity resulting in a constant blood backflow and, as a consequence, in venous hypertension. A higher pressure in blood vessel induces an increase in wall permeability with leakage of plasma components, like fibrin, into the perivascular space. Fibrin accumulation gives rise to vessels “fibrin cuffs” that could trap growth factors and matrix materials, attempt a down-regulation in collagen synthesis and produce a barrier against the oxygen exchange between blood and dermis. (Falanga V and Eaglstein WH., 1993; Higley H.R. et al., 1995)

Karatepe et al. (2010) observed an increased presence of oxidative stress markers and MMPs in tissues collected from patients with healing venous ulcers. These findings suggest a role of oxidative stress in venous stasis ulcer onset. (Karatepe O. 2010)

Also Wlaschek M. et al. (2005), in a perspective article underline the effects of the oxidative stress as an important cause of the hostile microenvironment of chronic venous leg ulcers. The capability of high amount of ROS to generate a continuous damage in the wounded tissue, stimulate pro inflammatory cytokines and MMPs, leads to a non-healing phenotype of the ulcers. (Wlaschek M. et al., 2005).

Arterial ulcers follow an arterial insufficiency caused by atherosclerosis or embolism. The consequent reduction in arterial lumen and the accompanying ischemia affects appropriate healing of traumatic injuries (Boateng J.S. et al., 2007). Aging and diabetes may aggravate vascular pathologies.

Pressure ulcers

Pressure ulcers origin from decrease in oxygen tension, ischemia-reperfusion injury and tissue necrosis following a constant pressure exerted on skin and underlying muscle tissue. (Demidova-Rice T., 2012). It should be stressed that aging and diabetes may aggravate vascular pathologies and pressure ulcers.

Diabetic ulcers

Among 15%–25% of patients, suffering from diabetes, may develop a diabetic foot ulcer and 50%–70% of them are subjected to a relapse in the next 5 years. Foot ulcers are the most common cause of hospitalization in these patients, with high morbidity and mortality.

Diabetes pathophysiological abnormalities interfere with the complex process of wound healing showing anomalous expression of growth factors, chemokines, cytokines and MMPs. A prolonged inflammatory response was observed as macrophages reduce their skill in removing necrotic tissue. Moreover, TNF-α increased expression compromises fibroblasts proliferation, hinders angiogenesis and cells proliferation, and increases apoptotic events. (Karen L Andrews, 2015).

Diabetic patients skin display glycation of collagen (non-enzymatic covalent addition of sugar molecules) and higher levels of advanced glycation end products (AGEs). Neutrophils are capable to bind AGEs inducing the release of inflammatory cytokines. Qing C. (2017) mentioned a reduction in collagen and hyaluronic acid synthesis, anomalous expression or activity of cytokines, growth factors and MMPs in fibroblasts cultivated in high glucose concentration medium or medium added with AGEs. (Qing C., 2017)

As mentioned above, ROS play a key role in regulation of wound healing. In diabetic patients, the signaling mediated by oxidants fail, occurring an imbalance between ROS generation and their scavenging that damage ECM components. (Kunkemoeller B et al., 2017). In a human *in vivo* study, Bolajoko EB et al., demonstrated a role of oxidative stress in the pathogenesis and progression of diabetic ulcers. (Bolajoko EB, 2008).

Chronic wound phenotype

There are different and several causes for impaired wound healing. Activated neutrophils induce the overexpression of matrix metallic proteinases (see below) and inflammatory cytokines in the wound which causes ECM degradation and a disproportionate degradation of collagen thus inhibiting mature scar development. Increased levels of MMPs cause the degradation of growth factors, their receptors and adhesion proteins, avoiding normal cell adhesion essential for wound repair. After an injury usually hypoxic status occur, due to a decrease in blood supply, with a consequent decrease in oxidative bursts and antimicrobial activity typical of polymorphonuclear leukocytes. These cells of immune system counter the hypoxia releasing proteinases and reactive oxygen species, damaging endothelial cells and fibrin deposition, affecting negatively the nutrient and oxygen supply (Kenneth Fan, 2010). Moreover, the keratinocytes migration, differentiation and releasing profile are affected in chronic wounds.

Falanga and Eaglstein (1993) in their ‘trap’ hypothesis, underline how the fibrin complexes prevent the passage of oxygen and other nutrients, which normally sustain the cells of the dermis, the epidermis and the vasculature. This leads directly to cell death and ulceration.

The theory of ageing called “free radical theory”, purposed by Harmann in 1956, suggest that high levels of reactive oxygen and nitrogen species and a decrease of both enzymatic and non-enzymatic antioxidants represent another important reason of tissue turnover (Farrar D., 2011).

Coleridge Smith et al. (1988) suggested the 'white cell hypothesis'. The venous hypertension decreases capillary flow rate and causes a leakage of leukocytes from the blood circulation that result entrapped in leg vascular, where they may occlude capillaries and induce ischemia. Leukocytes became activate and release reactive oxygen species, proteolytic enzymes and chemotactic molecules recruiting other white cells.

In chronic wounds, the abnormal overstimulation of immune response generate an irregular and persistent inflammatory status. In these conditions, Menke et al. observed a premature fibroblasts senescence with functioning impairment.

In addition, the increased vascular permeability, caused by the activation of endothelial cells, allow for the passage of fibrinogen into the pericapillary spaces leading to fibrin cuffs development (Shami S.K.et al., 1992; Menke N.B. et al., 2007; Demidova-Rice T.N. et al., 2012; Sabine A. Eming S.A. et al., 2007).

Matrix Metalloproteinases (MMP)

Among the proteases released during the wound healing process an enzyme family named matrix metalloproteinase (Tab. 2) play a key role in different steps of wound repair. MMP are involved in removal necrotic tissue, in angiogenesis, remodeling ECM and regulation of the activities of some growth factors.

The MMPs are zinc-dependent endopeptidases capable of breakdown ECM components. This skill is important to allow detachment and migration of cells, to remodel tissues in several physiological situations, e.g. developmental tissue morphogenesis, tissue repair, and angiogenesis (Saarialho-Kere U.K., 1998).

The MMPs concentration in healthy tissue is lower than in injured tissues and change in the different phases of wound healing. They have a role in several pro inflammatory processes and they are able to activate specific cytokines and chemokines (Wainwright C.L. et al., 2004).

Observation on cardiac ischemia evidence how peroxynitrite ($ONOO^-$) can activate matrix metalloproteinases; Wang W. et al. (2002) demonstrate the crucial role of MMP-2 in acute cardiac toxicity induced by $ONOO^-$ (Wang W. et al., 2002; McLennan S.V. et al., 2008).

Enzyme	Name	Main substrate	Subfamily
MMP1	interstitial collagenase	interstitial collagen and type I, II, III, VII, X collagens	Collagenase
MMP2	Gelatinase A	type IV,V,VII,X Collagens, fibronectin, laminin, inhibitors of preoteasis α-1	Gelatinase
MMP3	Stromelysin 1	Type III, IV, IX, X Collagens, type I, III, IV, X gelatins, proteoglycans, elastin, laminin, pro-collagenase, fibronectin	Stromelysin
MMP7	Matrilysin	type IV Collagens, type I, II, IV, V gelatins, elastin, fibronectin, laminin, entactin, proteoglycans, pro-collagenase	Matrilysin
MMP8	Neutrophyl collagenase	type I, II, III, VII, VIII, X Collagens, gelatins	Collagenase
MMP9	Gelatinase B	Gelatins, type IV, V collagens	Gelatinase
MMP10	Stromelysin 2	type III, IV, V, IX, X Collagens, type I, III, IV gelatins, elastin, laminin, fibronectin, pro collagenase	Stromelysin
MMP12	Macrophage Metalloelastase	Elastin, type IV collagens, laminin, fibronectin, vitronectin, heparin sulfate	Metalloelastase
MMP11	Stromelysin 3	Tissue remodeling	
MMP13		type IV, IX, X, XIV Collagens, tenascin C, fibronectin	Collagenase
MMP14	MT1-MMP	Pro-MMP2 - type I, II, III collagens, gelatin, fibronectin, laminin-1, proteoglycans	Transmembrane
MMP15	MT2-MMP	Pro-MMP2, gelatins, fibronectin	Transmembrane
TIMP1	Tissue inhibitor of metalloproteinases	All MMP except MMP-14	
TIMP2	Tissue inhibitor of metalloproteinases	All MMP	
TIMP3	Tissue inhibitor of metalloproteinases	All MMP, pro-MMP-2 and pro-MMP-9	
ELASTASE	Neutrophil elastase	Elastin, type I, II, III, IV, VIII, IX, XI collagens, fibronectin, laminin, TIMPS Activates pro-collagenases, pro-gelatinases and pro-stromelysin	
INHIBITORS OF PREOTEASES α-1	α-1 Antitrypsin		

Tab. 2 Main matrix metalloproteinases and respective tissue inhibitors. (Adapted from: PubMed Gene website; Saarialho-Kere U. K., Arch Dermatol Res. 1998; Schultz G.S. et al. Wound repair and regeneration. 2003)

Aging in skin

A dysfunctional healing is related with ageing. Prolonged inflammation, a defective ECM status due to the presence of senescent fibroblasts, increased ECM turnover due to an increase of proteolytic enzymes were observed. Dysfunction in collagen synthesis and cross-linking occur and it undergos glycation reaction. Elastin, glycosaminoglycans (GAG) synthesis and deposition change, as well as collagen organization, leading to a lack of mechanical resistance of the skin. Moreover, defects in re-epithelialization and keratinocytes function result in aged skin. (Farrar D., 2011; Ashcroft, Horan, & Ferguson 1995).

Exudate

Exudate is a biological fluid derived from blood and is described by Thomas as "*a liquid formed from chronic wounds or other more acute injuries*". It affects all the phases of wound healing, moistures the environment (the ideal condition for healing), supplies nutrients and provides advantageous conditions for epithelial cells migration. (Thomas S., 1997; Boateng J.S. et al., 2007)

Chronic wound fluid impairs cells proliferation and is different from acute wound fluid (Schultz G.S, 2003).

1.1.2 Free radicals, reactive molecules and oxidative stress

In biology, free radicals (Tab. 3) are referred to highly reactive molecules, produced during the metabolic processes in all cells and in small amount and can be grouped in these categories:

GROUP	MOLECULES
reactive oxygen species (ROS)	Superoxide Anion
	Hydroxyl Radical ($HO^{-\bullet}$)
	Peroxyl Radical
	Hydroperoxyl radical
	Hypochlorous Acid (HOCl)
	Ozone (O_3)
	Singlet Oxygen
reactive nitrogen species (RNS)	Nitric Oxide
	Nitrogen Dioxide Radical
	Nitrogen Dioxide Radical
	Nitrous acid
	Nitrosyl Cation (NO^+)
	Nitrosyl Anion (NO^-)
reactive chlorine species (RCS)	Atomic Chlorine (Cl^-)
	Hypochlorous Acid (HOCl)
	Chorine (Cl_2)
	Nitronium Chloride (NO_2Cl)
non-radicals	Hydrogen Peroxide (H_2O_2)
	peroxynitrite anion ($ONOO^-$)
	peroxynitrous acid (ONOOH)
	nitrosoperoxycarbonate anion ($ONOOCO_2^-$)
	nitronium cation (NH_4^+)
	dinitrogen trioxide (N_2O_3)
	dinitrogentetraoxide (N_2O_4)

Tab. 3 Free radicals classification. (Adapted from Pavelescu LA; 2015)

They play a key role in different physiological mechanisms that involve for example the skill of immunity system cells to fight pathogens. In particular, ROS were largely studied and, at low levels, are known to affect some critical points of wound healing as the intracellular signaling. Low concentrations of H_2O_2 supported wound healing by promoting angiogenesis. Roy S. et al. (2006) demonstrate *in vivo* the activity of the redox environment of the wound site on healing outcomes. (Roy S. et al., 2006)

On the other hand, ROS high reactivity causes impaired wound healing. The presence of ROS was observed in particular in chronic wounds (Eming S.A. et al., 2007). H_2O_2 is not a radical, but it can react with iron or cupper ions forming hydroxyl radicals $OH^{-\bullet}$. ROS are dangerous due to the oxidation of cellular macromolecules and excessive ROS amounts lead to oxidative stress (Fig. 2), resulting in severe cell damage, premature aging or neoplastic transformation.

The presence of ROS-detoxifying enzymes protects the body against oxidative stress; nevertheless, also a number of non-enzymatic low molecular weight antioxidants provide ROS neutralization.

In vivo concentrations of ROS are difficult to measure because of their short half-life. Different methods for directly and indirectly quantification were developed. (Schäfer M. et al., 2008; Pavelescu L.A. et al., 2015)

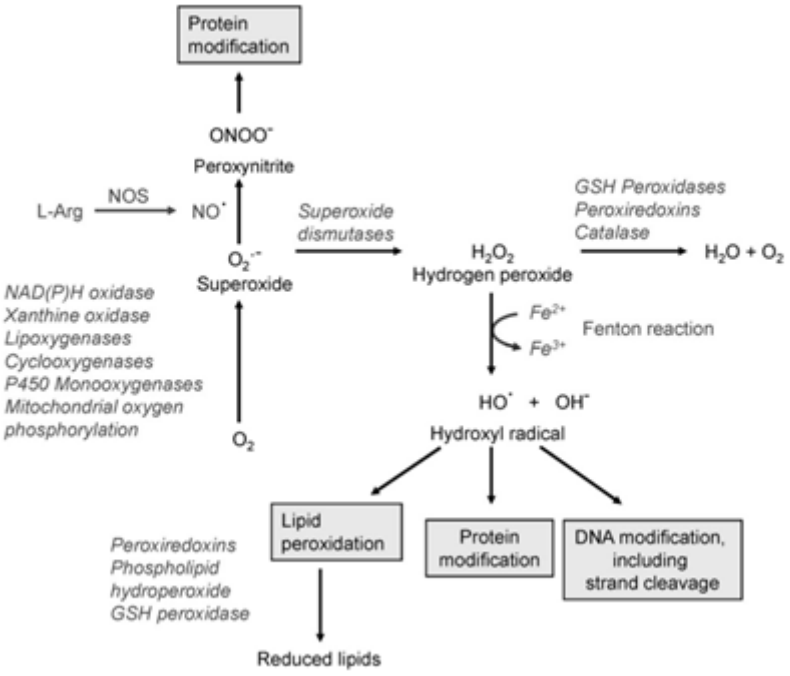

Fig. 2 Effects of free radicals and ROS on living tissue macromolecules. Reprinted from Pharmacological Research vol. 58, Schäfer M. and Werner S. Oxidative stress in normal and impaired wound repair. pp. 165–171 Copyright (2008) with permission from Elsevier

ROS and angiogenesis

Blood vessels allow oxygen and nutrients supplementation to all cells. Endothelial cells employ oxygen also to produce reactive oxygen species (ROS) and nitric oxide (NO) as signaling molecules, which have different biological activities. (Fraisl P. et al., 2009). ROS play a role in endothelial cell

proliferation, vessel permeability and in expression changes of surface adhesion molecules in these cells (Ushio-Fukai and Nakamura, 2008).

1.1.3 Bacterial imbalance and infections

Another important aspect in chronic wound concerns the bacterial colonization of the injured area. As the skin undergoes breakdown, bacteria and foreign bodies enter the wound. Bacteria endotoxins (i.e. lipopolysaccharide) stimulate white cells to release cytokines that intensify the expression of MMPs (Bruce A. M. et al., 1996).

On the other hand, some bacteria, producing proteolytic enzymes (i.e. hyaluronidase), help the debridement of the injured site. Microorganisms are typically present in a chronic wound. Resident or environmental microorganisms may enter the wounds. Often their presence does not affect the healing and an infection does not occur.

The presence of bacteria in the wound may evolve in wound contamination, wound colonization or chronical colonization and infection.

Wound contamination indicates the presence of microorganisms not able to replicate in the wound, usually because of the hostile environment of human tissue.

Wound colonization indicates that microorganisms capable of replicating adhere to the wound without causing damage to the host. A delayed healing due to the presence of Microorganisms results in a critical colonization. They can release MMPs and pro-inflammatory molecules. Infection consists in the presence of replicating microorganisms in the wound that causes a damage to the host. An infection become dangerous as the bacterial load increase strongly. (Schultz G.S. et al., 2003)

An infected skin wound may lead to a life-threatening systemic infection, sepsis and multiple organ dysfunction syndrome. In chronic wounds, the pathogen species may be more important than the number of microorganisms. Commensal skin bacteria are the main microorganisms in early acute wounds. After about 4 weeks, gram-negative strains usually start to colonize chronic wounds. It was also observed that the contamination of deeper tissues involves anaerobic bacteria.

Cutting and Harding, in 1994, suggested some conceivable signs of infection: friable red granulation, exuberant granulation, increased discharge, and new slough areas within the wound base. (Schultz G. et al., 2003; O'Meara S et al. 2000; D. Leaper 2015)

Antimicrobials

The role of antimicrobials in wound healing is not completely clarified. When topical agents fails to improve healing, physician may use systemic antibiotics. An infection in a diabetic foot ulcer may cause gangrene or death. In pressure ulcers, an infection may cause septicemia or osteomyelitis.

Local antiseptics and disinfectants kill microorganisms or limit their growth in their vegetative state. Usually antiseptics can be applied directly on tissues while disinfectants may be used for decontamination of instruments and surfaces. (O'Meara S. et al. 2000)

Biofilm

Biofilms consist of microorganisms that live attached to surfaces or living tissues and aggregate in a community, within an exopolysaccharide matrix. The presence of biofilms improves the microorganisms survival providing a protection against environmental threats and helping to elude host immune system and antibiotics treatment. Palanisamy N.K. et al (2014) demonstrated that silver nanoparticles inhibit the biofilm formation of multidrug resistant strains of Pseudomonas aeruginosa. (Karatan E. and Watnick P., 2009; Palanisamy N.K. et al 2014) The presence of biofilms require specific strategies to disrupt the embedding matrix to attack bacterial contamination.

1.2 Nanoemulsions

Emulsions

"Emulsions are dispersions of one liquid phase in another immiscible liquid phase that are made using mechanical shear [9, 10]. Due to differences in attractive interactions between the molecules of the two liquid phases, an interfacial tension, σ, exists between the two liquids everywhere they are in contact [11]. This interfacial tension can be reduced significantly by adding amphiphilic surface-active molecules, or 'surfactants', that are highly soluble in at least one of the liquid phases. Surfactants preferentially adsorb at interfaces, since their molecular structures have non-polar hydrocarbon tails that prefer to be in non-polar liquids, such as oils, and polar or charged head groups that prefer to reside in polar liquids, such as water. The energy required to create additional interfacial area, A, between the two liquids in contact is σ A, so the interfacial tension always acts to minimize the interfacial area between the two liquid phases and keep the interfaces smooth."

Emulsions are formed applying an external shear to disaggregate larger droplets into smaller ones, overcoming the surface tension. (Mason T.G. et al., 2006)

Emulsions can be divided in: oil-in water (O/W) emulsion in which water represents the continuous phase, surfactant is water soluble and allows stabilization of the water film at interface; water-in-oil (W/O) emulsions in witch oils represents the continuous phase, the surfactant is soluble in the oil phase and allows stability of oil films at interface. (Tadros T. et al., 2009; Mason T.G. et al., 2006)

The formation of emulsion needs energy necessary to increase the interfacial area (ΔAγ). The following equation describe the free energy (G) required by these systems:

$$\Delta G = \Delta A\gamma - T\Delta S$$

where: A=interfacial area γ= interfacial tension

When γ is positive, also the energy necessary to increase the interfacial area is positive and the entropy in this system is also positive but not abundant yet, resulting in a total free energy (G) positive. Consequently, this process is non-spontaneous and requires energy. Emulsions are therefore physically unstable due to the excess free energy but can be kinetically stabilized by

reducing the surface area or lowering the interfacial tension. Surfactants cause a decrease of the interfacial tension and allow the formation of small droplets. Literature reports that some surfactant blends and polymer-surfactant blends may present synergetic activity in the reduction of interfacial tension.

Nanoemulsions

Nanoemulsions belong to the broad category of multiphase colloidal dispersions. The distinctive properties of colloidal systems is that droplet diameter is usually under 500 nm (Singh Y. et al., 2017) In principle, nanoemulsions are kinetically unstable due to the high surface area generated by the nanosized droplet dimensions. However, if kinetically stabilized by the addition of suitable type and amount of surfactants, they offer distinctive advantages with respect to coarse emulsions.

The small droplet size of nanoemulsions reduces the force required to resist to the gravity force and the Brownian motion may be adequate and to prevent flocculation and coalescence and to avoid subsequent phase separation/creaming. (Tadros 2004, 2009). It should be stressed that nanoemulsions demonstrate a long-term physical stability described in literature as “approaching thermodynamic stability”. However nanoemulsions are to be clearly differentiated from microemulsions that are the typical thermodynamically stable systems.

For sake of completeness, it has to be mentioned that also micelles belong to the category of colloidal dispersions. They consist in self assembled colloidal particles distributed in a continuous phase. Self-assembled micelles form spontaneously in certain conditions from amphiphilic molecules, like surfactants. Amphiphilic molecules at low concentrations in aqueous medium persist separate, however, when the critical micelle concentration (CMC) is reached, aggregation occurs with the consequent formation of an hydrophobic core (formed by the lipophilic moieties) surrounded by a hydrophilic shell (formed by the hydrophilic moieties) thus creating the so-called core-shell configuration. Micelle structure shows the hydrophobic blocks of amphiphilic molecules disposed in the internal core, while the hydrophilic blocks shape up the external shell. (Torchilin V. P., 2007). This process also depends on the temperature and micellization occurs when the critical micellization temperature (CMT) is reached. The thermodynamic reason for this process consists in a decrease of free energy in the system due to the subtraction of hydrophobic blocks from the aqueous media and the re-establishing of hydrogen bond network in water.

It could be inferred that micelles represent the first step towards the formation of a thermodynamically stabilized system.

However, the differences between the above described colloidal dispersions are not yet completely understood as witnessed by the various attempts, described in literature, to categorize them.

Surfactants and nanoemulsion stabilization

Surfactants are critical excipients in dispersed systems. They should prevent flocculation, coalescence and Ostwald ripening. The use of non-ionic surfactant or polymers and the ratio of the

adsorbed layer thickness to droplet radius lead to a steric stabilization that are crucial for the stability of nano-systems.

Polymeric surfactants, when strongly adsorbed at the interface, represent the most proficient method to stabilize an emulsion. For example, Tadros et al. (2009) explain the effectiveness of INUTEC®, a polysaccharide grafted with several alkyl groups, that allows to obtain a stable emulsion thanks to improving steric stabilization, the alkyl multi-point attachments, the strong hydration of the polysaccharide "loops" (also at high osmotic pressure) and the high amount of loops at the interface. (Tadros T. et al., 2004; Tadros T. et al., 2004)

The addition of an insoluble dispersed phase in the continuous phase helps to reach smaller drops and avoid Ostwald ripening. A high concentration of the insoluble compound in the smaller droplets and a partitioning between different droplets occurs.

A significant excess of surfactant added to the continuous phase turns out in the formation of micelles that can dissociate into monomers rapidly and adsorbed on the surfaces of newly formed droplets during emulsification process. (Mason T.G. et al, 2006; Tadros T. et al. 2004)

Nanoemulsions preparations methods

High-energy methods and low energy methods are the main techniques for nanoemulsion preparation. They are illustrated in Figs. 3 and 4, respectively.

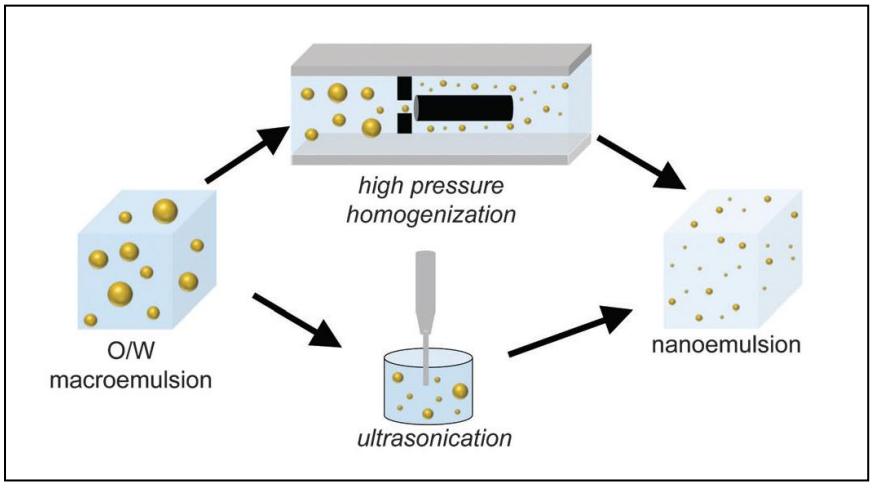

Fig. 3 High energy methods in nanoemulsion preparation (108-1010 w/kg). Reprinted from Gupta A. et al. Soft Matter, 2016, 12, 2826. Published by The Royal Society of Chemistry).

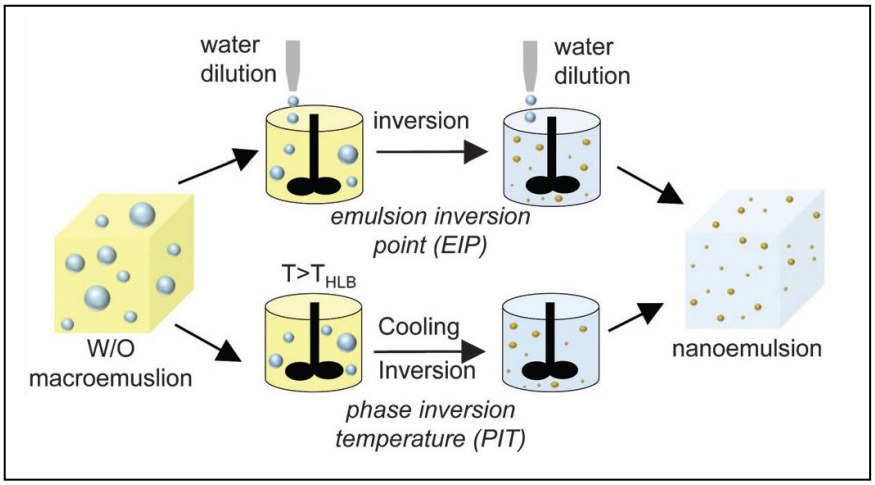

Fig. 4 Low energy methods in nanoemulsion preparation (103-105 w/kg). (reprinted from Gupta A. et al. Soft Matter, 2016, 12, 2826. Published by The Royal Society of Chemistry).

Whereas high pressure homogenization, the most common high shear method, consists in submitting a premixed emulsion of microscale droplets to extreme elongation and shear stress, in addition ultrasonic methods add high-energy waves that produce turbulence causing the breaking of droplets. The process is repeated or continued until a constant droplet size is achieved.

High-pressure microfluidic is a similar high shear method which consists in pumping rapidly premixed emulsion through rigid microchannel generating a strong extensional flow at high pressure; the droplets undergo a high shear rate that cause their breaking. Commonly the emulsion needs to stream several times through the device at high shear.

The main low energy methods include emulsion inversion point (EIP) and phase inversion temperature (PIT) and consist in the conversion of a W/O emulsion into an O/W emulsion altering either the composition or the temperature. In these processes, the system experiences a state of low interfacial tension and a phase inversion takes place in response to changes in composition (EIP) or temperature (PIT). The energy required for these processes is lower with respect to the methods previously described. (Gupta A. et al. 2016, Mason T.G. et al., 2006).

Evaporative ripening method (Fig. 5) is another interesting approach to nanoemulsion production. Fryed and Mason in a study (2010) investigated the combination of high-flow emulsification with solvent evaporation to obtain very small nano-droplets. Nanoemulsions size reduction resulted from using a mixture of low molecular weight volatile oil and high molecular weight non-volatile oil or solvent, insoluble in the continuous phase. This mixture is emulsified with a surfactant by high-pressure homogenizer. Thereafter the system is heated and the low molecular weight oil or solvent are removed by evaporation. This results in the formation of very small droplets. (Fryed and Mason, 2010; Gupta A. et al., 2016)

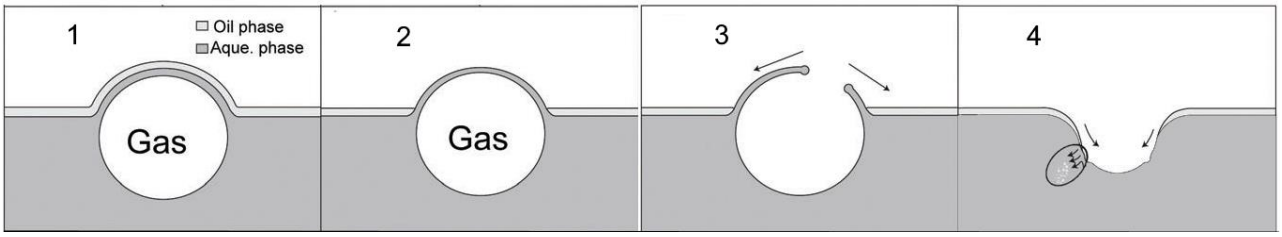

Fig. 5 Phases of evaporation ripening method for nanoemulsion preparation. 5.4 shows the formation of nanodroplets by evaporation of organic oil or solvent. (Adapted from Gupta A. et al. Soft Matter, 2016, 12, 2826. Published by The Royal Society of Chemistry)

Spontaneous emulsification

It is considered a low energy method but it is poorly defined, however it should account not only for the rate of the emulsification process, but also for the volume and the particle size distribution of the emulsion. Briefly, in a water miscible solvent, an oil and a surfactant are dissolved. Then, the solution are poured into an aqueous solution under moderate stirring. Spontaneous emulsification can occur. It may result out of a fortunate combination of a number of mechanisms/factors including the system composition and the physicochemical features of the components, the interfacial tension, the interfacial and bulk viscosity, the surfactant structure and concentration. (Bouchemal K. et al., 2004; Bonferoni M.C. et al., 2017).

Pharmaceutical use

These systems may be used as drug carriers in aqueous media, improving the solubility of poorly soluble molecules hosting them inside (Torchilin V. P., 2007). As drug delivery systems, these formulations may enhance drug loading, modify release properties, improve shelf life and decrease the toxicity. The properties of colloidal dispersed materials could present significant difference with respect to those in the bulk (Muller-Goymann C.C. et al., 2004).

1.3 Antioxidants in wound healing

Free radicals reaction mechanisms may be summarized in electron donation, reducing radicals, and electron acceptance, oxidizing radicals, hydrogen abstraction, addition reactions, self-annihilation reactions and by disproportionation. These reactions cause the formation of ROS and RNS. (Carocho M. et al., 2013)

Antioxidants are capable of donating electrons and/or hydrogen atoms to oxidant species, preventing or stopping the oxidant chain reactions (Wang et al. 2013). “Radical scavenging” consist in the delocalization and stabilization of a spare electron by reaction with a free radical. Halliwell & Gutteridge (1989) describe an antioxidant as a substance that delays or prevents the oxidation process of a substrate in a significant way, at a lower concentrations compared with that of the reaction’s substrate. Litescu et al. (2010) propose a concentration ratio of 100:1 between free radicals and antioxidant to report a molecule as an effective antioxidant. (Siti H.N. et al., 2015)

Antioxidants are classified into non-enzymatic and enzymatic (Fig. 6).

Non-enzymatic antioxidants

The polyphenolic flavonoids group includes flavonols, flavanones, anthocyanidins, flavones, flavonols and isoflavonols. A polyphenol can be defined an antioxidant when, at low concentration compared to the substrate, prevents the autoxidation or the oxidation caused by free radicals; furthermore, the resulting product formed after scavenging must be stable. Flavonoids present multiple beneficial biological activities, for example anti-inflammatory, vasodilatory, antibacterial and anticarcinogenic action.

The effectiveness of ascorbic acid (Vitamin C) as antioxidant can be explained with its radical scavenging activity and with the ability to reestablish α-tocopherol after reaction with a radical (tocopheroxyl radical). α-tocopherol is an isoform of Vitami E group, a hydrophobic group of molecules, found in the lipid compartment of cellular membranes, very effective against lipid peroxidation chain reactions.

Vitamin A group consists of different molecules such as retinol, retinal, retinoic acid, and numerous carotenoids (beta-carotene, lycopene, etc.) Carotenoids antioxidant activity is mainly referable to singlet molecular-oxygen quenching and lipid radical chain reaction blocking.

A numbers of low molecular weight antioxidants play a role in the control of redox environment in skin wounds.

Musalmah M et al. observed that the supplementation of vitamin E decrease the MDA levels and, consequently, lipid peroxidation activity in the wounds of diabetic rats (Musalmah M et al., 2005).

Matthias Schäfer and Sabine Werner (2008) observed that topical application of curcumin decreases the levels of lipid peroxides and increases the activity of some endogenous enzymatic antioxidants systems, speeds up the healing in a wound murine model. (Schaffer M. et al., 2008)

Coenzyme Q is a hydrophobic compound associate to the mitochondrial respiratory chain, which is present in cell membranes. It acts as antioxidant preventing or neutralizing lipid radicals and aiding the restoration of Vitamin E.

Glutathione is an endogenous peptide that promotes the restoration of other antioxidants (i.e. ascorbic acid) and exerts a radical scavenging activity through donation of a hydrogen atom or an electron.

(Rice-Evans C.A. et al., 1996; Palace V. P. et al., 1999; Halpner A.D. et al., 1998; Turunen M. et al.1998)

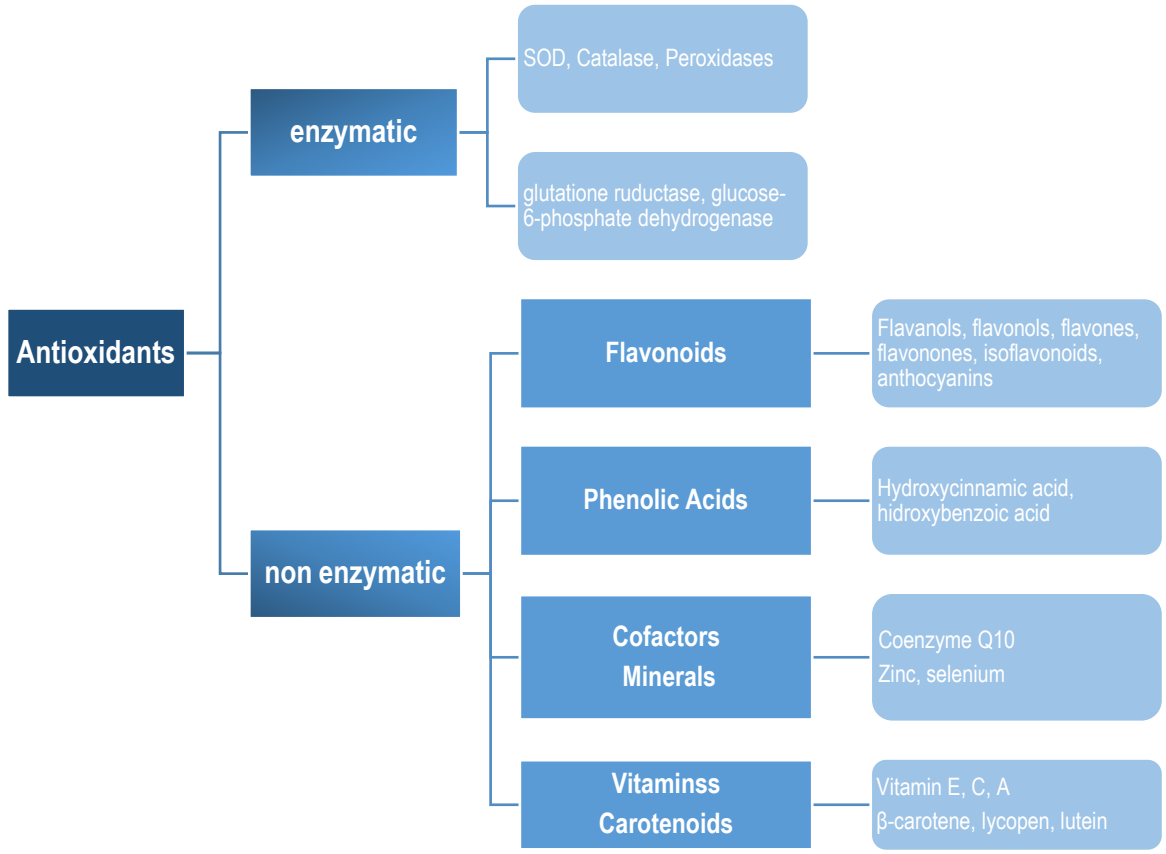

Fig. 6 Antioxidants classification. (Modified from Carocho M. and Ferreira I.C.F.R. Food and Chemical Toxicology 51 15–25 2013; Rice-Evans C.A. et al. Free Radical Biology & Medicine 20(7) 933-956 1996)

The lack of these antioxidants in healing skin wounds seems to indicate their crucial role.

1.4 Probiotics

Probiotics are "*live micro-organisms which, when administered in adequate amounts, confer a health benefit on the host.*" (Food and Agricultural Organization of the United Nations and World Health Organization. 2001)

Live bacteria and yeasts or their parts or metabolites may be administered to obtain a beneficial effect. The beneficial effect of administration of probiotics require microorganisms to be alive, a specific dose should be defined and proven to be beneficial to the host.

Researchers have hardly defined the most effective dose and always the highest reasonable dose is supplied. A plethora of probiotics has been studied to unveil their potential beneficial effect, including *Lactobacillus rhamnosus* GG, several *Lactobacillus* and *Bifdobacterium* strains and the yeast *Saccharomyces boulardii* (Hickson M., 2013).

Probiotics may act in three different way on human health. Probiotics can act directly against pathogen or commensal bacteria, they can modulate the host immune system or carry out the inactivation of toxic compounds. In particular, probiotics are active in the gastro-intestinal tract of humans but can also be helpful in dermatological field.

Metabolites, ranging from small molecules to peptide, produced from probiotics often play an antimicrobial role (Oelschlaeger T.A., 2010).

Several proteins seem to carry out their role on cells surface, for example by making easier the interaction with host epithelial cells or extracellular matrix proteins, by inducting an immunomodulation route and by aiding the colonization of the gastrointestinal tract. Probiotic metabolites may be interesting compounds in clinical applications for prevention and treatment of different diseases. (Yan and Polk, 2011)

The major mechanisms of probiotics-mediated immunomodulation are the regulation of gene expression and signaling pathways in the host cells. Probiotics are effective in the regulation of defense immune responses directly interacting with intestinal epithelial cells, stimulating the responses of white blood cells after internalization by M cells and triggering toll-like receptors in immune system cells.

As described above, bacterial colonization and infection represent distinct features of chronic wound phenotype. Antibacterial treatments are effective (i.e. silver sulfadiazine) but often present side effects. Biofilm formation are another cause of persistent infections and impaired healing. Bacteria develop resistance or growth in biofilm; consequently, they are not sensible to immune defenses and antibiotics. Novel antimicrobial agents are required. A novel approach in the management of infected wounds consists in the topical application of probiotics, also called bacteriotherapy. (Peral M. et al., 2009)

In the last years, the use of probiotics for skin treatment has increased and confirmed their safety profile. The probiotics commonly employed usually belong to the intestinal microflora: *lactobacilli, bifidobacterium*, and *enterococci*. Probiotics and prebiotics may play an important role in wound healing due to inflammatory response modulation and antibacterial properties. (Baquerizo Nole K.L. et al., 2014).

The extracts or supernatants from *Lactobacilli* cultures have been employed for their antibacterial effects and showed ability to improve the different phases of wound healing. (Ramos A. et al., 2012). Chemical composition of *Lactobacillus plantarum* ATCC 10241 cultures supernatants (LAPS) was investigated and Ramos et al. postulated that these chemical compounds in wound healing and wound infections. LAPS was tested on a murine model. It resulted no cytotoxic, helpful in wound healing and active against *P. aeruginosa*. LAPS was analyzed and a number of active molecules were found. Organic acids, alcohols, benzoic acid, 5-methyl hydantoin, 2,5-mevalonolactone, and isobutyl-piperazinedione, AI-2, DNAse, demonstrate antimicrobial properties and a biofilm disrupting ability. In addition, phenolic compounds were found present, that could be helpful in contrasting reactive oxygen species typically present in chronic or infected wounds. Another interesting molecule detected is lactic acid, which is reported in literature as having antimicrobial activity, and seems to stimulate angiogenesis. Finally, barbituric acid derivatives found in LAPS may promote wound healing improving collagen production. (Ramos A et al., 2014; Cabral M. et al., 2014)

LAPS represent an "*active pharmaceutical ingredient (API) from biological origin*". Topical application of LAPS requires a suitable formulation. To ensure a correct application in wounds,

Cabral M. et al. (2014) developed a semi-solid dosage form loaded with LAPS. The formulation of probiotics in general deserves dedicated studies.

2. AIM OF THE THESIS

Literature data, including those cited in the introduction section, suggest that antioxidants and probiotics stimulate and support tissue regeneration by promoting the various phases of wound healing. There is therefore a need to develop formulations suitable for releasing antioxidants and probiotic agents to the damaged tissue in order to promote tissue repair. New active dressings are needed to allow the simultaneous use of antioxidants and probiotics in wound treatment, that are easy to find and less expensive compare to the use of biotechnological products (i.e. growth factors). The present thesis work was intended to support the treatment of "chronic ulcers" by preventing potential imbalance. The project aimed to the optimization of antioxidant delivery to wounds using a nanotechnology approach and to realize medications/medical devices for topical supplementation of antioxidants and probiotics.

In the first section, α-tocopherol, used as model lipophilic antioxidant, was loaded in nanoemulsions stabilized with hydrophobically-modified chitosan with the aim to improve drug solubility and stability. To further improve chemical stability and to increase drug concentration, nanoemulsions were converted into a spray-dried solid. Both were used as prototypes to be tested *in vitro*, *ex vivo* and *in vivo* to check safety and to obtain a proof of concept of their activity in the healing process. As biological tests the use of *in vitro studies* on cell culture, *ex-vivo* studies on human skin biopsies was envisaged and, finally, tissue repair was studied on an *in vivo* murine model.

In the second section, the practical problem of topical application to wounds had to be solved. To this purpose, different formulations, to be used as advanced dressings or films have been developed. It is known that dressings/films are particularly useful to protect and maintain the optimal moisture conditions in wounds. In particular, based on previous results, nanoemulsions were incorporated in films, whereas probiotics were loaded either in lyophilized dressings or in films. In both cases, well-known natural and synthetic hydrophilic polymers and mixtures thereof were used as base materials.

3. SECTION ONE

Nanoemulsion of α-tocopherol stabilized with hydrophobically modified chitosan and spray-dried in microparticles.

3.1 PREFACE

Classification of dressings for wound healing

Dressings for skin lesions can be classified using different approach:

- the function in the wound (e.g. antibacterial, occlusive, absorbent),
- the dressing materials (e.g. hydrocolloid, collagen),
- the physical form of the dressing (ointment, film, foam, gel, powder).

Nevertheless, dressings can be classified into primary dressing (in physical contact between medication and the wound surface), secondary dressing (cover the primary dressing) and island dressings (equipped with a central absorbent region surrounded by an adhesive slice.)

Other classifications include traditional or modern dressings, advanced dressings, skin replacement products and medical devices.

Modern medications have been developed to maintain a moist environment on the wound and can be classified according to their primary material (eg. hydrocolloids, alginates). Generally, they are produced in form of gels, films or foam sheet.

Films have been used and studied since a long time. Originally these dressings were occlusive, made in nylon placed on an adhesive polyethylene structure.

Semi-permeable film dressings were then proposed obtained from polyurethane. Their porous and permeable structure allows gas exchange and absorption of liquid exudates. Most commercialized brands offer different levels of vapor permeability, adhesiveness, conformability and extensibility. (Boateng J.S. et al., 2008)

Chitosan and chitosan-based nanoparticles

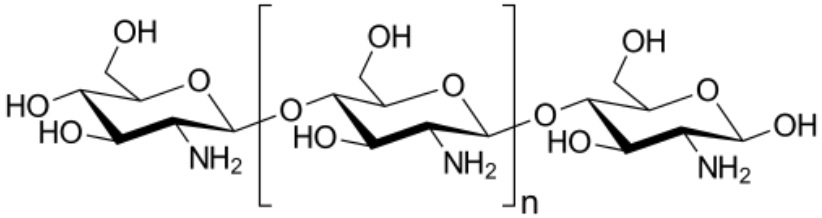

Fig. 7 Chemical structure of chitosan.

Chitosan (Fig. 7) is a linear polycationic amino-polysaccharide, composed of glucosamine and N-acetyl-glucosamine monomers. It is a semisynthetic derivative of the completely acetylated amino-polysaccharide Chitin, a natural polymer mainly extracted from the exoskeletons of crustaceans and cell walls of fungi and is obtained from Chitin by a controlled partial deacetylation process. Chitosan is generally recognized as a safe (GRAS) pharmaceutical ingredient.

Chitosan shows hemostatic and antibacterial activities, biodegradability and biocompatibility. Further, it is able to speed up tissue wound healing when applied in powders, microparticles, sponges or other forms. Chitosan promotes neutrophils and macrophages migration and fibroblasts proliferation, helping wound cleaning, granulation tissue formation and re-epithelilization. (Muxika A. et al, 2017; Patrulea V. et al., 2015).

Numerous chitosan derivatives derivatives have been made available even commercially and proposed for a variety of applications.

In particular amphiphilic polymers like hydrophobically-modified chitosans are also proposed as polymeric surfactants to stabilize o/w nanoemulsions. Indeed whereas the bulky hydrophilic blocks of the polymers interact with water molecules in aqueous media, thus exerting a positive effect on steric stabilization and interfacial activity, the high number of contact points between the oil droplets and the multiple chains of the polymer hydrophobic blocks, result in a strong attachment of the polymeric surfactant to the oil/water interface. In addition, the macromolecular shell formed by the polymeric surfactant in aqueous environment may display potential biological activities. For example, the vast family of amphiphilic palmitoylglycol chitosan derivatives have been shown to maintain the mucoadhesion and penetration enhancement properties typical of chitosans.

Advantages related to the use of hydrophobically-modified chitosan derivatives are largely described in the literature. For example, semisynthetic amphiphilic derivatives of chitosan have been tested for the ability to form polymeric micelles and to solubilize difficult to treat drugs. Deshmukh et al. used stearic acid-grafted chitosan oligosaccharide to solubilize doxorubicin. The incorporation in micelles slowed down the drug release due to the hydrophobic interaction between doxorubicin and the hydrophobic moiety of chitosan oligosaccharide represented by oleic acid. (Deshmukh A.S. et al., 2017).Different N-acyl modified chitosans, like the above mentioned palmitoylglycol chitosan family are described in the literature. An alternative approach to obtain such derivatives includes the preparation of hydrophobically-modified chitosan salts by electrostatic interaction between the cationic groups of chitosan, and the anionic groups of fatty acids. These interaction products were used to obtain polymeric micelles suitable to increase the solubility of hydrophobic drugs. (Bonferoni M.C. et al., 2017)

Spray dried powders

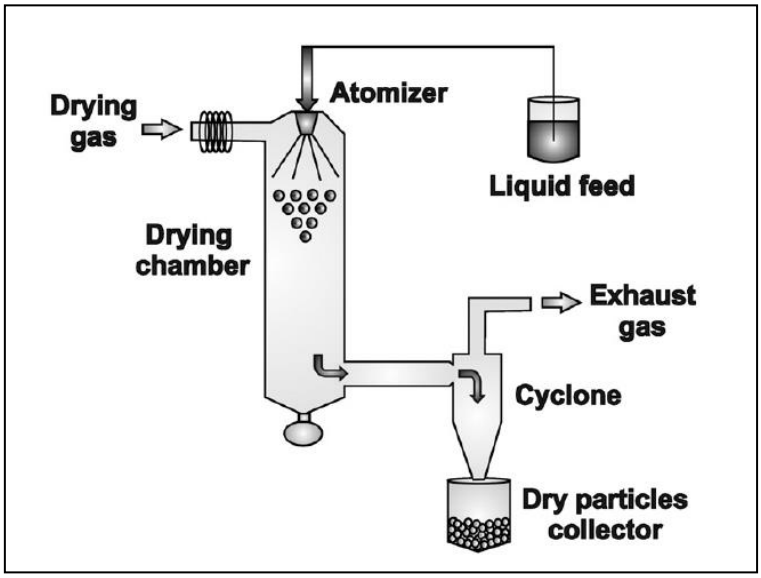

Fig. 8 Scheme of a classic spray-drier.

Fig 8 Reprinted from Advances in Colloid and Interface Science, Vol 223, A. Sosnik, K.P. Seremeta, Advantages and challenges of the spray-drying technology for the production of pure drug particles and drug-loaded polymeric carriers, Pages No. 40–54., Copyright 2015, with permission from Elsevier.

Spray-drying technique (Fig. 8) employs the atomization in a hot drying gas flux to transform a fluid solution, suspensions, melts or emulsions into a powder. There are four main steps in this process:

1. atomization of the inlet fluid
2. drying of liquid into drying gas,
3. dry particles formation,
4. separation and collection of the dry product.

A peristaltic pump pushes the fluid through an atomizer or a nozzle into the drying chamber. The micrometer droplets produced are subjected to fast solvent evaporation (due to a high surface area-to-volume ratio) that leads to the formation of dry particles. A cyclone allows the separation of the particles from the gas flux storing them in a glass collector. Solid products obtained present a higher chemical and physical stability compared to liquids. An important advantage of spray drying process consist in the ability to dry several heat-sensitive compounds without degradation. During the drying process, the droplets could be exposed to high temperature for a very short time, milliseconds or seconds avoiding drug degradation. This technique is particular interesting in pharmaceutical field to encapsulate drugs and oils into polymeric nanoparticles and microparticles carriers. (Sosnik A. and Seremeta K.P., 2015)

Photon correlation spectroscopy (PCS)

Photon correlation spectroscopy (PCS), based on laser light scattering, provides a reliable method to measure the dimension of nanoparticles (Fig. 9). Variations in the powers of the scattered light result from the molecular motion (Brownian motion) in the dispersion and hence PCS results with time. As the particle size decreases, the Brownian motion raises and these variations increase. A correlation may be found among the different intensities measured. (Muller-Goymann C.C. et al., 2004)

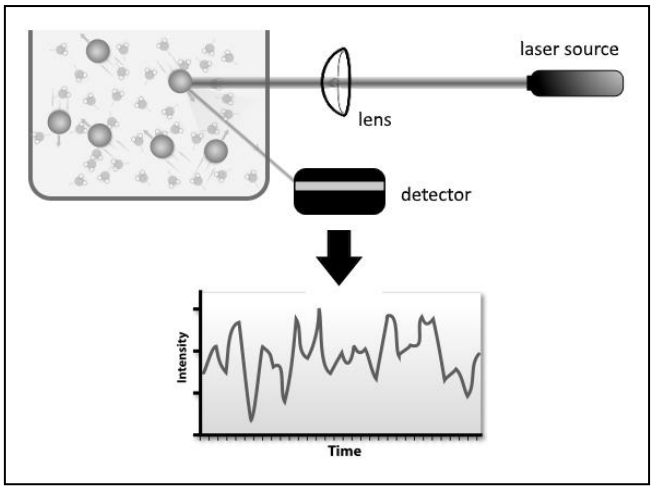

Fig. 9 Schematic representation of PCS. The laser beam hits the particles and light intensity is registered to calculate the particles radius. (Adapted from DLS, Mike Jones. CC License)

Vitamin E

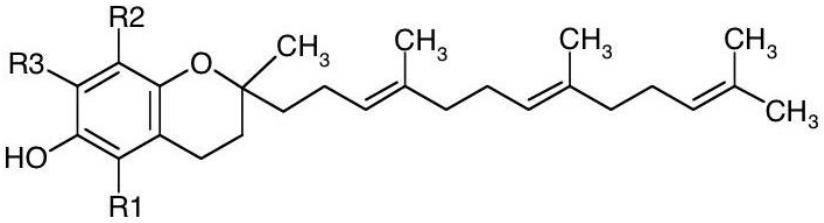

Fig. 10 General chemical structure of Vitamin E.

R1, R2, R3 = H or CH_3

Vitamin E consists of a group of fat-soluble compounds classified into two groups of four isomers, tocopherols and tocotrienols (Fig. 10). The most effective and abundant radical-scavenging antioxidant *in vivo* is α-tocopherol. Vitamin E protects cell membranes and other lipids from ROS damages, acting as antioxidant, and may modify the activity of different enzymes regulated by oxidation or reduction reactions involved in signal transduction by influencing their redox state. Furthermore, Vitamin E induces the activation of different biochemical transduction pathways, gene

transcription and modulates the expression of Connective Tissue Growth Factor. Another role of Vitamin E concern a modulation of cell signaling that protects the structural integrity of all human cells. Taking into consideration globally its beneficial effects, Vitamin E play a key role in the tissues healing. (Hobson R., 2014; Zingg J., 2015)

Oleic acid

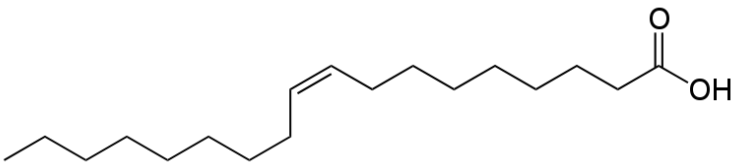

Fig. 11 Chemical structure of oleic acid.

Oleic acid is fatty acid with a hydrophobic tail of 18 carbon (cis-9 double bond) and a polar carboxylic acid group (Fig. 11). Behavior of free fatty acids in solution is complex and pH-dependent. Janke et al. (2014) observed the aggregation of oleic acid monomers into micelles, vesicles, and oil phases, depending on the protonation state of the oleic acid group. Unsaturated fatty acids are able to modulate immune responses. Fatty acids play an important role in angiogenesis and cell proliferation and modulate the functions of neutrophils that release various cytokines during wound healing process. Essential fatty acids, such as linoleic and oleic acid, help to ensure epidermal integrity and to maintain the water barrier in the skin. Nevertheless, they may be effective in prevention and treatment of pressure ulcers. Cardoso C.R. at al. (20011) concludes that oleic acid can modulate inflammatory and immune responses in skin lesions, thus may be an interesting compound for treatment of cutaneous wounds. (Janke et al., 2014; Cardoso et al., 2011; Pereira et al., 2008)

3.2 SCOPE OF SECTION ONE

Hydrophobically-modified chitosan was employed in the preparation of nanoemulsion suitable for loading hydrophobic antioxidant. α-tocopherol was chosen as pilot compound because it is one of the most effective fatty soluble antioxidant in nature. The resulting nanoemulsion was characterized for dimension, stability and *in vitro* radical scavenging activity. Furthermore, different biological tests were effectedon fibroblast cultures, keratinocyte cultures and human skin *ex vivo* biopsies to study the biological effects of this formulation. Finally, an *in vivo* test was carried out on a rat wound model. By means of a spray-drying process a powder suitable for the treatment of skin lesion was developed, increasing significantly the chemical and physical stability of the loaded antioxidant.

3.3 EXPERIMENTALS

3.3.1 MATERIALS

- Oleic acid (Fluka, Milan, I)
- Chitosan low molecular weight. mol wt 50,000-190,000 Da, viscosity 20-300 cP, 1 wt. % in 1% acetic acid 25 °C, Brookfield Acetone HPLC grade (Sigma-Aldrich, Milano, Italy)
- Absolute ethanol (Sigma-Aldrich, Milano, Italy)
- Alpha-tocopherol (Fluka, Sigma-Aldrich, Milano, Italy)
- Sodium acetate (Carlo Erba, Milano, Italy)
- Acetonitrile Cromosolv per HPLC (Sigma-Aldrich, Milano, Italy)
- Glacial acetic acid (Carlo Erba, Milano, Italy)
- Acetic acid 96% (Carlo Erba, Milano, Italy)
- Hydrochloric acid 1M (Carlo Erba, Milano, Italy)
- DPPH, 2,2'-diphenil-1-picrylidraziyl radical (Sigma-Aldrich,Milano,Italy)
- Sodium hydroxide (Carlo Erba, Milano, Italy)
- D-Mannitol (Fluka, Sigma-Aldrich, Milano, Italy)
- Methanol HPLC-PLUS gradient (Carlo Erba, Milano, Italy)
- Isopropyl Myristate (Sigma-Aldrich, Milano, Italy)
- Tween 80: polyoxyethylene sorbitan monooleate (Sigma-Aldrich, Milano, Italy)
- PBN (α-phenyl-N-tert-butyl nitrone) (Sigma-Aldrich, Milano, Italy)
- Fibroblast (bNHDF) (baby Normal Human Dermal Fibroblast) (Promocell, Milano, Italy)
- Human epidermal keratinocytes (Sezione di Chirurgia Plastica,I.R.C.C.S. Fondazione Salvatore Maugeri, Pavia, Italy)
- Culture medium 10% FBS: Dulbecco's Modified Eagle's Medium (DMEM with glutamine, Sigma-Aldrich, Milano, Italy) addition with FBS 10% v/v (FBS, Foetal Bovine Serum, Euroclone, Milano, Italy), previously free from complement proteins by thermostatic bath at 56°C for 30 minutes, and 1% v/v of a sterile solution of Penicillin, Streptomycin and Amphotericin (Sigma-Aldrich, Milano, Italy)
- Culture medium 20% FBS: Dulbecco's Modified Eagle's Medium (DMEM with glutamine, Sigma-Aldrich, Milano, Italy) addition with FBS 20% v/v (FBS, Foetal Bovine Serum, Euroclone, Milano, Italy), previously free from complement proteins by thermostatic bath at 56°C for 30 minutes, and 1% v/v of a sterile solution of Penicillin, Streptomycin and Amphotericin (Sigma-Aldrich, Milano, Italy)
- HBSS: Hans Balanced Salt Solution, modified (Sigma-Aldrich, Milano, Italy)

- PBS: Dulbecco's Phosphate Buffered Saline 10 (sterile filtered, endotoxin tested, without calcium chloride and magnesium chloride) (SigmaAldrich, Milano, Italy) diluted 1:10 with distilled sterile water sterile
- Trypsin with EDTA 2,5% (Sigma-Aldrich, Milano, Italy)
- MTT: [3- (4,5-dimethyl-2-thiazolyl) -2,5-diphenyl-2H-tetrazolium bromide] (Sigma-Aldrich, Milano, Italy)
- DMSO: dimethyl sulfoxide (Sigma-Aldrich, Milano, Italy)
- Flask T25: Cellstar tissue culture flasks, 75 cm^3, 250 ml, PS, red standard cap, sterile (Greiner bio-one, Milano, Italy)
- Flask T75: Cellstar tissue culture flasks, 25 cm^3, 50 ml, PS, red standard cap, sterile (Greiner bio-one, Milano, Italy)
- 96-well plate: Cellstar tissue culture plate, 96 W, flat bottom, with lid, sterile (Greiner bio-one, Milano, Italy)
- Criovials: cryogenic vials (Nalgene Cryoware, Nalgene Labware, New York, USA)
- Counting chamber: KOVA Glasstic Slide 10 with grids, combination cover slip-Microscope slides (Hycor Biomedical Inc., Garden Grove, California, USA)
- Filter 0.22µm: Minisart single use filter unit, non-pyrogenic, hydrophilic, 0,22 µm (Sartorius Stedim Biotech GmbH, Goettinggen, Germany)
- Protease IX (Sigma-Aldrich, St. Louise, MO, USA)
- Petri multiwell 12 wells (Costar, Corning, New York, USA)
- Transwell® Permeable Supports System 12-well (Corning Costar, Corning, NY)
- Culture medium EpiGRO (Merck Millipore, USA)
- Glass coverslips (Bio-Optical, Milano, Italy)
- Primary mouse monoclonal antibodies anti-BrdU (GE Healthcare UK Ltd, Amersham Place, Buckinghamshire, England)
- Primary mouse monoclonal antibodies anti-PCNA (Biocare Medical, Concord, CA, USA)
- Fluorescent secondary antibodies anti-mouse FITC-conjugate (SigmaAldrich, USA)
- Kit MACH1 Universal HRP-Polymer detection Biotin-free (Biocare Medical Concord, CA, USA)
- Mounting Solution DPX (VWR International PBI S.r.l., Milano, Italy)
- Hoechst 33258 (Sigma-Aldrich, USA)
- Equitensine (pentobarbital 0.972% w/v, chloral hydrate 4.25% w/v, ethanol 10% v/v, propylene glycol 39.6% v/v, distilled water)
- Tramadol hydrochloride solution 15% w/v
- Physiological solution (NaCl 0.9% w/v)
- PBS (phosphate buffer) pH 7,4 (SigmaAldrich, Milano, Italy)

- HEC (Natrosol® hydroxyethylcellulose 250 HX Pharm, Natrosol® Hydroxyethyl cellulose 250 HHX Pharm, Aqualon® Hercules Incorporated®, Castelmaggiore, Italy)

3.3.2 METHODS

3.3.2.1 Preparation and characterization of nanoemulsion

The nanoemulsions were prepared from low molecular weight chitosan (mol wt 50,000-190,000 Da, viscosity 20-300 cP, 1 wt. % in 1% acetic acid 25 °C, Brookfield) dissolved in distilled filtered water acidified with HCl 1M, in stoichiometric ratio with the amine groups of chitosan, under magnetic stirring. Chitosan HCl obtained was dialyzed (12-14 kDa, Emanuele Mires, Milan, Italy) in distilled filtered water and then lyophilized (Heto dry winner, Analytical de Mori, Milan, Italy).

α-tocopherol loaded nanoemulsions have been preparedusing chitosan oleate, a form of amphiphilic modified chitosan (AMC) obtained by addition of fatty acid chains. AMC, in fact, has the ability to self-assemble into nanoparticles structures, able to deliver hydrophobic substances, loaded into the core of the structure. In particular, chitosan oleate is the result of the electrostatic interaction between the polymer and the fatty acid and consists of electrostatic interaction among the amino groups of the chitosan and the carboxylic groups of the oleic acid.

The organic phase was obtained by solubilization in acetone of oleic acid (1.1 mg/ml) and α-tocopherol (1 mg/ml), while the aqueous phase was a solution of chitosan hydrochloride at 0.05% (w/v) (80% deacetylation degree) in filtered-distilled water (Millipore Sartorius Stedim Bioteh GmbH, Gottingen, Germany). One part of the organic phase was poured, under magnetic stirring, into three parts of the aqueous phase so that the chitosan/oleic molar ratio was 1:0.5. Solvent evaporation took place under vacuum in Rotavapor, rotation speed was fixed at 90 rpm, with mild heating (30-35 °C). Under these conditions, nanoemulsions were obtained by spontaneous emulsification. Finally, nanoemulsion underwent sonication for 15 minutes (Elmasonic S 80 H, Elma Hans Schmidbauer GmbH and Co, Singer, Germany) to reduce possible particle aggregates. (Bonferoni M.C. et al., 2014; Bonferoni et al, 2017; Bouchemal K. et al., 2004; Liakos I.L. et al., 2016)

(M. C. Bonferoni, G. Sandri, S. Rossi, F. Ferrari, C. Caramella, “Nanoemulsioni olio-in-acqua" – Patent (University of Pavia) MI2014A001812, 21 october 2014).

Dimensional analysis

Particle size analysis of nanoemulsions were carried out by means of Photon Correlation Spectroscopy (PCS) (N5 submicron particle size analyzer, Beckman Coulter, Italy). The correct concentration was chosen in accordance with the operating procedures of the instrument by dilution of the samples with filtered-distilled water (Millipore Sartorius Stedim Bioteh GmbH, Gottingen, Germany). Each analysis was performed at the temperature of 25°C by means of 30° and 90° detection angles. For each sample, the measurements were replicated 3 times.

ζ potential

The zeta potential was measured by Malvern Zetasizer Nano ZS90. The nanoemulsion was diluted with water (ratio 1:5) and each sample was loaded in disposable cuvettes.

Quantification of α-tocopherol

The concentration of the active ingredient was assessed by RP-HPLC analysis. The HPLC system is a Perkin-Elmer Series 200 instrument and consists of a pump, an autosampler, a UV-Vis detector and is interfaced with a PC that allows recording and reprocessing chromatograms. The analyzes were carried out using a Waters C18 column as stationary phase (3.9 · 150 mm, particle size 10 µm, 125 Angstrom) and a solution of acetonitrile:acetate buffer pH = 4, 95: 5 (v/v) as mobile phase. The flow rate was fixed at 1 ml/min, at room temperature, and detection wavelength was settled up at 292 nm. The injection volume of the sample was 20µl and for each sample were performed two replicates with a 12-minute analysis time. The concentration of α-tocopherol in nanoemulsion sample was calculated by the calibration curve prepared in the concentration range from 2.5 to 50 µg/ml (R^2 = 0.999). Samples for HPLC analysis were directly solubilized in mobile phase (Castana S. et al., 2005; Bele C. et al., 2013).

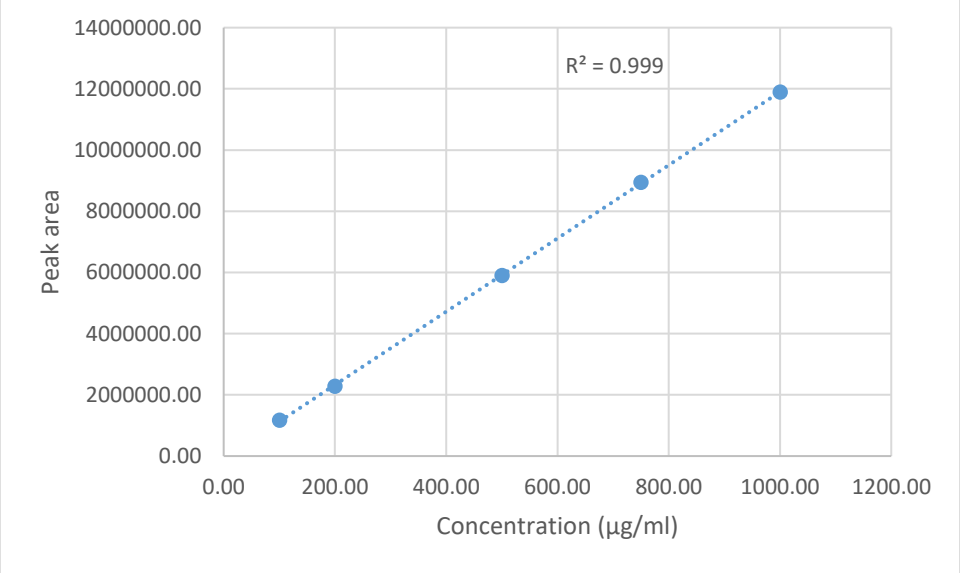

Fig. 12 Calibration curve for analysis of α-tocopherol by HPLC.

100µl of sample were diluted in 600µl of mobile phase splitting up the emulsion components; the concentration of the samples remained in the range of the calibration curve.

The encapsulation efficiency (EE%) and the loading capacity (L.C.%) were calculated by the following the equations:

$$EE(\%) = \frac{\alpha\text{Tph quantified in NE}}{\alpha\text{Tph added to the system}} * 100$$

$$L.C.(\%) = \frac{\text{of } \alpha\text{Tph quantified in NE}}{\text{Chitosan OA } + \text{ } \alpha\text{Tph added to the system}} * 100$$

Stability Study

The nanoemulsion samples loaded with α-tocopherol at concentration of 314±22 µg/ml were stored in dark vials and under nitrogen flux to avoid the oxidation due to the atmospheric oxygen at different storage temperatures, room (25°C) and fridge temperatures (4°C). HPLC-RP method, as previously described, was employed to assayα-tocopherol concentrations at time 0 and at day 1, 2, 7, 14, 22, 28, 35.

In vitro antioxidant activity (2,2'-diphenil-1-picrylidraziyl (DPPH•) assay)

Use of DPPH• provides an easy and rapid method to evaluate the antiradical activities of antioxidants, (Bondet V. et al., 1997).

A number of studies on DPPH• reaction chemistry (Fig.13) have shown that absolute and relative concentrations of DPPH•, solvent polarity and hydrogen bonding strength, pH, temperature and oxygen affect the rate and the kinetic of DPPH• reaction with antioxidants (Xie J. et al., 2014). Hence, we worked preserving the radical from light, at room temperature (25°C), without salt in the solutions, at the same pH.

Employing the 2,2'-diphenil-1-picrylidraziyl (DPPH•) assay, the antioxidant activity of α-tocopherol loaded in nanoemulsion was evaluated *in vitro*. DPPH• is a stable radical molecule in methanol solution. It appears violet and it shows the best absorbance at λ=515nm; however, in presence of antioxidants molecules it reacts with and gives a hydrogen atom becoming an instable non-radical molecule, the 2,2-diphenil1-picrylidrazine, unable to absorb at λ=515nm, that shift the color of the solution to yellow.

The reaction among antioxidant and DPPH• occurs directly in a quartz cuvette (1.5 ml). A solution containing only the solvent $MeOH_3$ was used as control.

DPPH• assay was carried out on α-tocopherol in nanoemulsions and alone by measuring the intensity in UV absorbance at λ=515 at the beginning of the experiment (T=0) and at different times. The residual value of absorbance, determined at steady state (plateau), provides an evaluation on the radical scavenging activity that doesn't depend on the antioxidant kinetic behavior, but it is affected by the molar ratio between the antioxidant and DPPH•. Therefore, the same molar ratio of antioxidant and DPPH•, and the spectrophotometric measure at the steady state are critical parameters to compare the radical scavenging ability of different antioxidants species.

The radical scavenging capability of nanoemulsions was evaluated following a standardized procedure. The DPPH• methanol solution was prepared at the concentration of $6x10^{-5}$M using dark vials to protect the compound from the light. The analysis was carried out with an UV-VIS

spectrophotometer (Perkin Elmer Lambda 25 UV-VIS instrument spectrometer, Monza, Italy) with a quartz cuvette (high precision cells, Hellma Analytics, Germany), containing 975µl of DPPH solution and 25µl of sample. The absorbance value of the DPPH• solution was fixed as "zero point" in the construction of the absorbance/time curve. The kinetic of the reaction between DPPH• and the sample was monitored by measuring the absorbance at λ=515 nm at different times up to 1 hour (time 0, 1min, 5min, 10 min, 15min, 20 min, 30 min, 40 min, 50 min, 60min) or until the signal appeared stable (plateau). The absorbance value residues at steady state (A_{DPPH}^{R}) and the absorbance value at time zero (A_{DPPH}^{0}) allow the evaluation of the radical scavenging activity by calculation of the percentage of inhibition of DPPH•:

$$DPPH\ radical\ scvenging\ rate\ (\%) = \left(1 - \frac{A_{DPPH^R}}{A_{DPPH^0}}\right) x100$$

Similarly, analysis on unloaded nanoemulsion was carried out to determine the eventual antioxidant activity attributable to the chitosan oleate.

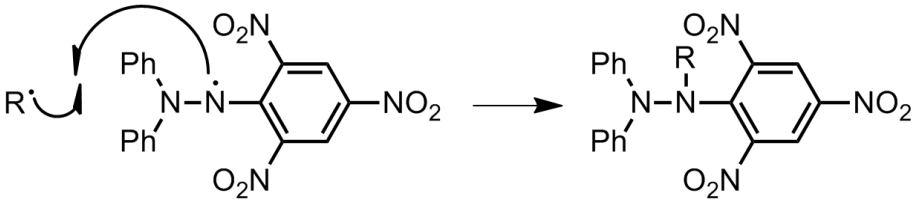

Fig. 13 2,2'-diphenil-1-picrylidraziyl (DPPH•) reaction with a radical species.

3.3.2.2 Biological evaluation of nanoemulsion

In vitro test on fibroblasts

Fibroblasts cell cultures and growth conditions

Normal Human Dermal Fibrobasts (NHDF, Promocell) were grown in Dulbecco's Modified Eagle's Medium (Lonza, Milan, Italy) supplemented with 10% (v/v) Foetal Bovine Serum (Euroclone, Milan, Italy), 1% v/v Penicillin–Streptomycin 100x and 1% (v/v) Amphotericin (WVR, Milan, I). Fibroblasts were maintained in a humidified (95 RH%) atmosphere with 5% CO_2 at 37 °C and routinely trypsinized every 7 days using trypsin–EDTA solution 0.25%. The cells used were between the 5th and the 13th passage.

Fibroblast proliferation test

Fibroblasts were seeded at a density of 20,000 cells/well into a 96-well plate (CELLSTAR Greiner®, Sigma Aldrich, MI, I) and were incubated with 200 µl of NE samples at different concentrations for 24 h in culture medium without serum (DMEM w/s). After that the Neutral Red test was performed: the medium was removed, fibroblasts were washed with PBS and treated with 200 µl of Neutral Red 0.5 mg/ml in HBSS. After 3h the medium was removed, the cells were washed with PBS. 200 µl of 50% v/v ethanol and 1% v/v glacial acetic acid were added to each well to disrupt cell membranes and solubilize NR present in vital cells. The plate was kept away from light for 5–10 min and the absorbance was read by a Microplate Absorbance Reader iMARK™ (Bio-Rad Laboratories S.r.l., Segrate, MI, Italy) at a wavelength of 490 nm, with a reference at 655 nm. The percentage of viability was calculated considering as 100% the viability of the control represented by the culture medium without serum (DMEM w/s). For BrdU test, 50,000 cells were seeded in growth medium without serum (DMEM w/s) on 2x2 cm2 slides introduced in Petri dishes. After 30 minutes, 200 µl of samples were added and incubated with the cells for 24 h. 1 h before the end of the test, 20 µl of BrdU were added at 30 µM final concentration. Cells were washed with PBS, fixed with 70% ethanol and stored at -20°C. BrdU staining was performed as described for keratinocyte cell cultures.

Antioxidant activity evaluation on fibroblast cell culture

A cytotoxicity test was carried out to evaluate the sensitivity of fibroblasts to H_2O_2. 34,000 cells/well were grown in a 96 well plate in complete medium (DMEM 10%). After 24 h cells were incubated with increasing H_2O_2 concentrations, 0.5-2.5 mM final concentration range, for 24 h. Cell viability was assessed by means of the Neutral Red test as previously described. 1.5 mM and 2.0 mM H_2O_2 concentrations were chosen to induce significant oxidative damage, and the test was repeated in presence of αTph NE. In this case, after 24 h of initial growth 200 µl of NE diluted in DMEM until α-α-tocopherol concentrations ranging from 0.1 to 100 µM were added to fibroblasts. Corresponding dilutions of unloaded nanoemulsion were also tested for comparison. After 4 h H_2O_2 at final 1.5 and

2.0 concentration was added and after 24 h NR test was performed. The % of cell viability was calculated referred to DMEM 10% control. 8 replicates for each condition were assessed.

In vitro test on keratinocytes

Keratinocytes isolation and culture

For in vitro experiments, human primary cell cultures of epidermal keratinocytes were used, obtained from surgical biopsies according Häkkinen et al. 2001, Riva et al., 2007. Biopsies was subjected to protease digestion to separate epidermis, that was in turn digested with trypsin (0.05% trypsin, 0.01% EDTA) under stirring for 10 minutes at room temperature to isolate keratinocytes. Cells were centrifuged 10 minutes 1200 rpm, and the pellet re-suspended in specific growth medium (EpiGROTM, Millipore, CA). Cells were directly seeded on round slides 12 mm diameter ($2*10^5$ cells/slide). Slides were introduced in 12 well plates and incubated at 37°C in 5% CO_2 atmosphere.

Keratinocytes proliferation test

Proliferation test was performed on keratinocytes grown to confluence on cover slides that were then introduced into a 12 well plate. Wells were added with amounts of α-tocopherol nanoemulsion corresponding to 67 µg α-tocopherol/well. Corresponding amounts of unloaded chitosan oleate were tested for comparison. Controls were represented by untreated cells. To each well 700 µl of keratinocytes growth medium EpiGROTM were added. The cells were maintained in culture for 24 h and 7 days. At the defined times and 1 hour before cell fixation, DNA synthesis was analyzed by measuring the incorporation of 5-bromo-2′ deoxyuridine (BrdU). BrdU was added to the medium at 30 µM final concentration during the last hour in culture. The samples were then washed with PBS and fixed in 70% ethanol. The incorporated BrdU was detected by an immunostaining reaction with Amersham monoclonal anti-BrdU antibody (GE Healthcare UK Ltd., Amersham Place, Buckinghamshire, England). Briefly, the dishes were washed with PBS and incubated with HCl 2 N for 30 min at room temperature. 0.1 M sodium tetraborate ($Na_2B_4O_7$ $10H_2O$, pH 8.5) was used to neutralize the solution for 15 min, and then the cells were washed twice for 5 min in PBS and incubated for 20 min in the blocking solution (1% w/v BSA and 0.02% w/v Tween 20 in PBS Tween Albumin (PTA)). Cells were then incubated for 1 h with mouse anti- BrdU antibody diluted 1:100 in PTA. The cells were washed three times (10 min each) in PTA and then incubated again for 30 min in PTA containing anti mouse IgG FITC-antibody (Sigma-Aldrich, Saint Louis, MO, USA) diluted 1:100. The slides were extensively washed in PBS, counterstained for DNA with 0.5 µg/mL Hoechst 33258 (Sigma- Aldrich, Saint Louis, MO, USA), and mounted in Mowiol (Sigma- Aldrich, Saint Louis, MO, USA). The slides were observed by means of a Confocal Laser Scanning Microscope (Leica, TCS SP5II, Leica Microsystems, Milano, Italy). Five/eight images were recorded in different fields of each slide for a total amount of at least 500 cells counted, and replicating cells were counted with respect to the total number (blue nuclei).

Ex vivo tests on human skin biopsies

Punch tests were performed on human skin biopsies ex vivo obtained from breast reduction surgery from young healthy patients (kindly provided by the Plastic and Reconstructive Surgery, Department of Clinical Surgical Diagnostic and Pediatric Sciences, University of Pavia, Pavia, Italy − Plastic and Reconstructive Surgery Unit, Istituti Clinici Scientifici Maugeri, Pavia, Italy). The study protocol conformed to the ethical guidelines of the 1975 Declaration of Helsinki and received informed consent of all patients. The IRB approved the use of human tissue biopsies for experimental purposes (approval number 921 CEC) on 28/10/2013. The skin, cleaned of the hypodermic layer, was cut with a penknife into fragments of approximately 7x7 mm^2 and each of them was scratched with sterile punch (Ø = 3 mm). The fragments were placed in transwell inserts for 12-well plates (membrane pores: Ø = 0.40 µm, insert area 1.12 cm^2, Constar, Corning, New York, USA). The nanoemulsions loaded with antioxidant (67 µg α-tocopherol/punch hole) and corresponding amount of unloaded nanoemulsions were added to the biopsies. As negative control a non-treated skin fragment scratched with punch was used. In the basolateral compartment 700 µl of the culture medium for fibroblasts with FBS 10% were added to promote the vitality of the skin, ensuring hydration and adequate intake of nutrients through a homogeneous diffusion from the deep dermis. After incorporation for 1 hour with bromodeoxyuridine (BrdU), added to the growth medium at the concentration of 30 µM, at different time, histological analysis was carried out, as described in the literature (Riva et al., 2007). Briefly, the skin fragments were fixed in a solution containing paraformaldehyde 4% and phosphate buffer PBS 0.1 M, pH=7.4 for 6 hours, dehydrated by an ascending alcohol scale (from 70% ethanol or absolute alcohol and xylene) and included in paraffin. Using a horizontal slide microtome Leitz (Leitz Wetzlar, Stuttgart, Germany), histological incisions of 5-10 µm were obtained, then rehydrated, and stained with hematoxylin and eosin or processed for immune reaction with proliferation markers, either BrdU or proliferating cell nuclear antigen (PCNA), previous steam treatment for 1 hour, followed by washing in distilled water. Hematoxylin and eosin are dyes of choice for common histological sections, allowing the observation of the morphological appearance of the tissues. Hematoxylin is a basic dye which has affinity for all acid structures (and therefore basophilic) of cells and tissues; eosin stains pink/orange all the acidophilus basic structures. Mouse monoclonal primary antibodies were used for immuno-labeling reactions, anti-BrdU and anti-PCNA respectively, diluted 1:100 in PTA. Later, after two washes in PBS, the sections were incubated with secondary antibody supplied with the kit MACH1 Universal HRP-Polymer Detection Biotin-free in accordance with the instructions provided by the protocol. Finally, the sample sections were rehydrated by immersion in descending gradation alcoholic solutions, attached with DPX and observed in transmitted light Zeiss Axiophot microscope (Carl Zeiss, Oberkochen, Germany). Proliferating cells positive for BrdU or PCNA were counted in each section. For comparison purpose, the number of cells was related to section areas (normalized cell number).

In vivo test on murine model

All animal experiments were carried out in full compliance with the standard international ethical guidelines (European Communities Council Directive 86/609/EEC) approved by Italian Health Ministry (D.lgs.vo 116/92). The study protocol was approved by the Local Institutional Ethics Committee of the University of Pavia for the use of animals. Male rats (Wistar 200-250 g) were anesthetized with Equitensina (3 ml/kg) and shaved to remove all hair from the site of injury. Three full thickness burns, having a circular diameter of 4 mm, were produced on animal back by contact with a brass rod (105 °C for 40 s). The day after, three 6-mm full-thickness excisional wounds were outlined using a punch biopsy tool on each animal back. Wounds were covered with a sterile gauze and the rat back was wrapped with a surgery stretch (Safety, Monza Brianza, Italy).

In vivo treatment with α-tocopherol nanoemulsion

Nanoemulsion loaded with antioxidant was slightly viscosized by dilution 1:1 with a hydroxyethyl cellulose (Natrosol™ 250 HX Pharm hydroxyethyl cellulose) 3% (w/v) solution, obtaining a final concentration α-tocopherol of about 150μg/ml and of HEC at 1.5% (w/v). A comparison was performed between wounds treated with α-tocopherol nanoemulsions (200μl ≅ 30μg of antioxidant) and controls treated with plain saline solution. At the end of the experiment (7 days), full thickness biopsies were collected, and the histological analysis of the tissues excised was performed.

Histological analysis

The eight animals employed were sacrificed, and tissue samples were bisected along the widest line of the wound, then fixed in 4% w/v neutral buffered paraformaldehyde for 48 h, dehydrated with gradient alcohol series, cleared in xylene and embedded in paraffin. Sections (8 μm) were obtained using a Leitz (Wetzlar, G) microtome and were stained with hematoxylin and eosin (H&E) The slices were examined at the magnification of 5X under a light microscope Axiophot Zeiss (Oberkochen, Germany) equipped with a digital camera.

EPR detection of free radicals

EPR (Electron Paramagnetic Resonance) is a spectroscopic technique used to detect and analyze chemical species containing one or more spared electrons (paramagnetic species). These species include: free radicals, transition metal ions. The EPR X-band Bruker 220 SE spectrometer was employed to detect ROSs and free radicals in the microenvironment of the wound in the murine model used in the present thesis work in order to analyze samples of both wounded skin and exudate collected during the experiments. The EPR analysis was carried out on sample treated with a spin trap, PBN (α-phenyl-N-tertbutyl nitrone) (Fig. 14), a chemical species able to intercept ROSs and forming EPR measurable stable radicals (Dikalov S.I. and David G. Harrison, 2014).

Samples (g) 0.01865 collected from three lesions wound fluid added with 200µl of PBN solution at 0.1 M in physiological solution (NaCl 0.9%).

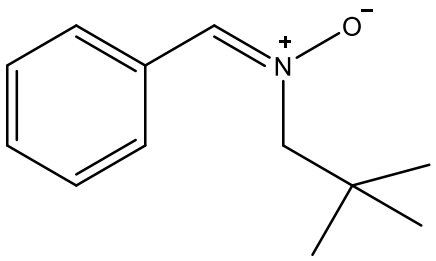

Fig. 14 Molecular structure of PBN spin trap.

Lipid peroxidation

Lipid peroxidation was investigated by quantifying malondialdehyde (MDA), a product of peroxidation in tissues, based on a calibration curve, the malondialdehyde content in rat skin samples was measured.

In details, firstly MDA was measured on samples obtained surgically from both injured and healthy rat skin. Then, after optimizing the method, samples from full thickness burned tissues treated with α-tocopherol-loaded formulation were compared to skin samples treated with formulation and to healthy skin as control, in term of lipid peroxidation. This method is based on the reaction between one molecule of MDA and two molecules of thiobarbituric acid (TBA) to form a red-pink dye complex (Fig. 15), measurable by UV-vis or fluorescence spectrophotometry. It should be stressed that among oxygenated products obtained from organic substrates, including lipids and fatty acids, it is common to detect compounds behaving like malonic aldehyde and reacting with TBA, i.e. Thiobarbituric Acid-Reactive Species (TBARS). In fact, TBARS may react with TBA producing the pink solution as describe above for TBA. The total concentration of TBARS is a representative of lipid peroxidation in the examined samples. (Gutteridge J.M., 1995; Baumbusch L.O. et al., 1998; Rael L.R. et al., 2004; Carocho M. et al., 2013)

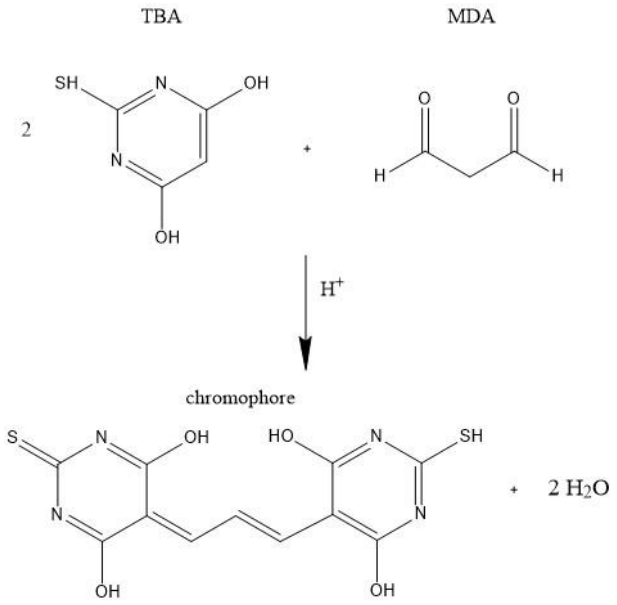

Fig. 15 Reaction between thiobarbituric acid and malondialdehyde to give a detectable chromophore.

A calibration curve (R^2 = 0.999) was obtained using MDA reagent solutions at different concentrations: 0.010 mM - 0.025 mM - 0.050 mM - 0.100 mM (Fig.16).

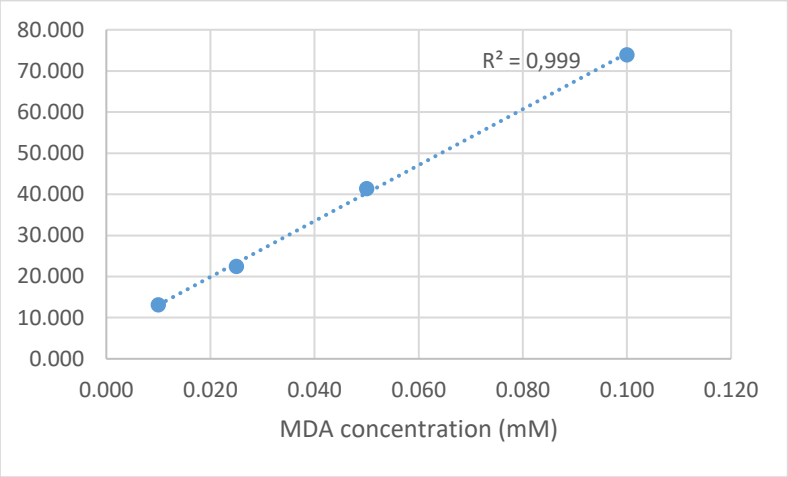

Fig. 16 Calibration curve of MDA by spectrofluorometric analysis.

Rat tissues were stored in freeze at -80°C after withdrawal. Tissues were homogenized in ice by means of an ultrasonic probe in 1.15% KCl solution. An aliquot (100 µl) of the homogenate was added to a reaction mixture containing 200 µl of 8.1% SDS, 1500 µl of 20% acetic acid (pH 3.5), 1500 µl of 0.8% thiobarbituric acid and 700 µl distilled water. Samples were then boiled for 15 minutes at 95°C, centrifuged at 3000rpm for 10 min and filtered on a 0.22 µm filter of cellulose acetate. Subsequently, the samples undergo were subjected to a spectrofluorometric analysis at excitation wavelight 532nm and emission wavelight 553nm. Thiobarbituric acid reactant substances were calculated by interpolation with calibration curve. (Mariotto S. et al., 2008)

3.3.2.3 Preparation and characterization of powders

Ultrafiltration and Concentration

A crossflow tangential flow concentrator (Vivaflow 50 | 50 R | 200, Sartorius Stedim Biotech GmbH, Goettingen, Germany) equipped with an ultrafiltration polysulfones membranes Hydrosart, with 50 m^2 of active area, was employed to obtain a concentration of nanoemulsion suitable for spray-drying. The volume of the emulsion was reduced and, consequently, the concentration of nanoemulsion was increased reaching a α-tocopherol concentration of 1mg/ml and 2mg/ml.

Dosage of tocopherol in powders

In a tube, 10 mg of recovered powder were dissolved in 250µl of acetate buffer pH=4, to solubilize the mannitol, then 1.250ml of acetonitrile were added to extract the α-tocopherol from the chitosan. The suspension in the tube was stirred by vortex for 2 minutes (Vortex Stirrer mod. 714, Riccardo Passoni, Milano, Italy); subsequently was centrifuged for 10 minutes at 3000 rpm (ALC 4218 centrifuge, ALC International, Cologno Monzese, Milan, Italy) and re-assayed by HPLC to assess the percentage of α-tocopherol residue.

Optimization of spray dried powders preparation

The nanoemulsion obtained by solvent evaporation presents a concentration in the range of about 300 and 400 µg/ml.

A preliminary assessment of the condition of spraying drying was carried out using 4 samples with mannitol alone to verify the influence of the aspiration rate and the inlet rate on the yield, in accordance with a full factorial design (2^2). The parameters of the protocol used are summarized in Tab. 4. Furthermore, the inlet temperature for spray drying the NE was 150°C (Li X. et al. 2011). The nozzle (∅ 0.7mm) pressure was fixed at 600L/h as suggested in the manufacturing instruction of the instrument (Buchi B-191 mini spay-drier, Cornaredo, Milano, Italy).

DoE Parameters	
Inlet rates (ml/min)	Aspiration rates (m^3/h)
1.9	21
3.5	28

Tab. 4 Parameters used in a preliminary screening of mannitol spray dried powder.

Preliminary experiments showed that a 46% yield powder, using mannitol (90% respect the total of solid present in the emulsion) as bulk agent, could be considered a good target. The system

preserves 87% ± 3 (measured by HPLC) of α-tocopherol loaded in nanoemulsions and the antioxidant activity of the powder was confirmed by DPPH• assay.

The concentrated by means of ultrafiltration allow the spray drying of nanoemulsion without mannitol or with low mannitol percentage. Preliminary trials of atomization alone and with bulk agent at the concentration of 1 mg/ml and 2 mg/ml were carried out.

A similar percentage of α-tocopherol residue and yield of recovered powder were obtained both at α-tocopherol concentrations of 1mg/ml and 2mg ml. Consequently, the concentration chosen for the following experiments was 1mg/ml.

A screening study of the condition of atomization was carried out using 4 samples to investigate the influence of the aspiration rate and the inlet rate on the yield of powder and the percentage of antioxidant residue, in accordance with a full factorial design (2^2). The parameters of the protocol used are summarized in Tab. 5. Lower (-1) and higher (1) values were established to assess the design of experiment. The central point (0) represents the mean value and was repeated 2 times.

The inlet temperature for spray drying the nanoemulsions was 150°C (Xiang Li et al., 2011) and the nozzle pressure was fixed at 600 L/h. The response variables were yield of powder and percentage of α-tocopherol residue.

Inlet rate (ml/min)		Aspiration rate (m^3/h)	
-1	1.9	-1	21
1	3.5	-1	21
-1	1.9	1	28
1	3.5	1	28
0	2.7	0	24.5

Tab. 5 Inlet rate and aspiration levels of spy-dried nanoemulsion chosen for the screening of the atomization condition.

Scanning Electron Microscopy (SEM)

Scanning electron microscopy (SEM) analysis was carried out using a scanning electron microscope Zeiss, model EVOMA10 (CarlZeiss, Oberkochen, Germany). The samples were made conductive by the deposition of a gold layer in vacuum vapor phase.

Release study

A release study of α-tocopherol from powder was carried out by means of Franz vertical diffusion cells (Permeagear, Inc., Hellertown PA, USA) (Fig. 17). A cellulose acetate membrane (0.45µm, Sartorius Stedim Biotech GmbH, Gottingen, Germany) was employed to separate the donor chamber from the acceptor chamber. On the membrane the samples were placed to evaluate the

release. In the donor compartment 1.5ml of physiological solution (NaCl 0.9% p/v) were added. The temperature was fixed at 32°C as model of skin condition.

In a preliminary phase comparative experiments on different media used in the acceptor compartment of the Franz cells were carried out.

- Ethanol:H_20 20:80
- Ethanol:H_20 20:80 + Tween 80 0.5% (v/v)
- Ethanol:H_20 40:60
- Ethanol:H_20 40:60 + Tween 80 0.5% (v/v)
- Ethanol:H_20 60:40
- Ethanol:H_20 60:40 + Tween 80 0.5% (v/v)
- Absolute ethanol
- Isopropyl myristate

Three Franz cells were prepared for each experiment, and the samples were taken at 1, 2, 3, 4, 5, 20 hours. A known volume of the receiving phase (500 µl) was withdrawn at certain times by a Hamilton micro syringe and the collected volume was replaced with an equal amount of receiving phase. The samples were subjected to HPLC analysis, as previously described, for the determination of the amount of α-tocopherol released. (Rozman B. et al., 2009; Pereira G.G. et al., 2014; Proniuk S. et al., 1998; Garcıa P. et al., 2013)

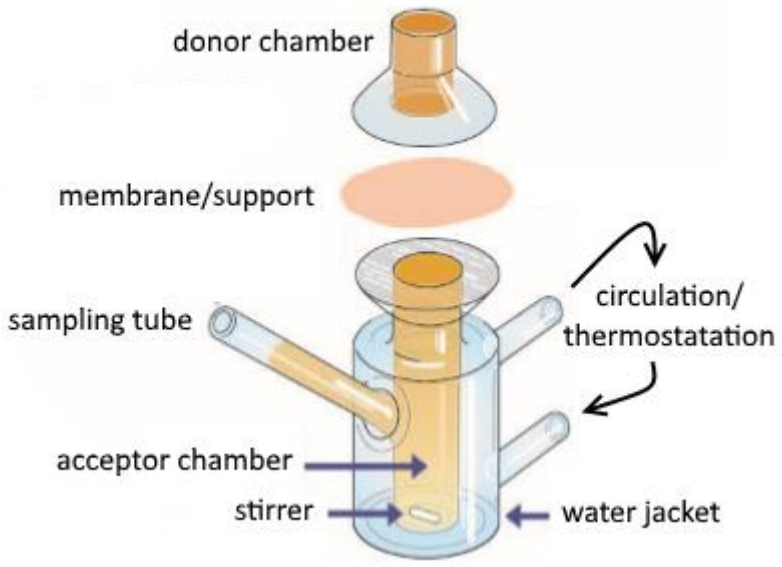

Fig. 17 Franz vertical diffusion cell. (adapted from Permeagear Inc. http://permegear.com/wp-content/uploads/2015/08/primer.pdf)

Resuspension of powders

The spray dried powders were dispersed in aqueous media (PBS) under magnetic stirring at room temperature and the dimension of the particles redispersed were measured by Photon Correlation Spectroscopy.

Powder stability study

10 mg of the powder stored at room temperature, in dry a vessel, were placed in a tube and dissolved in 250µl of acetate buffer pH=4, to solubilize the mannitol, then 1.250ml of acetonitrile were added to extract the α-tocopherol from the chitosan. The suspension in the tube was stirred by vortex for 2 minutes (Vortex Stirrer mod. 714, Riccardo Passoni, Milano, Italy); subsequently was centrifuged for 10 minutes at 3000 rpm (ALC 4218 centrifuge, ALC International, Cologno Monzese, Milan, Italy) and re-assayed by HPLC (as previously described) to assess the percentage of α-tocopherol residue. The test was carried out after 30 days and 60 days on 2 different samples (2 repetition for each ones).

Statistical analysis

Statistical evaluations of the Central Composite design used to optimize the spray drying process were performed by means of Stat Graphics 5.0, Statistical Graphics Corporation, MD, USA. Differences were determined according to One-way ANOVA or by means of a multifactor ANOVA. Differences were considered significant at $p < 0.05$.

3.3.3 RESULTS

3.3.3.1 Characterization of nanoemulsions

The results of the dimensional characterization of nanoemulsions are reported in Tab. 6. Immediately after preparation, the dimensions were less than 300 nm, both at 30° and at 90° of detection angles. The determination of the size at 30° is more sensitive to the presence of larger particles, and the proximity of the values obtained at the two angles agrees, in this case, with the very low values of PI, to indicate monodisperse samples. This result is confirmed 24 hours after the preparation, both at room temperature (25°C) and in the fridge (4°C), indicating good physical stability of the system.

	T0		**T24h (25°C)**		**T24h (4°C)**	
Angle	*Diameter (nm)*	*P.I.*	*Diameter (nm)*	*P.I.*	*Diameter (nm)*	*P.I.*
30°	247 (±34)	0.32 (± 0.11)	343 (±52.75)	0.34 (±0.01)	323 (±97)	0.38 (±0.11)
90°	241 (±50)	0.14 (±0,01)	268 (±27.44)	0.14 (± 0.06)	326 (±27)	0.27 (±0.06)

Tab. 6 Diameter of nanoemulsion measured by PCS at different diffraction angles (30° and 90°). The analysis was conducted immediately after preparation (T0) and after 24h in different storage condition (25°C and 4°C).

Nanoemulsion concentration of α-tocopherol

The dosage of α-tocopherol loaded in nanoemulsions was carried out by direct injection of nanoemulsions in the HPLC column, previously dissolved in an appropriate mobile phase. The direct solubilization in the mobile phase is faster and reliable. The amount of α-tocopherol in different nanoemulsion batches was quantified and a value of association efficiency (± SD, n = 3) of 93.64 ± 7.97% resulted, corresponding to a loading of 25.79 ± 2.17%.

ζ Potential

The measurement of the ζ potential showed a high and positive value, +56.8 mV, in agreement with the cationic character of the polymer used for the preparation of the NE. This number suggests a higher system stability and good dispersion of the particles that do not aggregate and therefore do not undergo coagulation and flocculation. This is in agreement with the results obtained from the dimensional analysis.

Nanoemulsions stability study

Fig. 18 represents the variations in time of the concentration of α-tocopherol in nanoemulsions, considering 100% the initial value of 371 µg/ml., The test was continued up to about one month of storage at room temperature (25°C) and in the fridge at 4°C. Considering the instability of the

molecule known in the literature (Liang L, et al. 2011), the decrease is conceivably due to the α-tocopherol oxidation, and it is in agreement with the literature data for encapsulated α-tocopherol, while much quicker degradation is described for the free molecule. As expected, the decrease is more pronounced in the sample maintained at room temperature with respect to sample stored in the fridge.

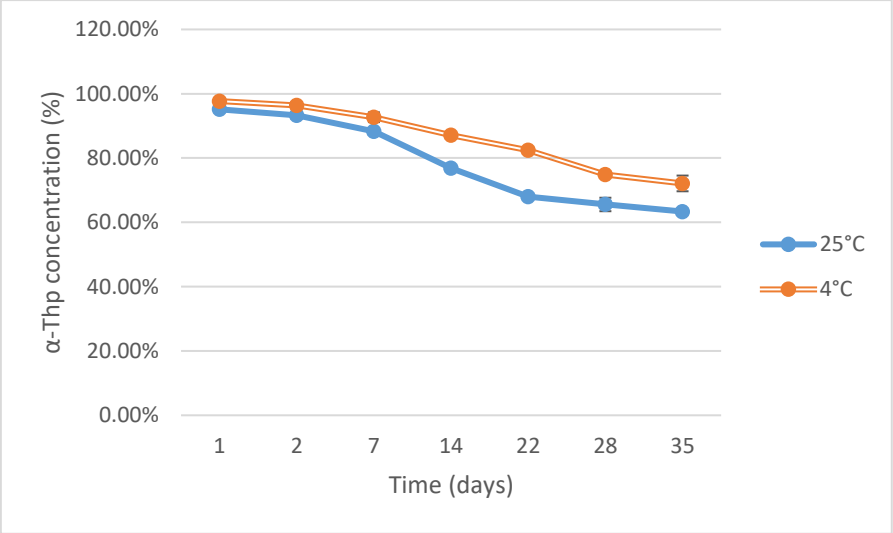

Fig. 18 Percentage of αTph residual in nanoemulsion dispersions during storage time at 25 °C and at 4°C.

DPPH radical assay

The antioxidant activity *in vitro* on free α-tocopherol was evaluated, using samples in a concentration of 3.7 µ/ml, and loaded in nanoemulsions at the same concentration and in a halved concentration (1.86 µg/ml).

As shown in Fig. 19, the antioxidant activity is fully preserved even for loaded α-tocopherol, and it is noticeable a relationship between the concentration of the loaded antioxidant and its activities, as expected. The activity of the unloaded nanoemulsions is significant lower than the loaded system. The unloaded chitosan oleate does not show antioxidant activity.

Nevertheless, the activity of the antioxidant in NE reach a plateau in about 30 minutes while free antioxidant activity arises faster and reach a plateau in about 10 minutes; this is probably due to a slow release from the nano-systems.

In Fig. 20 the different kinetics behavior of free antioxidant and NE loaded are compared plotting the mean (±sem) absorbance values obtained during the experiments at different times.

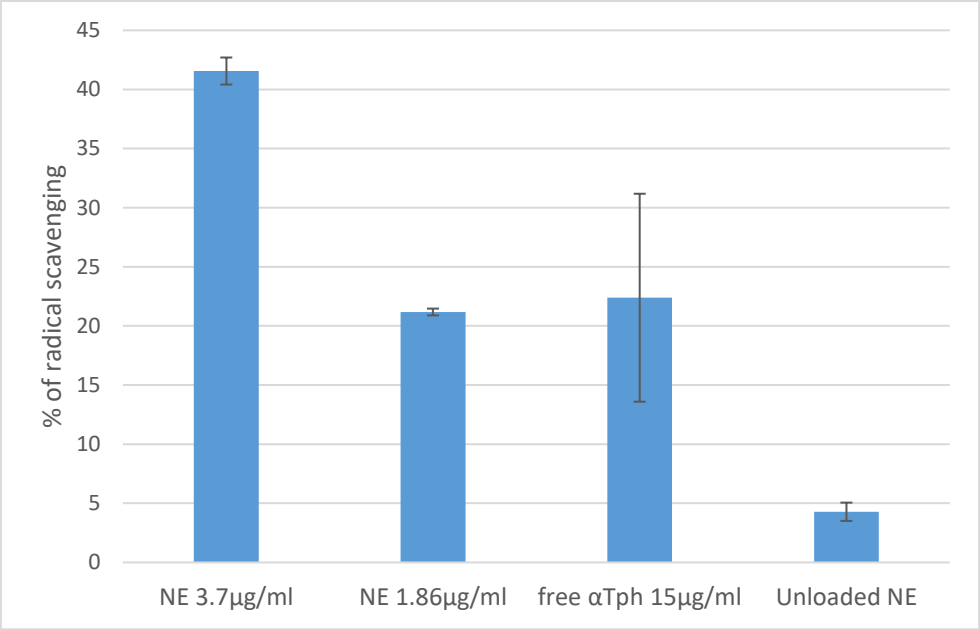

Fig. 19 Comparison among radical scavenging ability (%) of free α-tocopherol, α-tocopherol loaded NE and unloaded NE.

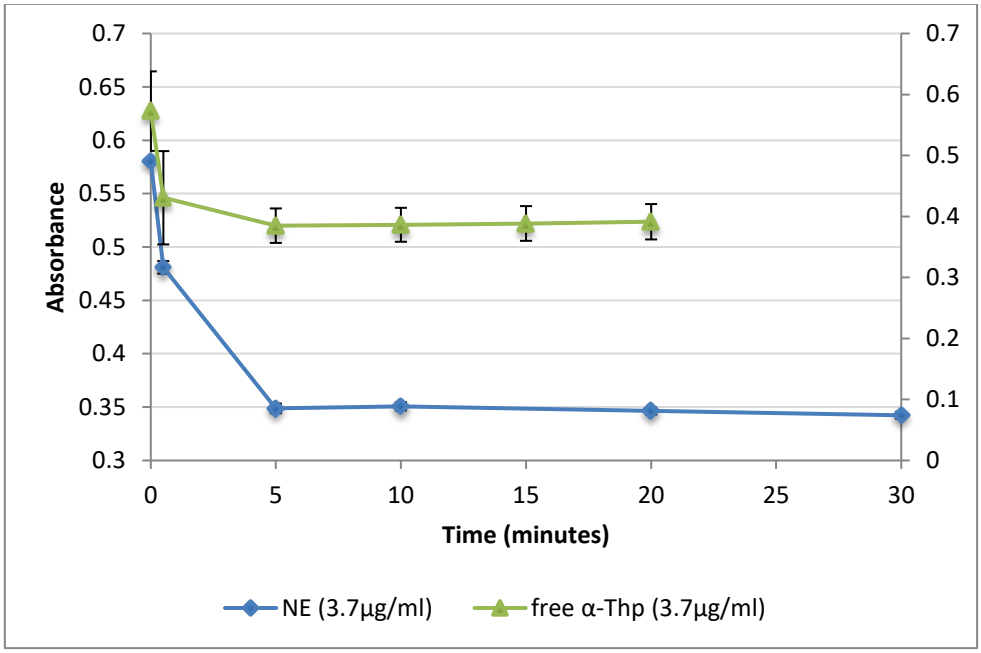

Fig. 20 Comparison of kinetics behaviors of free α-α-tocopherol and NE loaded with antioxidant. The free antioxidant reached a plateau in few minutes whereas the NE seem to release the antioxidant slowly

3.3.3.2 Biological evaluation of nanoemulsions

In vitro test on fibroblasts

In Fig. 21 is represented the decrease of the fibroblasts cell viability after exposure for 90 minutes at various concentrations of H_2O_2, compared to the viability in complete medium. A significant decrease in cell viability starting from the concentration 1mM was observed.

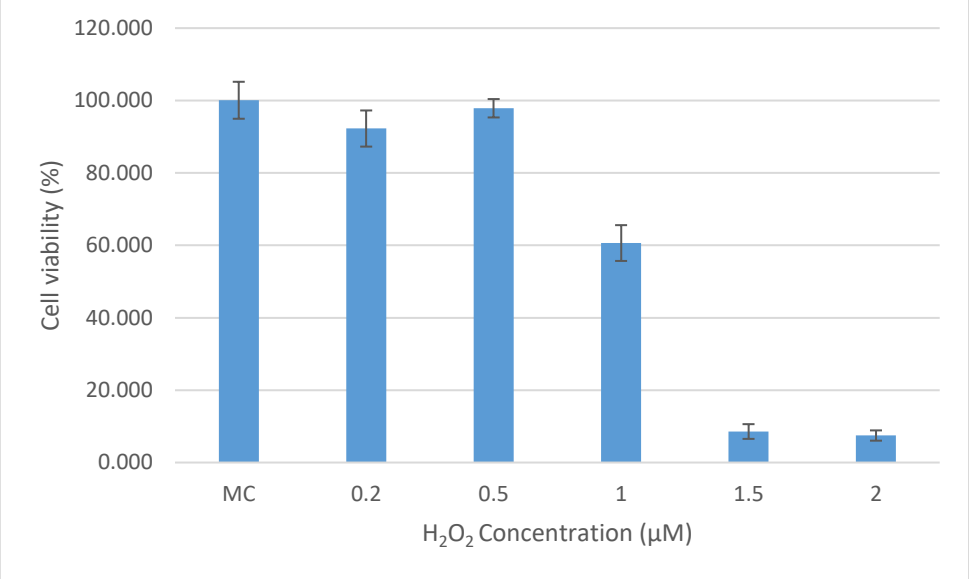

Fig. 21 Viability of the culture of fibroblasts exposed to H_2O_2 for 90 minutes.

It could be observed that the cell resilience after oxidative stress is practically complete after the exposure to 1 mM H_2O_2, regardless of the presence or not of nanoemulsions system. The recovery of the cells following exposure to higher concentrations is slower, as indicated from the controls that reach the vitality of about 50%. However, in these critical conditions the reparative action of the nanoemulsions can be pointed out. The treatments induce a global faster recovery of viability independently on the presence of the antioxidant. The antioxidant activity seems not any more relevant after the oxidative damage was completed, but the proliferative effects of the NE were probably responsible for the cell vitality improvement observed in comparison with the controls (Fig. 22).

Statistically significant differences can be observed among samples exposed to H_2O_2 (1.5mM and 2mM) and samples treated with different amount of α-tocopherol (student t-test unpaired, n=8, p value 0.05); differences were observed in particular between treatments with 5µM, 10µM and 20µM of NE both loaded and unloaded with antioxidant after exposure to H_2O_2 at concentration of 1.5mM with respect to their controls (as shown in Fig. 22); furthermore significant differences were observed between treatment with 5µM and 10µM of NE both loaded and unloaded with antioxidant after exposure to a concentration of 2mM of H_2O_2 with respect to their controls. No statistically significant different can be observed for treatment after exposure to H_2O_2 at concentration of 1mM.

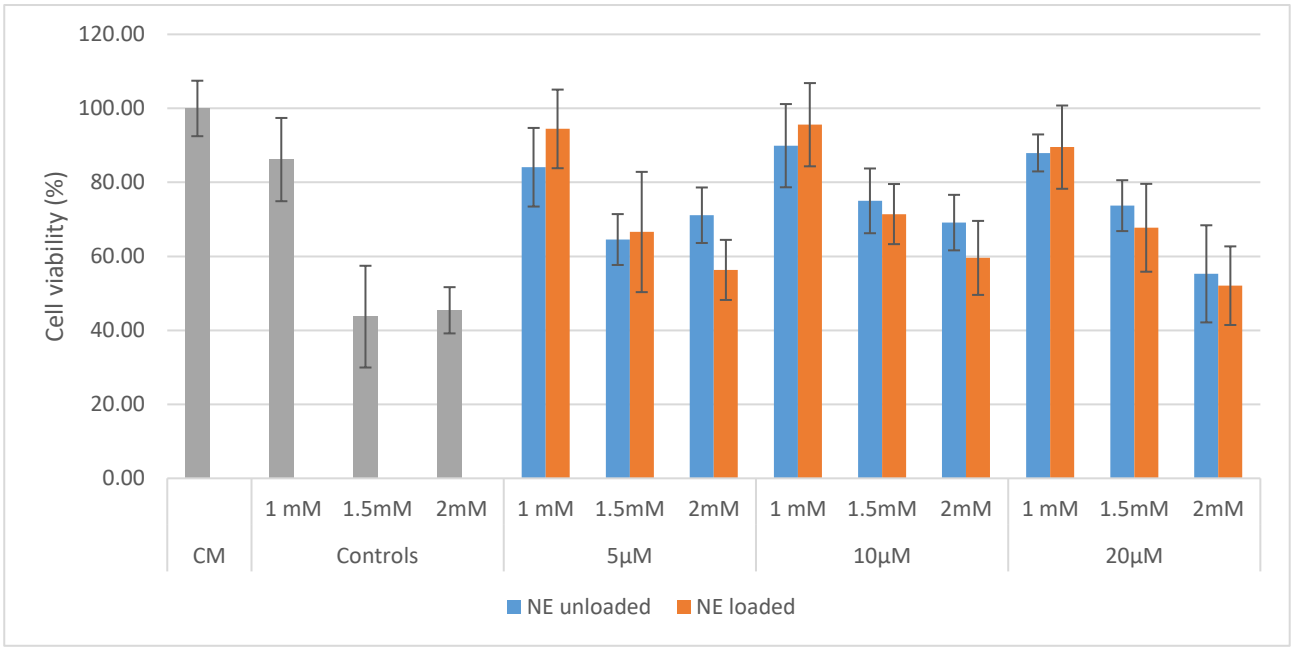

Fig. 22 Comparison among fibroblast cultures exposed to increasing concentration of H_2O_2 (1mM, 1.5mM and 2mM) treated with increasing concentration of nanoemulsions (NE) both unloaded and loaded with α-tocopherol (5µM, 10µM and 20µM), vs. controls.

In vitro test on keratinocytes

Both unloaded chitosan oleate and α-tocopherol loaded nanoemulsion were placed in contact with human keratinocytes cell cultures, that represent an important epithelial cell component damaged during skin injury, to evaluate the effect of the nano-systems in their proliferation.

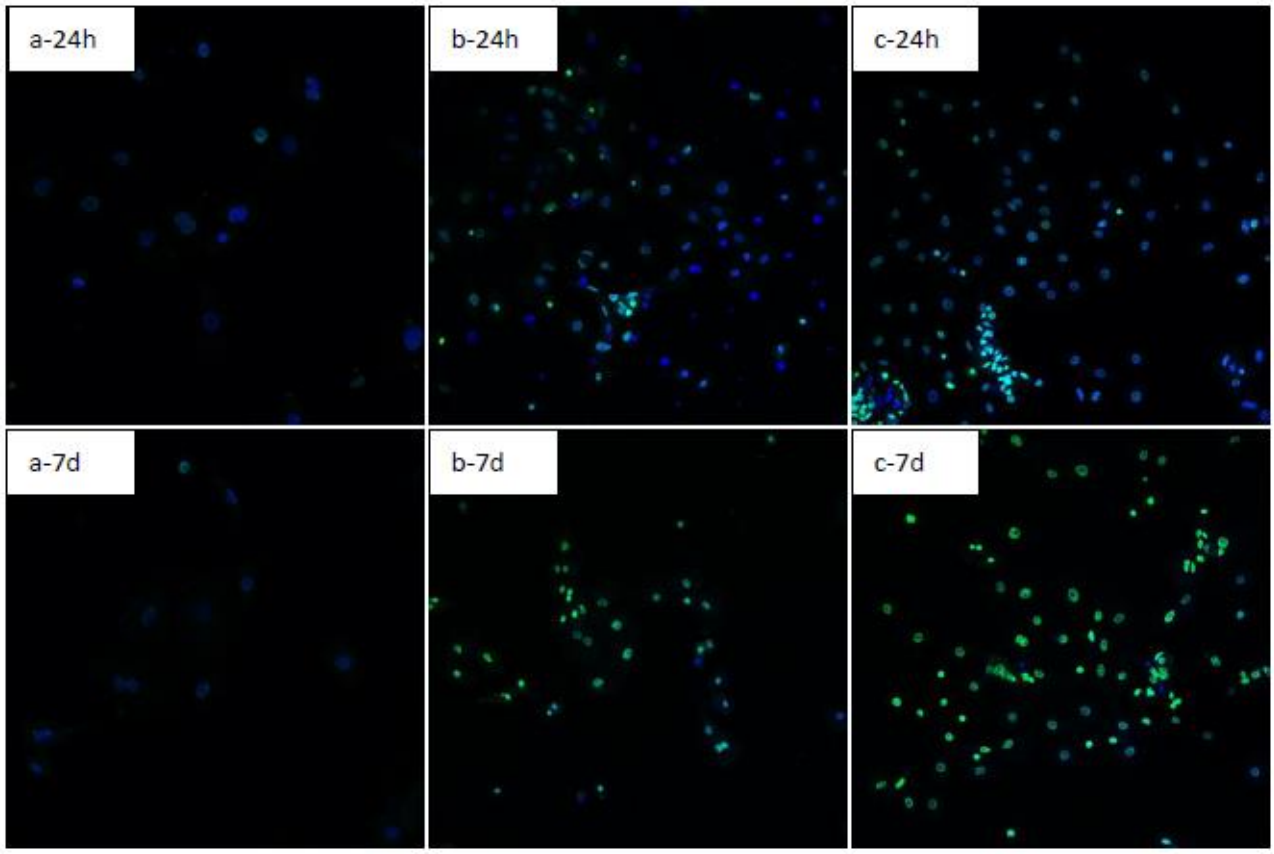

Fig. 23 CLSM microphotographs of keratinocytes at 24 h and at 7 days untreated (a) and after contact with CS-OA (b) and with αTph nanoemulsion (c). Green nuclear fluorescence (FITC): BrdU positive cells in proliferation. Blue nuclei (Hoechst 33258): total population of cells. [merge of fluorescences]

Fig. 23 shows the photomicrographs obtained at Confocal laser scanning microscope (CLSM Leica TCS SP5II, Leica Microsystems, Milan, Italy) for the cells after 24 hours (a24, b24, c24), and for the cells after 7 days of incubation (a7d, b7d, c7d, with the unloaded nanoemulsions (a) and with the NE loaded with antioxidant (c). The controls are illustrated in sections a-24h and a-7d, for the two times. A high percentage of cells positive for nuclear staining with bromodeoxyuridine (BrdU), green in relation to the total number of cells recognizable by blue nuclei, can be appreciated for the two samples compared to controls (a). The capability of nanoemulsions samples to stimulate cell proliferation is evident

In Figure 24 the ratios obtained by counting the BrdU labeled positive cells as percentage of the total cells counted at 24 h and 7 days were quantified for samples and controls. α-tocopherol nanoemulsions seem to be able to stimulate the proliferation of keratinocytes, quickly reaching a plateau of proliferating cells after 24 h. In addition, unloaded nanoemulsions shows a significant, but

slower, ability to stimulate cell proliferation. The proliferative activity in this case could be attributed to chitosan but also to oleic acid, which have been reported in the literature as active compounds in wound healing (Muzzarelli, R.A.A., 2009; Cardoso, C.R., at el., 2011).

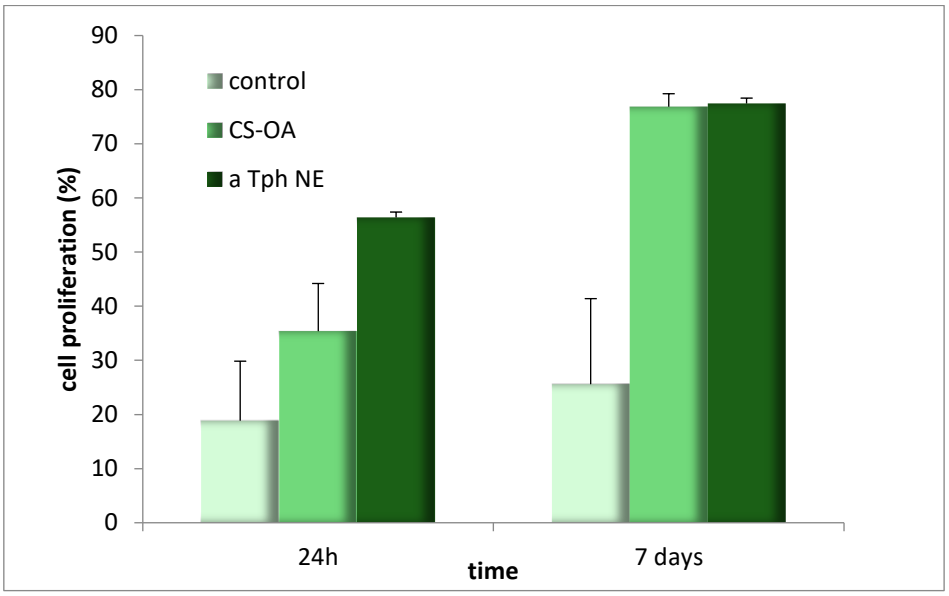

Fig. 24 Ratios of the proliferating/total cells (%) after 24 h and 7 days for control and cells treated with CS-OA and with αTph nanoemulsion. Statistically significant differences (ANOVA, P<0.05): control vs αTph NE 24 h; CS-OA vs αTph NE 24 h; control vs CS-OA 7 days; control vs αTph NE 7 days.

Ex-vivo test on human skin biopsies

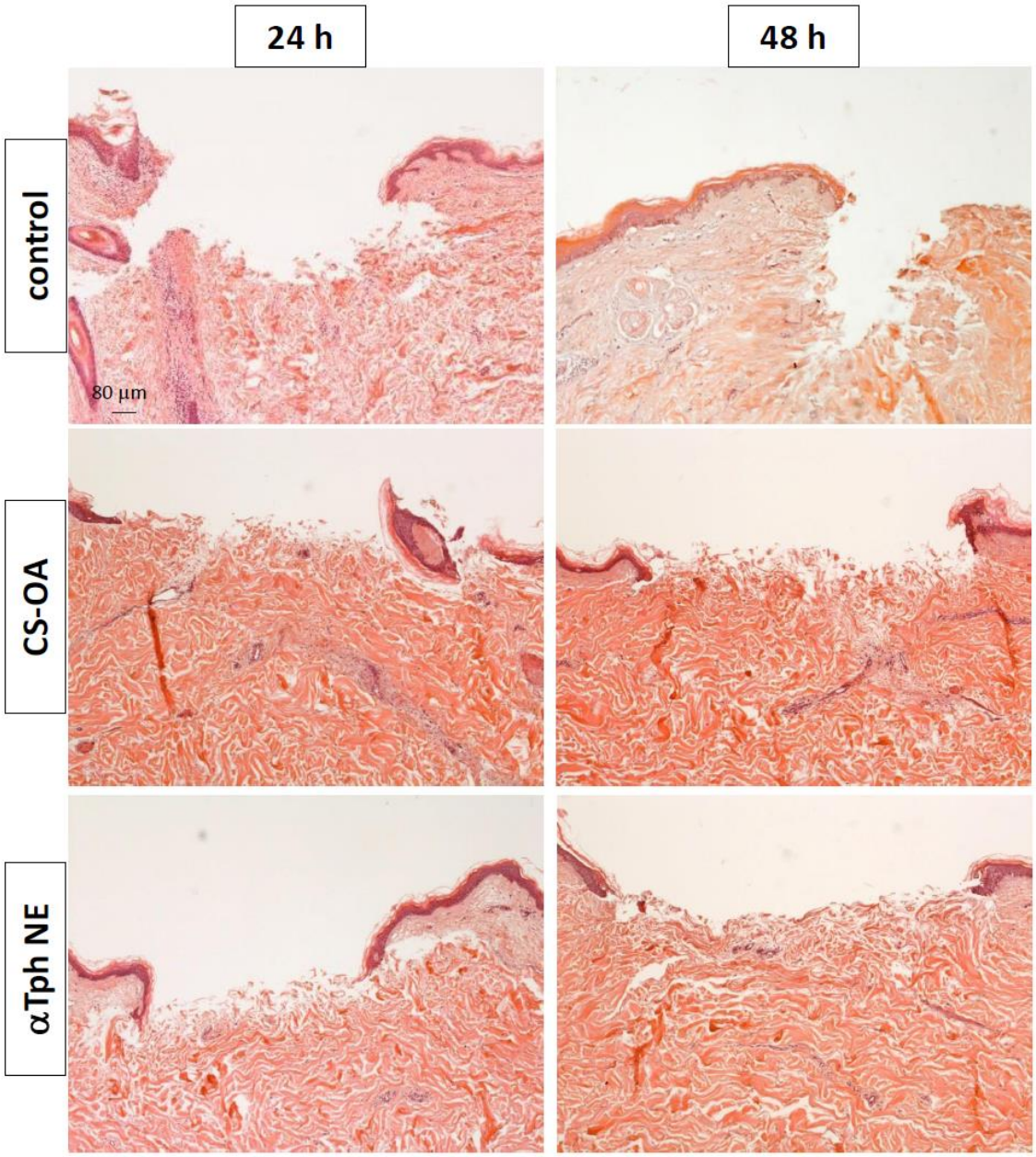

Fig. 25 Microscope images (5x) of histological sections of ex vivo cultured human skin biopsies untreated (controls) and treated for 24 h (on the left) and 48 h (on the right) with unloaded CS-OA and with αTph NE. Hematoxylin-eosin staining.

In Fig. 25, the histological images of human skin fragments excised by 3mm biopsy punch after 24 hours and 48 hours of incubation in vitro, treated with nanoemulsions either loaded of antioxidant and unloaded and stained with Hematoxylin-eosin are shown.

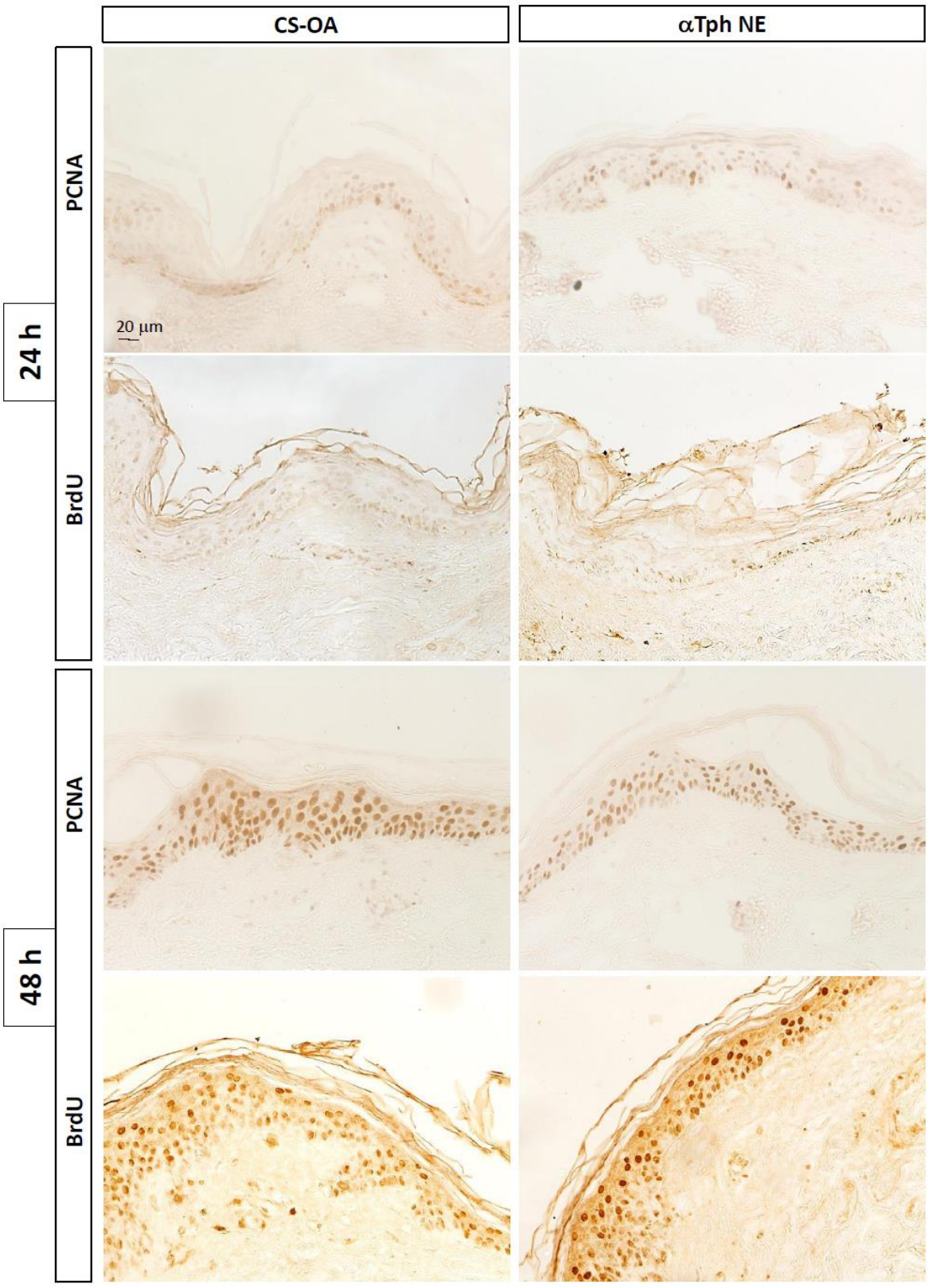

Fig. 26 Microscope images (20x) of histological sections of ex vivo cultured human skin biopsies treated for 24 h (upper part) and 48 h (lower part) with unloaded CS-OA (on the left) and with αTph NE (on the right). Immuno-staining performed with PCNA and with BrdU antigen.

The morphological analysis of hematoxylin and eosin stained histological sections shows a greater eosinophilia (pink/orange coloration associated with the collagen fibers) of the dermis in correspondence with the lesion created by punch in the sample treated for 24 hours with antioxidant loaded nanoemulsions, with respect to the sample treated with unloaded nanoemulsions. After 48 hours, an equilibrium seems to be reached, with increased acidophilia also in the skin treated with unloaded chitosan oleate. It is possible to assume that the antioxidant loaded nanoemulsions after 24 hours already activate the skin regeneration processes, stimulating the reorganization mechanisms of collagen fibers and the activation of protein synthesis by fibroblasts involved in the production of the extracellular matrix constituents, which give the intense coloration already at 24 hours after the treatment. In longer treatments, a similar effect was achieved with unloaded nanoemulsions.

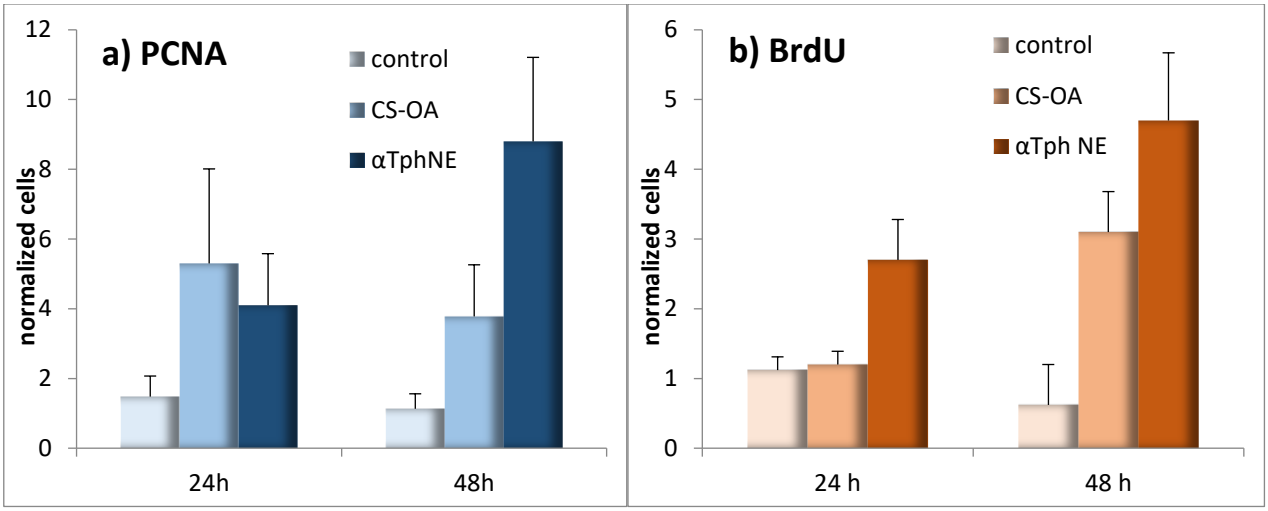

Fig. 27 Number of cells positive to PCNA (a) and to BrdU (b) staining counted per each microscope field, normalized per area (mean±sd) after 24h and 48h in controls and after treatment with unloaded CS-OA and with αTph NE.

Fig. 26 shows the skin section samples after 24 and 48 hours of contact with chitosan oleate and with the loaded nanoemulsion stained with the nuclear antigen of cellular proliferation PCNA and with BrdU.

In Fig. 27a and 27b are reported the quantification of the cells in proliferation for PCNA and BrdU immunostaining respectively, corresponding to images of Figure 26. Data are reported as mean and standard deviation of the counts performed on different sections. Both patterns (PCNA and BrdU) reveal an increase in cell proliferation both at 24 and 48 hours in the skin treated with loaded nanoemulsions. In the case of the biopsies treated with unloaded chitosan oleate, a greater increase in cell proliferation is seen at 48 hours and seems less evident at early time.

In vivo test on murine model

Histological analysis

The results of the histological analysis (Hematoxylin-eosin) performed on the rat wounds after 7 days of treatment with nanoemulsions loaded with α-tocopherol and with physiological solution (control) are shown in Fig. 28 and 29 respectively.

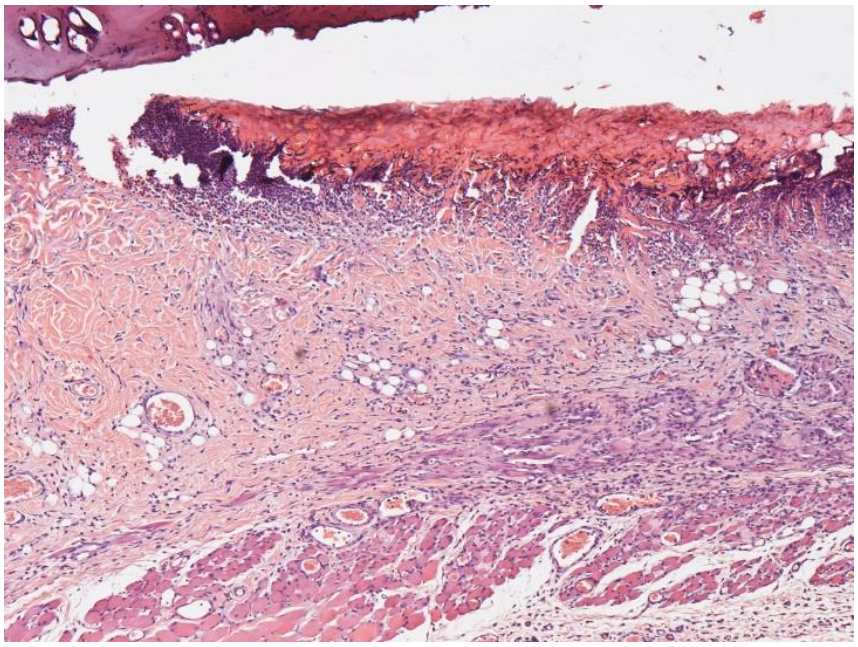

Fig. 28 Histological micrograph (20x) of tissue withdrawal after 7 days of treatment with NE loaded with α-tocopherol.

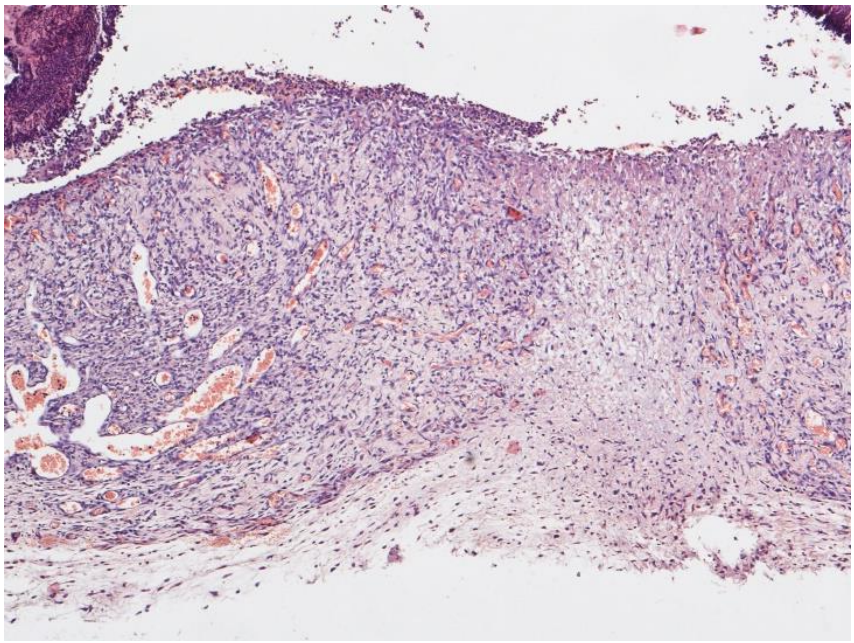

Fig. 29 Histological micrograph (20x) of tissue withdrawal after 7 days of treatment with physiological solution (control).

In the tissues treated with saline solution (Fig. 29) the epidermal layer was not yet re-epithelized, necrotic materials is partially detached from the lesions; the dermis is rich in inflammatory cells – in particular basophils nuclei are evident - and blood vessels, some of which appear very dilated. In the case of the tissues treated with α-tocopherol nanoemulsions (Fig. 28) the wound surface is not yet re-epithelized, it is covered of necrotic acidophilus material, while in the area immediately below the infiltrated inflammatory cells - of which basophils nuclei can be appreciated - necrotic acidophilus material is thinner. Many blood vessels are still evident, some of which dilated. Altogether, the presence of inflammatory infiltration in the treated sample compared to the control was considerably reduced.

EPR detection of free radical

The rat wound model involved the production of three 4mm diameter burns and removal of eschar after 24 h. Wounds are therefore characterized by high levels of inflammation and ROS. To confirm this, a preliminary study based on EPR method was performed on the biological material removed after 24 hours. This evaluation showed important peaks, as illustrated in Fig. 30, corresponding to the presence of high levels of ROS, and thus suggesting a microenvironment in the wounds of this "in vivo" rat model comparable/almost overlapping to a chronic wound (Wlaschek M. et al., 2005). In Fig. 31 the basal levels of health skin are given, for comparison purpose.

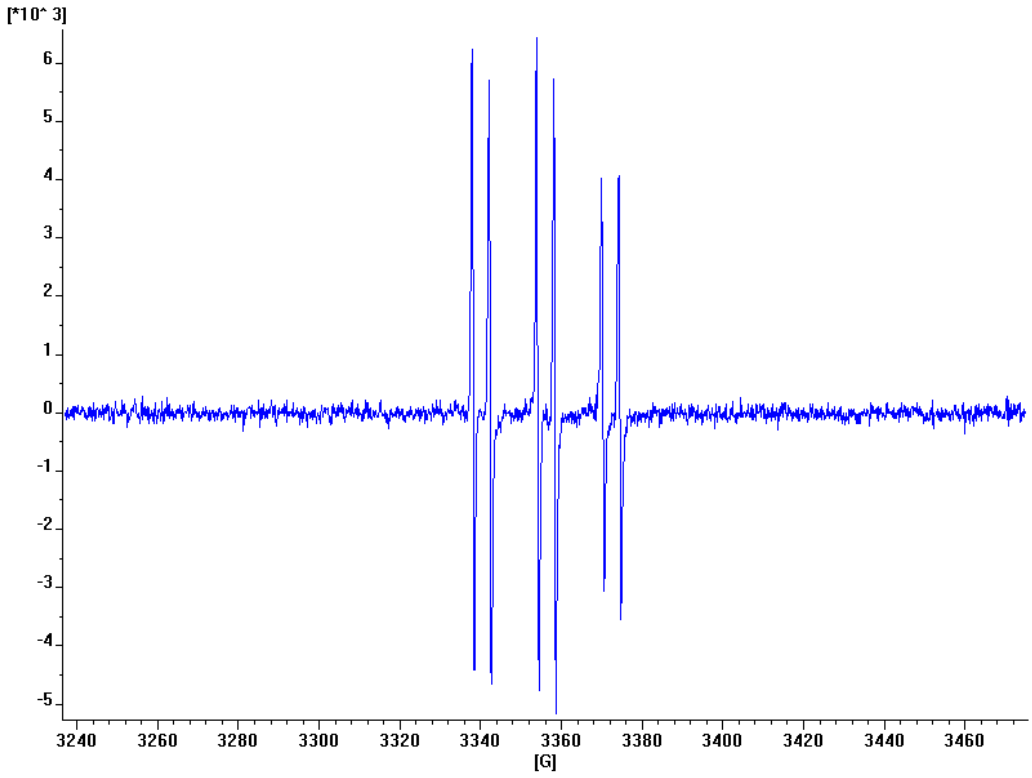

Fig. 30 In vivo sample signals indicating a high presence of ROSs.

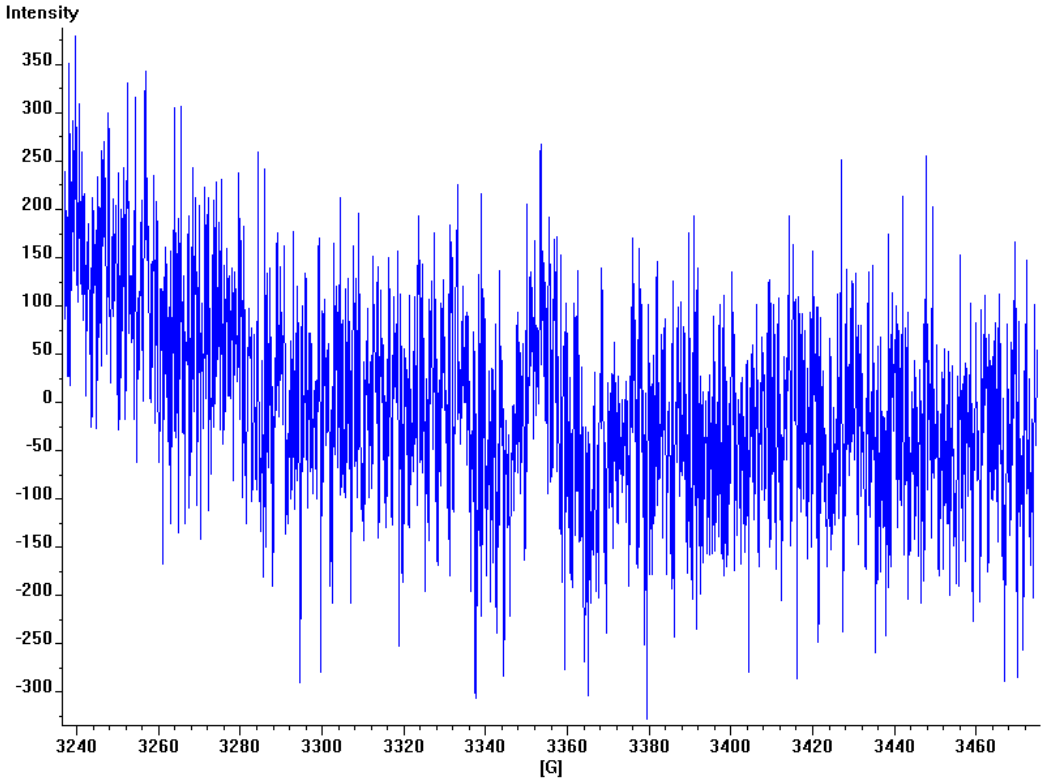

Fig. 31 Blank sample. Value below 200 (Measurable value = background noise)

Lipid peroxidation

Spectrofluorometric evaluations revealed a concentration of peroxided lipids, related to the sample weight, statistically different between healthy and injured rat skin samples. Whenever tissues from treated and untreated skin samples were compared, a statistically difference between α-tocopherol treatment and saline (control) was detected (Anova One-way, p value < 0.05, n=3). Data are reported in Tab. 7. These results are in agreement with the histological data.

SAMPLES	TBAR (nM/mg) MEAN±SD
UNTREATED WOUNDS	1.503 ± 0.152
HEALTHY SKIN	0.074 ± 0.018
NE TREATED WOUNDS	0.143 ± 0.014

Tab. 7 TBARS detected in different rat skin samples; untreated control, healthy skin and skin treated with α-tocopherol NE (mean±sd, n=3).

Section 1b

3.3.3.3 Preparation and characterization of powder

Optimization of spray dried powders preparation

To further stabilize the α-tocopherol, a method to obtain a powder formulation by spray-drying was developed. The aim of this part of the study was a powder formulation intended for topical administration to be applied to injured skin, consequently the product obtained in spray-drying can be advantageously used as an aspersoria powder.

A preliminary evaluation of the atomization conditions was piloted preparing 4 solutions with only mannitol to verify the influence of inlet rate and aspiration on the yield of recovered powder and the percentage of α-tocopherol residue, according to a full factorial design 2^2. The conditions used and the yields of powder (in percentage) obtained are reported in Tab. 8.

DoE		**Aspiration levels (m^3/h)**	
		17.5	28
Inlet rate	1.9	**32%**	**24%**
(ml/min)	3.5	**23%**	**46%**

Tab. 8 Summary of the condition investigated in a preliminary full factorial design to study the yield of the spray dried powder.

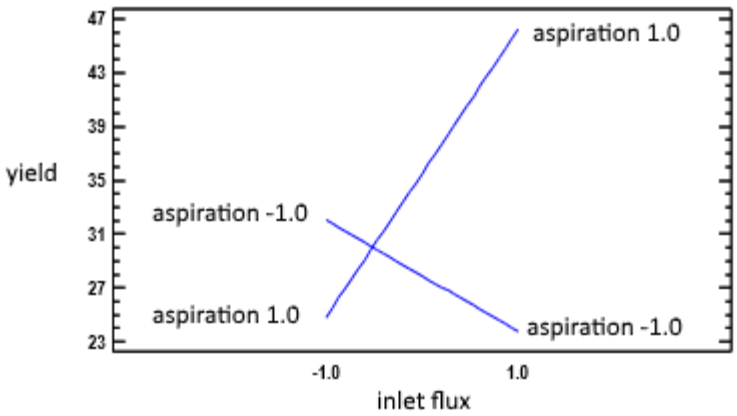

Fig. 32 Interaction plot between the different inlet and aspiration levels and the respective yield of recovered powder.

The graph in Fig 32 shows an increase in the yield of power produced increasing aspiration rate. Based on this preliminary study, a mixture of nanoemulsions loaded with α-tocopherol and mannitol was atomized, obtaining a yield of powder of 51.52%.

The nanoemulsion sample was concentrated by tangential flow about 3 times. The size and the polydispersion index were not changed compared to the original sample, the final concentration of α-tocopherol in emulsion was about 1000 µg/ml, determined by HPLC.

Trials of emulsion were tested by spray-drying, without addition of further bulk (mass forming) excipients. Preliminary results show that, in absence of any bulk agents, a large amount of powder adheres to the glass of atomization chamber with a very low yield (about 10%). To reduce this

negative effect, a 10% of mannitol (respect to the total amount of solids in colloidal dispersion) was then added as bulk agent. A similar percentage of α-tocopherol residue in the powder obtained with both α-tocopherol concentrations used (1mg/ml and 2mg/ml) was observed. The yield of the process was significantly increased, to approximately 17% of total solid mass.

To check the influence of the experimental conditions of the atomization process on the yield of recovered powder and the of concentration α-tocopherol residue, a central composite design was used, with inlet rate and aspiration rate at the levels indicated in Tab. 9.

The choice of atomization parameters, conducted by the experimental design, was carried out in the presence of mannitol 10%.

	Inlet rate (ml/min)		Aspiration rate (m^3/h)		% yield of powder	% of antioxidant residue
1	-1	1.9	-1	21	26.00	67.60
1	1	3.5	-1	21	28.20	74.50
1	-1	1.9	1	28	28.90	85.60
1	1	3.5	1	28	35.70	93.00
1	0	2.7	0	24.5	30.60	95.70
1	0	2.7	0	24.5	30.10	90.10
2	0	2.7	-1.4	19.6	24.98	74.80
2	1,4	3.90	0	24.5	25.70	87.80
2	0	2.7	1.4	29.4	36.70	94.90
2	-1,4	2.15	0	24.5	23.30	75.30

Tab. 9 Summary of parameters (inlet rate and aspiration rate) and response variables (yield of powder and percentage of α-tocopherol residue in powder) of experimental design.

As the results of screening design, the estimated response surface area (Fig 33a) and the corresponding response surface (Fig 33b), indicate an increase in the yield of recovered powder with the increase of aspiration, while inlet seems to induce just a slight curvature of the response values at intermediate levels. This is confirmed by the statistical evaluation, illustrated in the ANOVA table (Tab. 10) showing that only aspiration had a significant effect on the yield,

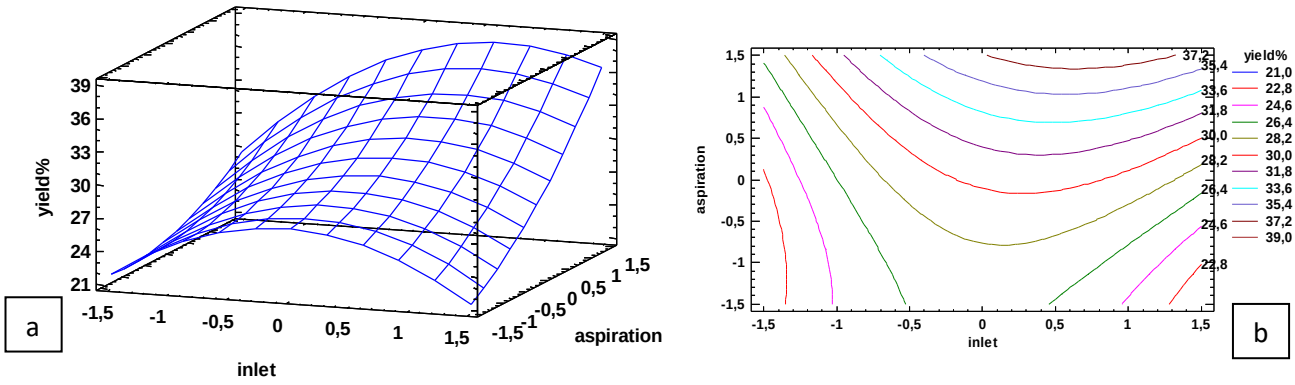

Fig. 33 a: estimated response surface area describes aspiration as the critical parameter for the yield of recovered powder; b: corresponding response surface also describes aspiration as critical parameters.

Source	*Sum of Squares*	*Df*	*Mean Square*	*F-Ratio*	*P-Value*
A:inlet	19.2018	1	19.2018	4.50	0.1011
B:aspiration	90.9535	1	90.9535	21.32	0.0099
AA	26.7167	1	26.7167	6.26	0.0666
AB	5.29	1	5.29	1.24	0.3278
BB	2.58867	1	2.58867	0.61	0.4795
Total error	17.0608	4	4.26521		
Total (corr.)	177.137	9			

Tab. 10 a: Analysis of Variance for yield (%) of recovered powder.

R-squared = 90.3686 percent
R-squared (adjusted for d.f.) = 78.3293 percent

Source	*Sum of Squares*	*Df*	*Mean Square*	*F-Ratio*	*P-Value*
A:inlet	127.821	1	127.821	11.74	0.0266
B:aspiration	526.918	1	526.918	48.39	0.0022
AA	189.079	1	189.079	17.36	0.0141
AB	0.0625	1	0.0625	0.01	0.9432
BB	104.505	1	104.505	9.60	0.0363
Total error	43.5558	4	10.889		
Total (corr.)	910.401	9			

Tab. 10 b: Analysis of Variance for yield (%) of recovered powder.

R-squared = 95.2158 percent
R-squared (adjusted for d.f.) = 89.2354 percent

Considering the concentration of α-tocopherol in the powder, the response surface is illustrated in Fig. 34a, while in figure 34b the isoresponse curves are given. The Anova table (Tab. 11) indicates a significant effect of both inlet and aspiration on this response. The response surface clearly shows a maximum of values corresponding to high aspiration levels and intermediate inlet settings This can be interpreted as a positive effect of quicker removal of the powder from the nebulization chamber. Looking therefore at the isoresponse curves, it is possible to find an interval of optimal parameter combinations that correspond to a maximum of concentration values.

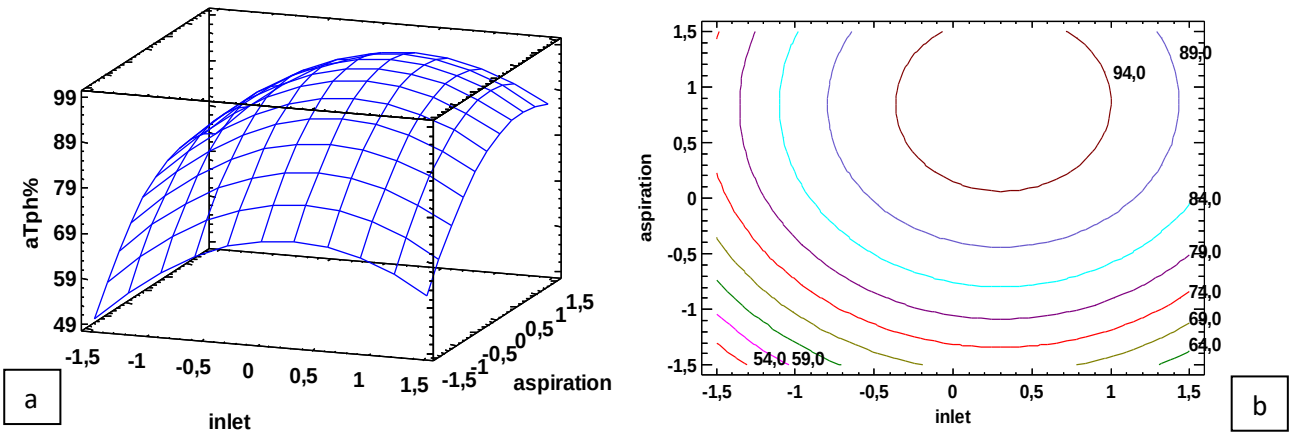

Fig. 34 Response surface (a) and contours plot (b) of the αTph (%) recovery response variable as a function of the spray drying parameters studied according to the central composite design.

Source	*Sum of Squares*	*Df*	*Mean Square*	*F-Ratio*	*P-Value*
A:inlet	19.2018	1	19.2018	4.50	0.1011
B:aspiration	90.9535	1	90.9535	21.32	0.0099
AA	26.7167	1	26.7167	6.26	0.0666
AB	5.29	1	5.29	1.24	0.3278
BB	2.58867	1	2.58867	0.61	0.4795
Total error	17.0608	4	4.26521		
Total (corr.)	177.137	9			

Tab. 11 Analysis of Variance for yield (%) of recovered powder.

R-squared = 90.3686 percent
R-squared (adjusted for d.f.) = 78.3293 percent

By comparing the concentration and the yield curves, high aspiration and intermediate inlet are suggested to obtain the better results in the spray drying process and were therefore chosen to prepare the optimized powder formulation. The aspiration was therefore maintained at the maximum level (70%), with inlet rate at 13%. The microparticle yield resulted in this case 39.7% and the analysis of αTph in the microparticles corresponded to a recovery of 93.3 %, in quite good accordance with the model (about 94% theoretical value) and corresponding to 20.4% of αTph loading in the microparticles.

Scanning Electron Microscopy (SEM)

The SEM micrographs show nanoparticles with a regular spherical shape embedded in a mannitol matrix and aggregate particles with dimensions of about a micron (Fig. 36), probably due to aggregation during the atomization process. The particle size is compatible with a powder intended for skin treatment. However, inside the microparticles, the presence of aggregates of fine round structures compatible with encapsulated α-tocopherol can be envisaged.

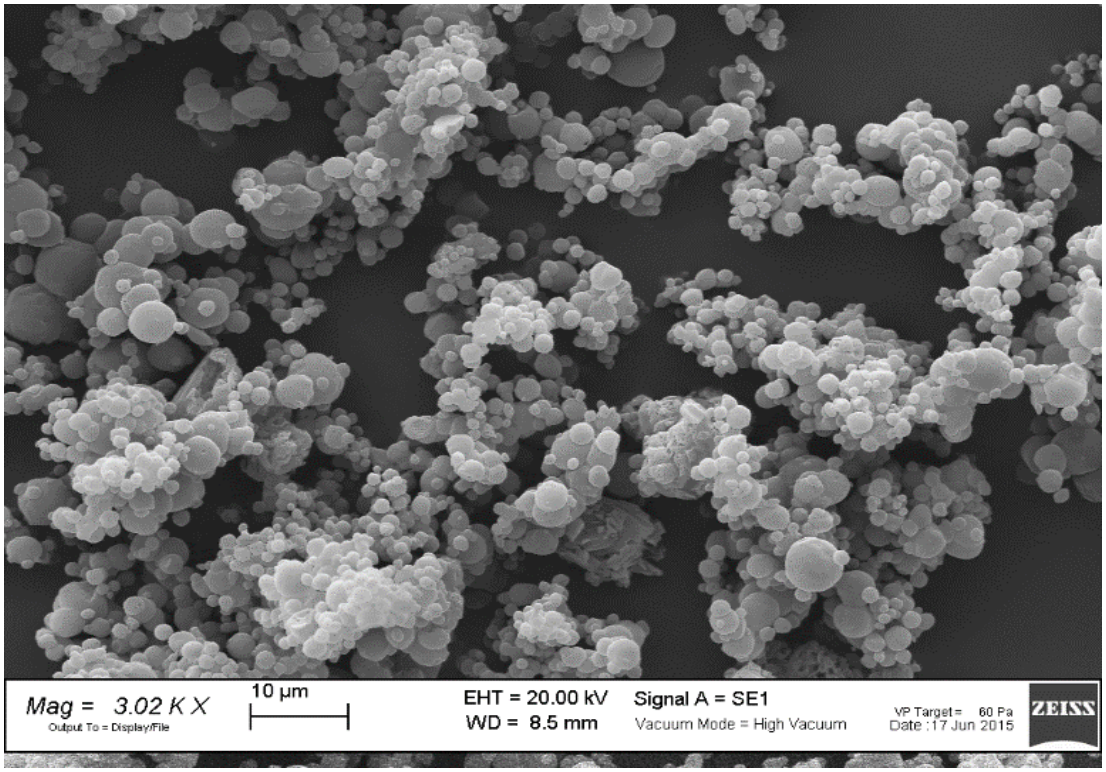

Fig. 35 a SEM micrograph of the powder embedded in a mannitol matrix, with rounded spherical shape and particle size in micrometer range. The nanodroplets seem to aggregate during atomization.

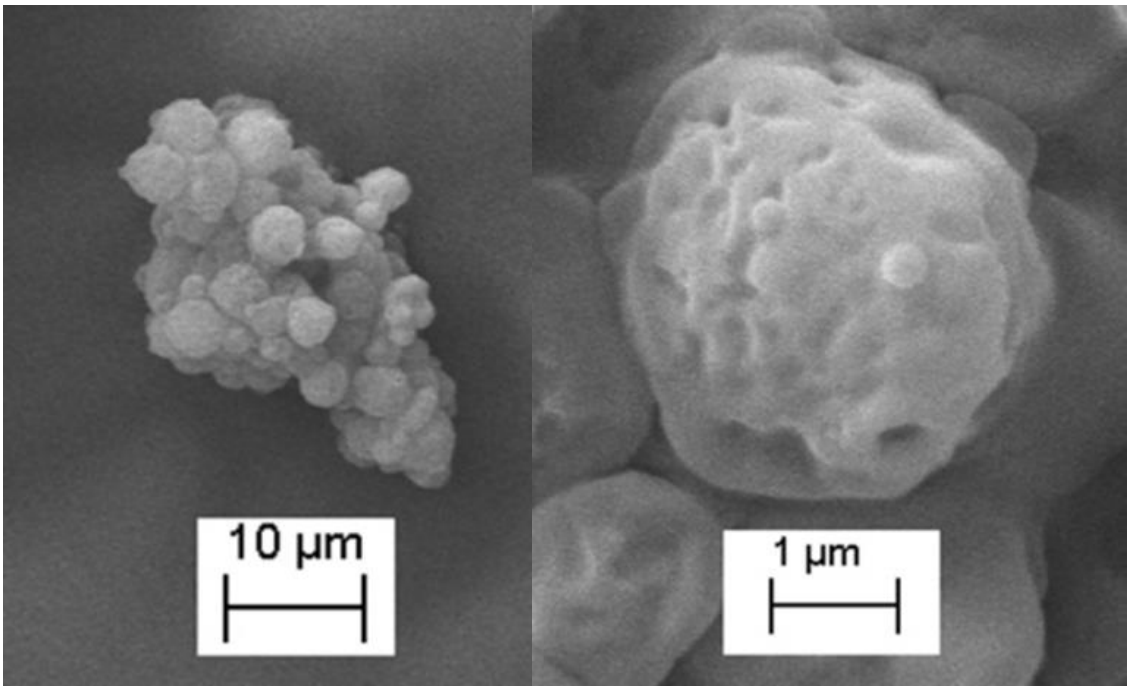

Fig. 35 b SEM micrograph of the powder embedded in a mannitol matrix, with rounded spherical shape and particle size in micrometer range. The nanodroplets seem to aggregate during atomization.

Release study

The development of a reliable release method consisted in a comparative study on different media used in the acceptor compartment of the Franz cells, investigating and modifying methods found in the literature.

Different combination of ethanol and aqueous phase (saline), resulted in non-significant release levels, either in the absence or in the presence of a surfactant in the receiving compartment (0.5% Tween 80), with the exception of ethanol/saline mixture (60:40) in the presence of Tween. In this case a detectable, but incomplete release was reached after 20 hours. Only ethanol allowed complete release of α-tocopherol but was considered unsuitable for its characteristics too far from the physiological conditions.

Isopropyl myristate in some cases proposed in the literature to mimic the skin as receiving phase, was therefore tested as acceptor media for the release test and allowed to obtain complete dissolution of α-tocopherol. In Fig. 36 the release curve of the antioxidant agent from the spray dried powder using isopropyl myristate as acceptor phase is shown.

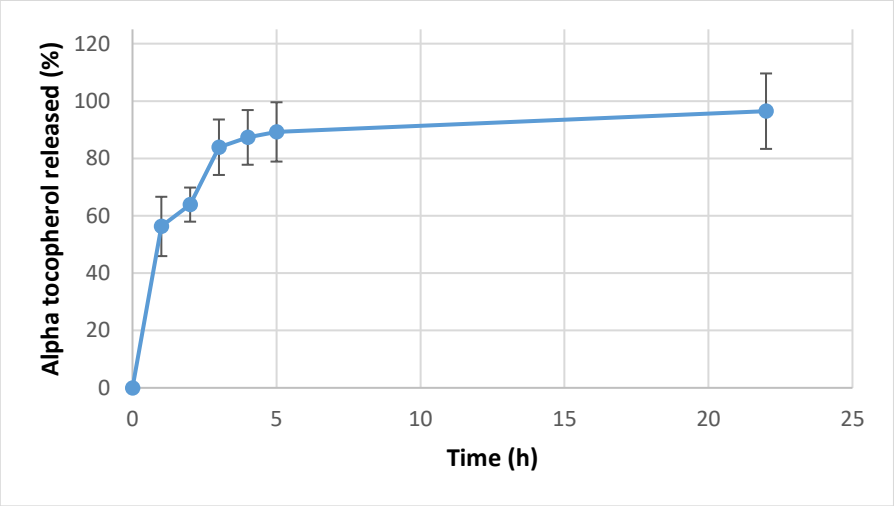

Fig. 36 Release profile of αTph from spray dried microparticles carried out in Franz vertical diffusion cells, using isopropyl myristate in the acceptor chamber.

Powder resuspension

The spray dried powder was resuspended in saline and the particle size was assessed by means of PCS. A certain increase in diameter could be observed, that resulted 862 (±132) nm at 90°, probably due to nanoparticle aggregation process occurring during the atomization process. However, the dimensions remained in the nanometer range and were compatible with a wounded skin treatment.

Powder stability study

The percentage of α-tocopherol residue in the powder was 98%±3 and 92%±5, respectively after 30 days and 60 days, confirming the improved chemical stability of the solid system.

DPPH assay

The powder maintains the radical scavenging activity improving the effectiveness of antioxidant loaded. The result suggests a higher radical scavenging activity with respect to the antioxidant alone (Fig. 37). The reaction reaches a plateau in 20-30 min suggesting a long-lasting effect, probably due to a modulation of the antioxidant release. In Fig. 38 the different kinetic behaviors of free antioxidant and NE powder are compared plotting the mean (±s.e.m.) Absorbance values obtained during the experiments at different times.

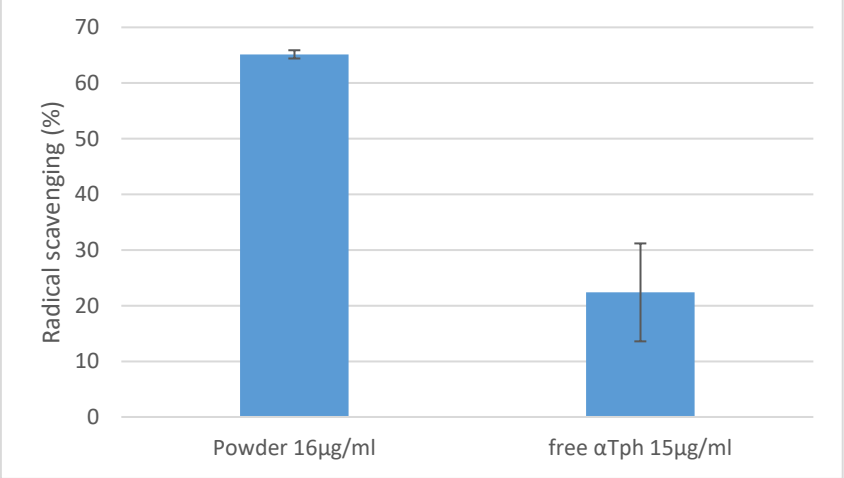

Fig. 37 Comparison between the radical scavenging activity of free α-tocopherol and nanoemulsion loaded with α-tocopherol embedded in powder. The powder exerts a higher radical scavenging activity, more reproducible with respect the antioxidant alone (mean+sd, n=3)

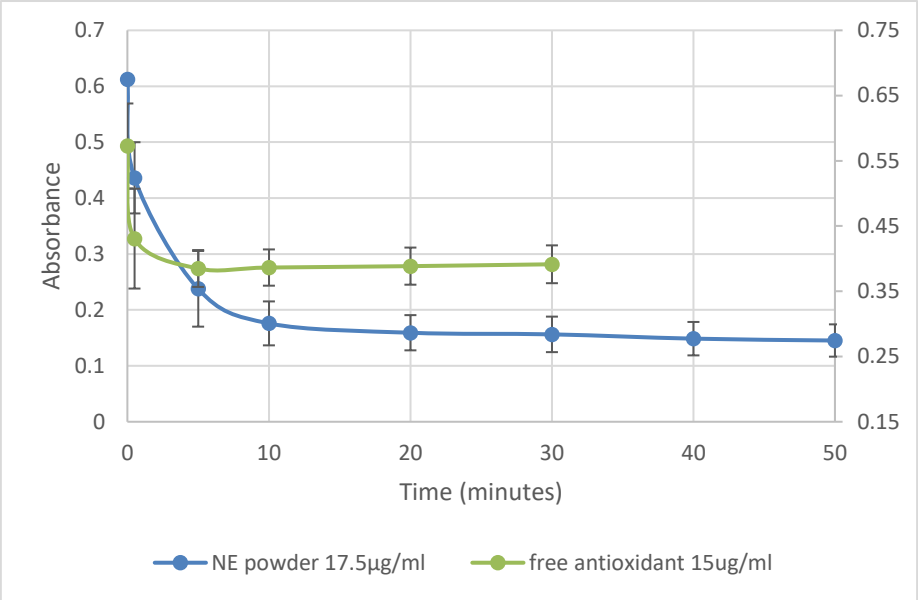

Fig. 38 Comparison between the different kinetic behavior of free α-tocopherol and nanoemulsion loaded with α-tocopherol embedded in powder. Free antioxidant exhausts its radical scavenging ability faster, in few minutes; the powder shows a long-lasting release (mean+sd, n=3)

3.3.4 CONCLUSIONS - SECTION ONE

Nanoemulsions

Nanoemulsions based on hydrophobically-modified chitosan were employed to load a hydrophobic antioxidant such as α-tocopherol. The nanodroplet size range between 200 and 250 nm (P.I. < 0.5). The results confirm a high encapsulation efficiency of α-tocopherol (93.64 ± 7.97%), corresponding to a drug loading of 25.79 ± 2.17%.

In vitro DPPH assay (2,2-diphenyl-1-picrylidrazil radical) demonstrates that the antioxidant loaded nanoemulsions show a more effective radical scavenging and a longer-lasting kinetic profile as compared to the free antioxidant.

The stability study indicates a decrease in antioxidant concentration with 70% of the theoretical concentration of α-tocopherol being found in samples stored at 4°C after 35 days.

Powders

As anticipated, the chemical stability of α-tocopherol could be improved by developing a solid formulation powder prepared by spray-drying. The preparation process, ameliorated by means of an experimental design, led to a yield of about 40% of recovered powder and to a α-tocopherol residual content ranging between 45 and 90%.

The release test, using Franz cell method, demonstrates that the powder releases over 90% α-tocopherol in few hours. The powder also maintains the radical scavenging activity (tested by DPPH assay). Stability tests show about 98% and 92% of antioxidant residual content after 1 and 3 months, respectively.

S.E.M. microphotographs show the presence of microparticles embedded in a mannitol matrix with a rounded spherical shape and a mean diameter in the micrometer range. The increase in dimension with respect to the nanosystem is probably due to nanodrops aggregation during the atomization process and it is confirmed by PCS dimensional analysis. Acceptable resuspendability of nanoparticles is confirmed.

Biological testing

In vitro viability test on fibroblasts shows the reparative actions of NE, independently on the presence of the antioxidant. Nanoemulsions, both unloaded and loaded with antioxidants, are able to stimulate cell proliferation in human keratinocyte cultures. Furthermore, NE, both loaded and unloaded, show a significantly higher ability to improve cell proliferation in the *ex vivo* test on human skin biopsies. In vivo evaluation on murine model showed that the injuries treated with nanoemulsions loaded with α-tocopherol resulted in a lower inflammatory response with respect to the negative control, seven days after the injury.

The overall results are promising for a possible use of the formulations on wounded skin especially if exacerbated by oxidative stress as in the case of diabetic foot ulcers.

Published papers/oral comunications poster presentations related to Section One:

Published papers

"**Alpha tocopherol loaded chitosan oleate nanoemulsions for wound healing. Evaluation on cell lines and ex vivo human biopsies, and stabilization in spray dried Trojan microparticles**."
M.C. Bonferoni, F. Riva, A. Invernizzi, E. Dellera, G. Sandri, S. Rossi, G. Marrubini, G. Bruni, B. Vigani, C. Caramella, F. Ferrari.
European Journal of Pharmaceutics and Biopharmaceutics 2018, 123:31-41.
doi: 10.1016/j.ejpb.2017.11.008.

"**Association of Alpha Tocopherol and Ag Sulfadiazine Chitosan Oleate Nanocarriers in Bioactive Dressings Supporting Platelet Lysate Application to Skin Wounds**."
M.C. Bonferoni, G. Sandri, S. Rossi, E. Dellera, A. Invernizzi, C. Boselli, A. Icaro Cornaglia, C. Del Fante, C. Perotti, B. Vigani, F. Riva, C. Caramella, F. Ferrari.
Marine Drugs 2018, 16(2), 56; doi: 10.3390/md16020056.

Oral communication:
"Nanoemulsion stabilized with chitosan oleate and loaded with antioxidant. Application to wound healing."
Advanced School in Nanomedicine 09/25-28/2017, Dipartimento di Scienze della Vita e dell'Ambiente, University of Cagliari.

Poster presentations:
"Sponge-like formulations for cutaneous ulcers. Evaluation on an in vivo model." 9° Annual Meeting A.It.U.N., Milano, 2015
"Evaluation of sponge-like dressing in a novel murine model of skin ulcer" 55° AFI symposium, Rimini, 2015
"Evaluation of chitosan based sponge-like dressing in a novel murine wound model" ICCC13TH/12TH EUCHIS Munster, Germania, 2015
"Evaluation of compatibility and antioxidant activity of SOD-loaded chitosan nanoparticles on fibroblast cells." ICCC13TH/12TH EUCHIS Munster, Germania, 2015
"Spray-drying process of tocopherol loaded nanoemulsions." 10° Annual Meeting A.It.U.N., Parma, 2016
"Tocopherol nanoemulsion stabilized with chitosan oleate: keratinocyte proliferation and spray drying to cutaneous powder." Congresso Nazionale Biomateriali, Politecnico di Milano, Milano, 2017

“Tocopherol nanoemulsion spray dryed powder intended for skin treatment” ULLA Summer School, Leuven, Belgium, 2017

“Spray-drying process of tocopherol loaded nanoemulsions.” 11° Annual Meeting A.It.U.N., Padova, 2017

“Spray drying to cutaneous powder of tocopherol nanoemulsion stabilized with chitosan oleate” Universidade da Beira Interior, Covilha, Portugal, 2017

4. SECTION TWO

Films and lyophilized dressings for delivery of probiotics or nanoemulsions.

4.1 PREFACE

Films

Based on IUPAC definition film is *"a generic term referring to condensed matter restricted in one dimension. A film which has lateral dimensions above 100μm is a macroscopic film."* (IUPAC, 1997)
Polymeric films have been extensively used to promote the healing of wounds. The film application points to cover the wound with a semipermeable material, avoiding dehydration, infection and protecting the damaged tissue from the environment. (Drago H. et al., 2010)
In solvent casting process polymers are dissolved in water and stirred to obtain a homogenous solution or semisolid (Fig. 39). If appropriate, the mixture is degassed and resulting solution or semisolid is casted on a support. Subsequently, the sample is subjected to evaporation of solvent and collected. (Vishwakarma P.K. et al., 2015)

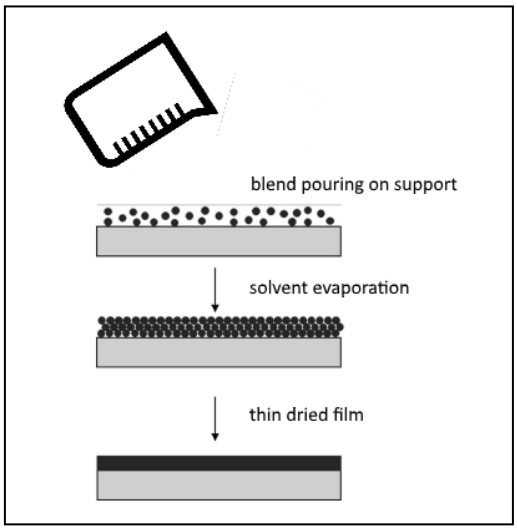

Fig. 39 Schematic representation of film solvent casting. (Adapted from Felton L.A., Int J Pharm. 2013)

Freeze-drying

The colloidal systems are largely used as drug delivery system for small molecules and macromolecules. In these systems a drug is hosted inside a core surrounded by a polymeric membrane. Nanoparticles could be prepared with biodegradable polymers; thus, water can be subtracted in order to improve the chemical and physical stability. Freeze-drying is a largely used and reliable process capable to remove water from different categories of formulations. It consists in a process of removing water from a frozen sample by sublimation under vacuum. Several stresses occur during freeze-drying and so-called cryo-protectants may be added to the solution or colloidal suspension to protect the nanoparticles. (Abdelwahed W. et al., 2006)
Freeze-dried probiotics are a convenient alternative to frozen cultures. The composition of probiotics' aqueous medium during freeze-drying influences their survival during drying and storage.

Polysaccharides are suitable cryoprotectants able to preserve biological material in the dry state. Polysaccharides interact, through hydrogen bond, with membrane phospholipids, protecting cells during dehydration, and cause the transition of water to glassy state, sustaining structural stability of possible nutrients. (Hoobin P. et al.,2013)

Probiotics and prebiotics

Probiotics effects in wound healing were described in Cap. 1.4. Gibson and Roberfroid in 1995, defined prebiotics as *"non-digestible food ingredient that beneficially affects the host by selectively stimulating the growth and/or activity of one or a limited number of bacteria in the colon, and thus improves host health."* [Reprinted from G.R. Gibson, H.M. Probert et al., Dietary modulation of the human colonic microbiota: updating the concept of prebiotics. Nutr Res Rev., 17(2), 259-75 (2004) Cambridge University Press, reproduced with permission.]

A variety of molecules can be prebiotics, but the great majority is dietary fibers. Prebiotics play a key role in the metabolism of the probiotics and comprehend a number of molecules, mainly fibers (e.g. oligosaccharides), especially helpful for maintaining advantageous microenvironment in the colon tract. Among oligosaccharides the most representative prebiotics are inulin, GOS, FOS, SOS, and xylooligosaccharides. Each probiotic species has a preferential prebiotic substrate. Lactobacillus specially use fructans rather than glucose (Gourbeyre P., 2011; Gibson G.R. et al., 2004).

Gums are complex hydrophilic polysaccharides extracted from plants, sea weeds, bacteria, and animal sources. The chemical structure of gums is suitable for gel formation absorbing a large amount of water. Gums are used as stabilizers, improving viscosity and texture, especially in pharmaceutical, cosmetic, paint and adhesive industries. Several polysaccharides present a prebiotics role by promoting growth and viability of probiotics.

According to their source, gums could be classified as:

- gums extract from terrestrial plants (e.g. locust bean, guar, pectin)
- gums extract from aquatic plants (e.g. carrageenan, alginate)
- gums extract from microorganisms (e.g. xanthan, gellan, pullulan)

Gums could favor the survival of probiotics in food and in the gut.

Guar gum (GG) is a galactomannan polysaccharide extracted from *Cyamopsis tetragonolobus* seeds and consists of a 1,4-β-D-mannose backbone and 1,6-α-D-galactose chains. The gelling properties of the polysaccharides are related to the interactions between their hydrophilic groups and water molecules through hydrogen bonds and the conformation of polysaccharide molecular chains.

Xanthan gum (XG) is an anionic polysaccharide produced by Bacterium *Xanthomonas Canpestris* and consists in a β-D-glucose backbone linked to a trisaccharide of mannose, glucuronic acid, and mannose. Xanthan gum presents poor gelling skill and therefore was considered a non-gelling polysaccharide. Thus, it could be used as a viscosity agent due to its high viscosity in water. (Karlton-Senaye B.D. and Ibrahim S.A., 2013; Naoi S. et al., 2002; Takahashi M. et al. 2006)

4.2 SCOPE OF SECTION TWO

Polymers mixture have been employed to obtain suitable film and lyophilized dressing to embed probiotics or nanoemulsion loaded with antioxidant. The pilot formulations have been characterized for rheological and mechanical properties, release profile of probiotics or antioxidants, water absorption capacity, structural integrity and water residue. The compatibility and survival of probiotics in these formulations have been studied and an *in vitro* preliminary test of biocompatibility on human fibroblasts has been carried out. Finally, a polyurethane backing has been developed to cast the polymers mixture loaded with probiotics and/or nanoemulsion to obtain an advanced medication intended for topical application

4.3 EXPERIMENTALS

4.3.1 MATERIALS

- Xanthan gum from *Xanthomona campestris* (Sigma-Aldrich, Milano, Italy)
- Guar gum (Sigma-Aldrich, Milano, Italy)
- Poly (vinyl alcohol) (Sigma-Aldrich, Milano, Italy)
- Glycine (Sigma-Aldrich, Milano, Italy)
- Glycerol (Carlo Erba, Milano, Italy)
- *Lactobacillus plantarum* ATCC:8014
- Acetone HPLC grade (Sigma-Aldrich, Milano, Italy)
- Acetonitrile Cromosolv per HPLC (Sigma-Aldrich, Milano, Italy)
- Glacial acetic acid (Carlo Erba, Milano, Italy)
- Oleic acid (Fluka, Sigma-Aldrich, Milano, Italy)
- Chitosan low molecular weight. mol wt 50,000-190,000 Da, viscosity 20-300 cP, 1 wt. % in 1% acetic acid 25 °C, Brookfield Acetone HPLC grade (Sigma-Aldrich, Milano, Italy)
- Alpha-tocopherol (Fluka, Sigma-Aldrich, Milano, Italy)
- Isopropyl Myristate (Sigma-Aldrich, Milano, Italy)
- Fibroblast (bNHDF) (baby Normal Human Dermal Fibroblast) (Promocell, Milano, Italy)
- Culture medium 10% FBS: Dulbecco's Modified Eagle's Medium (DMEM with glutamine, Sigma-Aldrich, Milano, Italy) addition with FBS 10% v/v (FBS, Foetal Bovine Serum, Euroclone, Milano, Italy), previously free from complement proteins by thermostatic bath at 56°C for 30 minutes, and 1% v/v of a sterile solution of Penicillin, Streptomycin and Amphotericin (Sigma-Aldrich, Milano, Italy)
- PBS: Dulbecco's Phosphate Buffered Saline 10 (sterile filtered, endotoxin tested, without calcium chloride and magnesium chloride) (Sigma-Aldrich, Milano, Italy) diluted 1:10 with distilled sterile water sterile
- MTT: [3- (4,5-dimethyl-2-thiazolyl) -2,5-diphenyl-2H-tetrazolium bromide] (Sigma-Aldrich, Milano, Italy)
- DMSO: dimethyl sulfoxide (Sigma-Aldrich, Milano, Italy)
- 96-well plate: Cellstar tissue culture plate, 96 W, flat bottom, with lid, sterile (Greiner bio-one, Milano, Italy)
- Petri multiwell 12 wells (Costar, Corning, New York, USA)
- Transwell® Permeable Supports System 12-well (Corning Costar, Corning, NY)

4.3.2 METHODS

4.3.2.1 Preparation of polymer solutions/mixtures

Polyvinyl Alcohol (PVA) solutions were prepared at different concentrations (1%, 2%, 5%, 10% w/v) in filtered bidistilled water (0.22 µm acetate cellulose filter, Sartorius Stedim Bioteh GmbH, Gottingen, Germany) under magnetic stirring.

Two guar gum solutions were prepared at 0.25% and 0.50% w/v in filtered bidistilled water under magnetic stirring. The solutions or mixtures were degassed in a centrifuge at 300 rpm for 10 minutes (ALC 4218 centrifuge), in case of bubbles formation during the hydration polymers. Finally, it was kept under stirring until the polymer was fully solubilized.

Six binary mixtures were prepared blending the 5% PVA solution and the two xanthan gum solutions at 0.25% and 0.50% w/v in different ratios (volume) to study their rheological characteristics. The percentages of each of the two mixtures are given in Tab. 12 and 13.

	PVA 5%	XG 0.25%
MIXTURE 1	50	50
MIXTURE 2	73	30
MIXTURE 3	30	70

Tab. 12 Composition (%) of binary mixtures PVA 5%: XG 0.25%

	PVA 5%	XG 0.5%
MIXTURE 4	50	50
MIXTURE 5	73	30
MIXTURE 6	30	70

Tab. 13 Composition (%) of binary mixtures PVA 5%: XG 0.5%

Nine binary mixtures were subsequently prepared using the 5% PVA solution and three xanthan gum solutions at 0.25%, 0.5% and 0.75% w/v. The two polymers were combined in the ratios (volumes) illustrated in Tab. 14 obtaining nine mixtures with the final concentrations of PVA and XG reported in the same table (Pandey S. et al., 2016).

TAB 14	TOTAL POLYMERS CONCENTRATION IN MIXTURES		
	PVA (1.5%)	**PVA (2.5%)**	**PVA (3.5%)**
XG (0.25%)	**α**	**β**	**γ**
	% of polymers on solid 89.6%PVA+10.4%XG	% of polymers on solid 95.2%PVA+4.8%XG	% of polymers on solid 97.9%PVA+2.1%XG
XG (0.50%)	**δ**	**ε**	**ζ**
	% of polymers on solid 81%PVA+19%XG	% of polymers on solid 90.9%PVA+9.1%XG	% of polymers on solid 95.9%PVA+4.1%XG
XG (0.75%)	**η**	**θ**	**ι**
	% of polymers on solid 74%PVA+26%XG	% of polymers on solid 87%PVA+13%XG	% of polymers on solid 94%PVA+6%XG

Tab. 14 Concentrations of polymers, in mixtures and after drying in solid samples, obtained by combination of PVA and XG solutions in different ratios (volumes).

The effect of the total polymer concentration in mixtures and the ratios between PVA and XG on the yield of lyophilized and film was investigated. Based on the previously results, mixtures were obtained in different ratios of PVA and XG (85:15, 75:25, 65:35) and at different total polymers concentrations (0.75%, 1.5%, 3.00% w/v), as exposed in Tab. 15a.

TAB 15 a	TOTAL POLYMERS CONCENTRATION IN MIXTURES		
Polymers ratios	**3%**	**1.5%**	**0.75%**
PVA:XG 85:15	A	D Dil. 1:1	G Dil. 1:4
PVA:XG 75:25	B	E Dil. 1:1	H Dil. 1:4
PVA:XG 65:35	C	F Dil. 1:1	I Dil. 1:4

Tab. 15 a: Composition of PVA:XG mixtures in different ratios and at various concentrations of total polymers in mixtures (3%, 1,5%, 0,75%).

Rheological evaluation of polymer solutions/mixtures

All the solutions or mixtures prepared were subjected to rheological evaluation with a rotational rheometer (Rheostress RS 600, Haake, Karlsruhe, G) equipped with a plate-cone system. The following measuring systems were used: C20, C35 and C60 of different sizes and angles depending

on the sample viscosity. The measurements were carried out at 25°C and at least three replicates were performed for each sample. The viscosity, which is indicated by η and expressed in Pa*s unit, measures the resistance of a flowing fluid. The sample, once deposited at the stator level, was subjected to the action of a tangential force on its surface. This produces a Shear rate (D) whose measuring unit is s^{-1}, which depends on the rotor movement speed and on the gap between stator and rotor (in this case the gap is equal 0.053 mm). The applied force, normalized for the surface of the sample, is defined as the shear stress (τ) and is measured in Pa. The viscosity measurements were carried out by applying increasing gradients in the range of 10-300 s^{-1} and measuring τ in relation to the shear rate. The viscosity of the fluids results from the ratio between shear stress and shear rate.

Measurement of pH of mixtures

By means of a pH Meter 210 (HANNA instruments, Woonsocket, RI. U.S.A.), the pH of different mixtures either in presence or absence of glycine or glycerol was assessed.

4.3.2.2 Preparation of lyophilized dressings and films loaded with probiotics

Preparation of lyophilized dressing

First, the mixtures in Tab. 14 have been freeze-dried. 2.5 ml or 5 ml of each polymer mixture were withdrawn and placed into a 19.62 cm^2 plastic holders, frozen at -20°C and then lyophilized for 24 hours in a lyophilizer (Heto drywinner Analitica de Mori, Milan, Italy).
The effect of the total polymer concentration in mixtures on the yield of lyophilized was evaluate and based on the results of the previous step, three mixtures were obtained in different ratios of PVA and XG (85:15, 75:25, 65:35) at 3% of concentration. Glycine 1% w/w was added as a cryo-protectant (Tab.15b), obtaining final mixtures at total concentration of 4%.

TAB 15 b

% w/v of compounds in mixtures	% w/w of compounds on solid
3% PVA:XG 85:15 + GLY 1%	PVA 64% - XG 11% - Glycerol 25%
3% PVA:XG 75:25 + GLY 1%	PVA 56% - XG 19% - Glycerol 25%
3% PVA:XG 65:35 + GLY 1%	PVA 49% - XG 26% - Glycerol 25%

Tab. 15 b: Composition of PVA:XG mixtures in different ratios and added with glycine, at total concentration of 4%. On the right, the percentage of each compounds with respect to the dried sample is reported.

Based on the preliminary results, the lyophilized dressings were achieved using 5 ml of each mixtures poured into a 19.62 cm^2 plastic holders. These are frozen at -20°C and subsequently lyophilized. The lyophilized dressings were evaluated also for the detachment aptitude from the plastic holders.

Preparation of films

In a preliminary phase, polymer mixtures were prepared to evaluate the influence of the percentage of PVA on detachment from the glass surface or PTFE after solvent casting as reported in Tab. 14. The mixtures were poured onto the glass support and laminated. The support is then placed into a vacuum stove (Bicasa, ISO 9001) at of 37°C and pressure fixed at 10mbar. Subsequently, the effect of total polymers concentration and ratios of PVA and XG on the yield of resulting films was investigated. Mixtures were prepared in different ratios of PVA and XG (85:15, 75:25, 65:35) and at different total concentrations (0.75%, 1.5%, 3.00% w/v), in according with Tab. 15a.

The solvent casting method consists on pouring the solution on a glass or PTFE support; however, in this case lamination was avoided because it affects negatively the thickness of resulting films. The samples were placed in a stove at 37°C and the pressure was fixed at 10mbar.

Finally, three mixtures at 3% of polymers concentration were prepared as illustrated in Tab. 16 by adding glycerol at 1% w/v in as plasticizer, obtaining mixtures at 4% of total concentration. Once the formulations have been dehydrated, the ratio of polymers and glycerol with respect to the total solid film matches to the percentage shown in Tab. 16. The ratio between PVA and XG outcomes the same.

TAB 16

% w/v of compounds in mixtures	% w/w of compounds on solid
3% PVA:XG 85:15 + 1% GLYCEROL	PVA 64% - XG 11% - Glycerol 25%
3% PVA:XG 75:25 + 1% GLYCEROL	PVA 56% - XG 19% - Glycerol 25%
3% PVA:XG 65:35 + 1% GLYCEROL	PVA 49% - XG 26% - Glycerol 25%

Tab. 16 Composition of PVA:XG mixtures in different ratios and added with glycine, at total concentration of 4%. *On the right, the percentage of each compounds with respect to film after solvent evaporation is reported.*

4.3.2.3 Characterization of lyophilized dressing and films

Thickness evaluation

Thicknesses of lyophilized dressings and films were measured whenever possible by means of a Starrett 216P-1 digital micrometer (Athol, Massachusetts, USA). Four replicates were carried out for each sample.

Mechanical properties characterization

Tensile breaking force

Mechanical resistance of both lyophilized dressing and films were characterized by means of TA.XT Plus (ENCO, Spinea, I), equipped with an A/TG measuring system and a 1 Kg load cell. The lyophilized dressings were placed on a hollow cylinder and was compressed with a conical probe P/30, for a distance of 25 mm and a trigger force of 0.5N until break. Test speed: 1 mm/sec. Film samples of 30 (length) x 10 (width) mm were characterized for tensile breaking force. The sample was placed between two jaws, a lower one, fixed, and the top one, movable, ensuring an initial distance of 3 cm. As soon as the analysis starts, the upper jaw moves upwards until film breaking. Test speed: 1 mm/sec.

Bending test

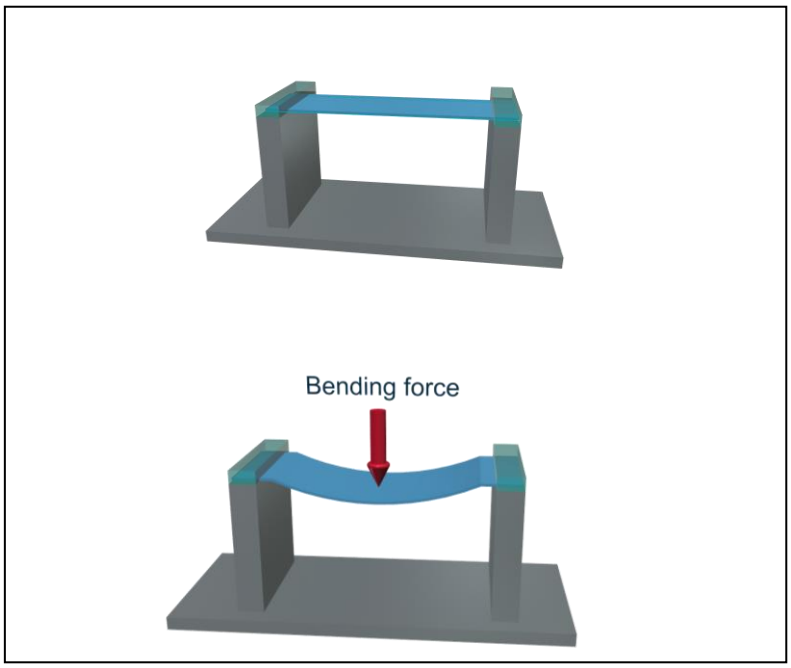

Fig. 40 A 3D model of apparatus coupled to TA.XT Plus texture analyzer to carry out bending measurements.

Films were fastened to a support as represented in Fig. 40. Thus, the texture analyzer equipped with an A/TG measuring system, a 1 Kg load cell and a cylindrical probe (∅5mm) was settled up to bend

the film sinking for a distance of 3mm. Test speed: 0.05 mm/sec. The recovered data were analyzed and plotted in graphs.

Elasticity of films

The measurement were carried out by means of a TA.XT Plus (ENCO, Spinea, I), equipped with an A/TG measuring system and a 1 Kg load cell. The results consist in a graph showing the Force (mN) or Stress (MPa) of the stretching film recorded by the loading cell on the ordinates axis and the distance (mm) moved by the jaw or the Strain on the ascites axis. The force values have been normalized for the area of the section and the samples were elongated of 2% of their length. Test speed: 0.05 mm/sec.

The young's modulus was calculated to characterize the stiffness of the formulations.

Young's modulus, E (MPa)

$$E = \frac{\sigma}{\varepsilon}$$

$$\sigma = \frac{F}{S}$$

$$\varepsilon = \frac{\Delta l}{l}$$

Where σ represent the tensile stress, F Force (N), S Surface (m^2), ε represent the extensional strain, l the starting length of the sample and Δl the elongation.

The slope of the stress/strain curves were calculated.

The evaluation of mechanical properties of the formulation were performed by means of Origin Pro 8.5.0 Northampton, Massachusetts, USA. Data are expressed as mean value and S.E.M (standard error) or SD (standard deviation). Differences were determined according to student t-test. Differences were considered significant at $p < 0.05$.

Loading of probiotics in lyophilized and films

For the preparation of the formulations loaded with *L. plantarum* sterilization of the glassware and the equipment was carried out in autoclave (pbi, ALFA-junior) at a temperature of 121°C for 20 minutes to obtain polymer mixtures in low contamination condition.

In addition, the mixtures were prepared twice as concentrated as reported and submitted to UV radiation to break down residual microorganisms and then diluted 1:1 with a probiotic suspension at a concentration of $2*10^7$ CFU/ml. These steps were carried out employing a laminar flow biological safe cabinet equipped with HEPA filters.

Other concentration of probiotics in suspension were tested, 10^8 and 10^9 CFU/ml.

The mixture at 3% of PVA:XG ratio 65:35 added with glycerol 1% was chosen to obtain the definitive film and mixture at 3% of PVA:XG ratio 75:25 added with glycine 1% was chosen to obtain the definitive lyophilized dressings. The processes employed to obtain the formulations persisted unchanged. Both the lyophilizer and the stove have been previously sanitized with an alcoholic solution of quaternary ammonium salts to reduce the contamination of environmental microorganisms during solvent-casting and lyophilization processes.

Once obtained, the formulations were detached from the support using sterilized instruments and placed in sterile containers for subsequent evaluation of probiotics viability.

4.3.2.4 Preparation of films loaded with nanoemulsion

Polymer mixtures of PVA and guar gum (GG) were used to prepare films containing nanoemulsions at various concentrations of total polymers and different PVA:GG ratios.
A mixture of PVA and guar gum (GG) at various total polymers concentrations (4%, 4.5%, 5%, 10% w/v) and with a PVA:GG ratio of 85:15, 75:25 and 65:35 were prepared.
Preliminary results suggest to take into account only the mixture reported in Tab. 17, added with glycerol 1% (w/v) as plasticizer.

TAB 17

% w/v of compounds in mixtures	% w/w of compounds on solid
5% PVA:GG 85:15 + 1% GLYCEROL	PVA 70.8% - GG 12.5% - Glycerol 16.7%
5% PVA:GG 75:25 + 1% GLYCEROL	PVA 62.5% - XG 20.8% - Glycerol 16.7%
5% PVA:GG 65:35 + 1% GLYCEROL	PVA 54.2% - XG 29.1% - Glycerol 16.7%

Tab. 17 Composition of mixtures at 5% of PVA:GG in different ratios added with glycerol 1% w/v and percentage of each compounds in film after solvent evaporation.

The polymers and the glycerol were added directly in the aqueous environment of the nanoemulsion in a dark container under magnetic stirring. The mixtures were poured on a PTFE surface and place the stove for 24h, the temperature was fixed at 35°C due to the heat sensitivity of chitosan based nanoemulsion, the pressure was fixed at 10mbar.

Franz cell release study

The release study was conducted following the method developed for the analysis of powder release, as described previously. Threes samples of 3mg of film with nanoemulsions was weight and placed on the acetate cellulose membrane on the acceptor chamber, full of isopropyl myristate under stirring. In the donor chamber 1.5 ml of physiological solution (NaCl 0.9%) were poured. The concentration of antioxidant released was assessed by HPLC at different times (1, 2, 4, 6 hours).

CLSM analysis

Nile Red is a fluorescent probe and its fluorescence properties depend closely on the polarity of the surrounding environment. A batch of nanoemulsion was prepared dissolving Nile Red fluorescent dye in the organic phase. The film loaded with these NE was analyzed by means of a Laser Scanning Confocal Microscope (LSCM)-coupled fluorescence detection system (CLSM Leica TCS SP5II, Leica Microsystems, Milan, Italy) to investigate the distribution of nanoparticles in the polymer matrix. (Kim H.H. et al., 2006; Maiti N.C. et al., 1997)

Evaluation of the hydration properties of films and lyophilized

The water absorption capacity of the lyophilized dressings and films was evaluated by weighing a sample and placing it on a cellulose acetate membrane rested and hydrated on a cylinder full of physiological solution (0.9% NaCl). At certain times, the membrane and sample were weighed. The measurements were carried out until a constant weight was reached. Three replicates were performed for each formulation.

The calculation of water uptake follows the equation:

$$\%W_g = \frac{w_t - w_0}{w_0} * 100$$

Where $\%W_g$ represent the percentage of water gain (uptaken), w_t the weight at a certain time and w_0 the weight of the dried sample. (Brachkova M.I. et al., 2012)

Bioadhesion analysis

The lyophilised and the films have been subjected to a bioadhesion test carried out by TA.XT plus equipped with a 1Kg (over) cell and equipped with a Mucoadhesion Test Ring (A/MUC). A cylindrical probe was fixed to the vertical arm of the instrument (P / 10, Ø = 10 mm, Cyl Delrin). A large beaker was placed on the horizontal base of the instrument, containing about 500 ml of bidistilled water, thermostated at 32°C, by means of a heating plate equipped with thermometer for temperature control. On the probe, a double-sided adhesive tape disk was applied to surface on which the samples were placed. The A/MUC measurement system consists of a cylindrical support for the substrate in which a sample of collected rat skin is inserted. Screws closed the cylindrical housing, to ensure the seal, and it was convoluted with parafilm. This device has been placed inside the beaker containing thermostated water, making sure that the water level does not exceed the height of the support wetting the rat skin sample.

Scanning Electron Microscopy (SEM) and samples preparations

Scanning electron microscopy (SEM) analysis was carried out using a scanning electron microscope Zeiss, model EVOMA10 (CarlZeiss, Oberkochen, Germany). The samples were made conductive by the deposition of a gold layer in vacuum vapor phase. The formulations were treated with liquid nitrogen at -195.8°C until complete refrigeration. In this condition, the formulations become particularly stiff and fragile. An accurate fracture of the formulation is practicable, that allow an accuracy observation of their section.

Differential Scanning Calorimetry (DSC)

The melting behavior of the samples of different formulations was examined using a TA Instruments DSC Q2000 differential calorimeter, New Castle, DE 19720, from -50°C to 250ºC at a heating rate of 10°C/min, under nitrogen at flux rate of 50 ml.min^{-1}.

4.3.2.5 Biological evaluation

Cultivation of probiotics and preparation of L. plantarum suspension

Lactobacillus plantarum was grown overnight at 37°C, in MRS Broth, in microaerophilic conditions. After 24 hours of incubation, it is centrifuged, eliminating the supernatant and washing the cells in PBS. Subsequently, a standardized suspension of microorganisms with an initial concentration of about $4*10^7$ CFU/ml was obtained. The following dilutions were then prepared in PBS from the initial suspension: II (dil 1: 100), IV (dil 1: 10˙000), VI (dil 1: 1 000 000), VIII (dil 1: 100,000,000) and were seeded in MRS Agar (Tarato). Finally, they were incubated at 37°C overnight in microaerophilic conditions and was counted the CFU/ml to confirm the standardized data.

Evaluation of the compatibility of probiotics with polymer mixtures

L. plantarum compatibility with polymers was evaluated on mixtures in ratios PVA:XG 85:15 and 75:25, at a total polymers concentration of 3% w/v. The evaluation took place at zero time, after 3 hours, 6 hours and 24 hours of contact.

Compatibility and stability of probiotics in lyophilized and films

Films (3% of PVA:XG ratio 65:35 added with glycerol 1%) while lyophilized dressings (3% PVA:XG ratio 75:25 added with glycine 1%) were loaded with probiotics and their vitality was evaluated at time zero immediately after preparation, and after 7 and 14 days of storage in a refrigerator at 4°C. The formulations were placed in a sterile Falcon and 20 ml (for films) or 5ml (for lyophilized) of PBS were added. The formulations were stirrer by vortex until complete dissolution (~15/20 minutes) and the following dilutions in PBS were prepared: II (dil 1:100), IV (dil 1:10˙000), VI (dil 1:1,000,000) and seeded in MRS Agar; a non-diluted sample was also seeded. Samples were incubated at 37°C, overnight, in microaerophilic conditions and the CFU/ml were counted. A comparison from the starting CFU/ml (Tarato) and CFU/ml obtained after dissolution of the formulations was carried out, taking into account the various dilutions and adapting the final results on them.
Antimicrobial effect was calculated in log scale following the equation:

$$AE = \log C - \log S$$

AE Antimicrobial effect

C= CFU/ml growth control

S= CFU/ml growth in sample

C and AE values were calculated by multiplying the number of CFU counted in the plates for the relative dilutions.

Release of probiotic from formulation to simulant wound fluid

For the selected probiotic formulations, a dissolution test was performed, in triplicate, by immersing the lyophilized dressings or film in an appropriate volume of sterile simulant wound fluid (1000g water, 0.368g calcium chloride, 8.298g sodium chloride - Thomas, S. and Fram, P., 2001). In particular, 20ml or 5ml were added to a film or lyophilized dressings, respectively (to reach the volume of starting mixture), at 37ºC (water bath), under mild agitation (120 rpm). Samples of 20 µl were withdrawn at predefined time intervals (0.5, 1, 3, 6 hours), and plated in MRS agar after serial dilutions in simulant wound fluid. The withdrawn volume was replaced with simulant wound fluid previously heated at 37ºC. After the first collection of samples, cell cumulative concentrations were corrected for the dilution factor, according to the following equation:

$$\text{Corrected CFU/ml} = \text{Determined CFU/ml} + \left(\sum \text{Previously determined CFU/ml} \times \frac{Vw}{Vt}\right) \quad \text{(Eq.4)}$$

where Vw represents the withdrawn (collected) volume (total volume 80 µl) and Vt the total volume inside the tube (5ml).

Concentrations were converted in CFU counts considering the volume of the tube and results were presented as CFU log versus time. (Brachkova M.I. et al., 2012)

In vitro test on fibroblasts

The effect of lyophilized, film loaded with *L. plantarum* and film loaded with NE on the viability of Normal Human Dermal Fibroblast (NHDF, 10th passage) (Promocell GmbH) was investigated.
A total of $1*10^5$ cells/well were seeded in the basolateral chamber of Transwell® Permeable Supports System 12-well (Corning Costar, Corning, NY) in presence of complete culture medium (CM) and left in incubator for 24 hours in order to reach confluence. Thereafter, a sample weighted portion of each formulation (5±0.5mg, n=3) was placed onto the filter of the apical chamber, hydrated with 500 ml of CM and left in contact with cells for 24 hours. CM was used as positive control. After incubation, Transwell® Supports, containing the samples, were removed and an MTT assay was performed. Briefly, CM was removed from the basolateral chamber, cell monolayers were washed with PBS and, then, 250 µl of MTT 7.5 µM in 500 µl of DMEM without phenol red were added to each well and incubated for 3 hours. Finally, 500 µl of DMSO, used as solubilization agent, was added to each well. In order to promote the complete dissolution of formazan crystals, obtained from MTT dye reduction by mitochondrial dehydrogenases of alive cells, the solution absorbance was measured by means of an iMark® Microplate reader (Bio-Rad Laboratories S.r.l.) at a wavelength of 570 nm and 690 nm (reference wavelength) after 60 s of mild shaking.

Results were expressed as % viability by normalizing the absorbance measured after contact with the samples with that measured for CM. Three replicates were performed for each sample.

Statistical analysis

Statistical evaluations were performed by means of Origin Pro 8.5, Origin Lab Corporation, MA, USA. Differences were determined according to One-way ANOVA or student t-test. Differences were considered significant at $p < 0.05$.

4.3.2.6 Preparation of composite films

A porous backing in polyurethane was developed as secondary medication. A combined medication can be obtained casting the mixtures directly on this support. The polymer film load with probiotic or nanoemulsions represent the active layer of the medication whereas the polyurethane represents the passive layer able to cover and protect the wound allowing gas exchange. In a typical lab-scale fabrication 1.5 g of thermoplastic polyurethane TPU (Estane 58887 - Lubrizol Corp.) were dissolved into 20ml of dimethylacetamide (DMAc) at 50°C over 4h. The TPU solution was poured into a petri dish filled with hand-grounded NaCl that absorb it over about 30 minutes. Once all the TPU solution was absorbed, DMAc was evaporated under vacuum in a stove at 80°C overnight, to obtain a NaCl-TPU disc that was removed from the petri dish. The NaCl contained in this disc was then removed by immersion in boiling water for 1-2 days, realizing a sponge-like TPU network that was then analyzed by SEM to verify the porosity and eventual NaCl residues presence (by EDX analysis).

PARTE II

4.3.3 RESULTS

4.3.3.1 Characterization of polymer solutions/mixtures

Rheological evaluation of polymer solutions/mixtures

PVA was completely solubilized in water at concentrations of 1%, 2% and 5%, while at concentration of 10% tends to form insoluble crystals that are evidenced in polarized light microscopy (Leica DM 2000). As a result, PVA solution at 5% was selected as a starting solution.
Xanthan gum was found excessively viscous and difficult to hydrate at concentration higher than 1% w/v.

Different mixtures were obtained by mixing PVA 5% w/v and xanthan gum 0.25% and 0.5% solutions in ratios specified in the methods section. These mixtures were subjected to rheological characterization. The rheological behavior of xanthan gum solutions at 0.25% and at 0.50% w/v was investigated, as illustrated in Fig. 41.

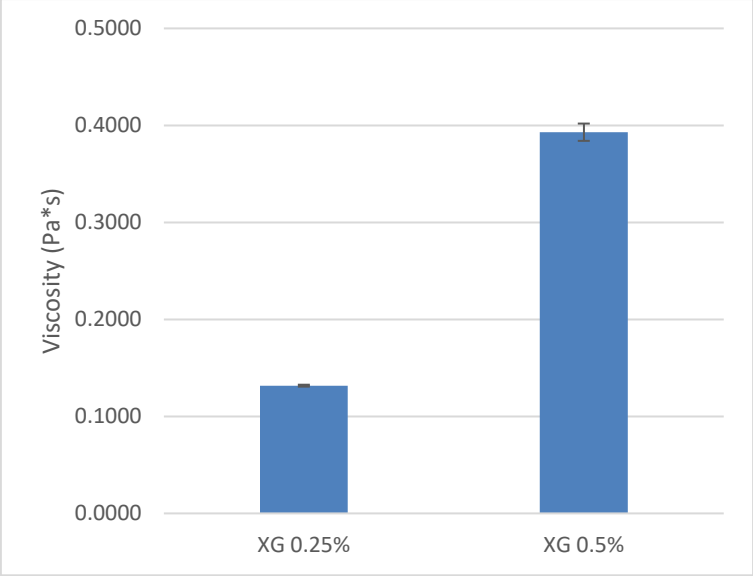

Fig. 41 Comparison between the viscosity values of XG solutions at 0.25% and 0.5% at share rate $25s^{-1}$. The solution at 0.5% of concentration is statistically significant more viscous respect the other at 0.25% (student t-test, p value 0.5; n=3).

Subsequently, the binary mixtures of PVA and xanthan gum reported in Tab. 12 and 13 of Methods were characterized by rotational rheometer. As illustrated in Fig. 42 and 43, an increase of the solutions viscosity occurs by increasing xanthan gum concentration.

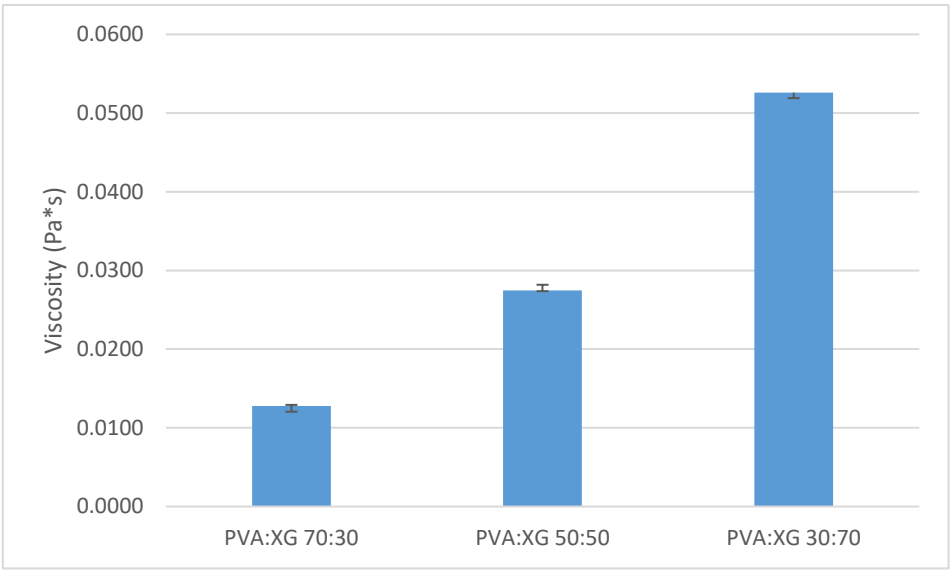

Fig. 42 Viscosity values at shear rate 25s-1 of PVA:XG binary mixtures 1, 2 and 3 corresponding to 0.25% xanthan gum solution blended in different ratios (volumes) with 5% PVA solution.

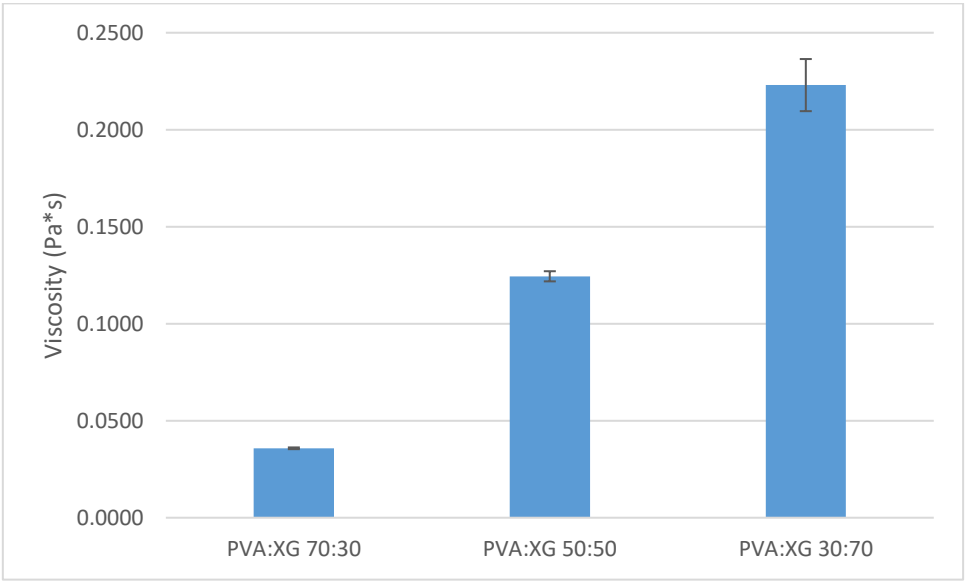

Fig. 43 Viscosity values at shear rate 25s-1 of PVA:XG binary mixtures 4, 5 and 6 corresponding to 0.5% xanthan gum solution blended in different ratios (volumes) with 5% PVA solution.

Mixture 6 (PVA:XG 30:70) was the most viscous among those studied.

The addition of glycine 1% w/v was envisaged to protect cell membrane of probiotics during freeze-drying process. Thus, the effect of glycine on the viscosity of mixtures was investigated. Fig. 44 illustrates the viscosity values at shear rate $25s^{-1}$ of solutions 4, 5 and 6 after adding glycine 1% w/v as cryoprotectant. The viscosity of mixtures results slightly different but this was not however considered relevant for the production of lyophilized dressings.

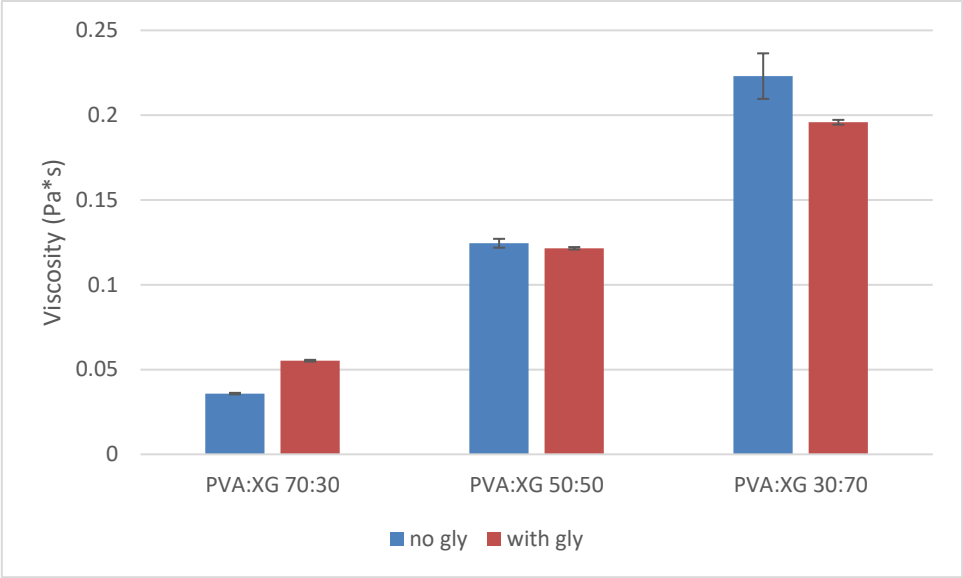

Fig. 44 Comparison between viscosity values at shear rate 25-1 of PVA:XG Binary mixtures 4, 5 and 6, corresponding to xanthan gum 0.5% and blended in different ratios with PVA, both with or without addition of glycine.

Consequently, glycine at 1% w/v was employed as a cryoprotectant in polymer mixtures aimed to prepare dressings by freeze-drying. These preliminary results show the effects of total polymers concentration and PVA:XG ratios on the viscosity of the mixtures, a crucial characteristic for obtaining suitable formulations by solvent casting.

The subsequent phase of the work concerned the rheological evaluation of the polymer mixtures described in Table 15a of the Methods, corresponding to mixtures with different PVA:XG ratios (85:15, 75:25, 65:35) and at different total concentration of polymers (0.75%, 1.5% and 3%).

Rheological evaluation confirms the significant increase in viscosity increasing the concentration of xanthan gum and increasing the total concentration of mixtures, as illustrated in Fig. 45, which report the viscosity values at shear rate 25s-1 of different samples.

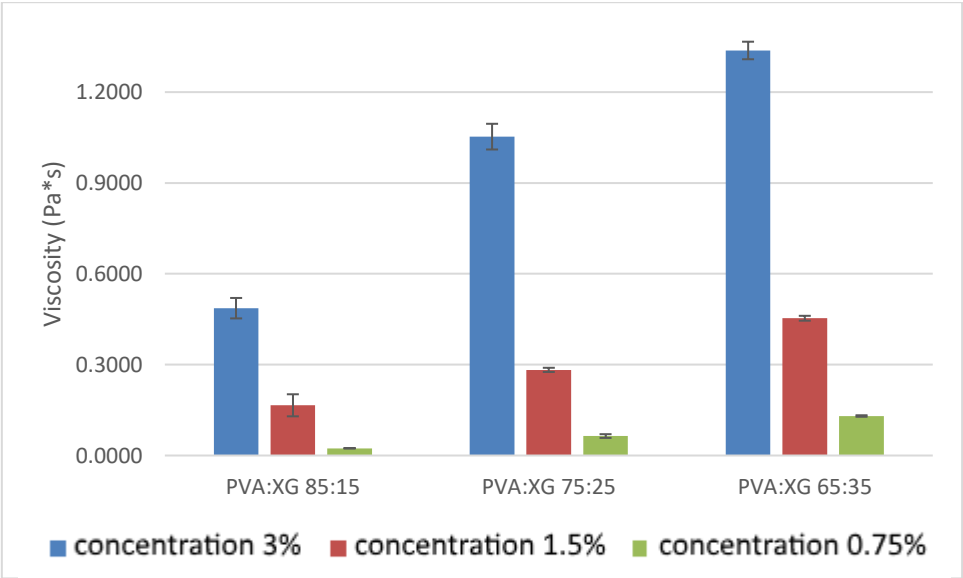

Fig. 45 Comparison among viscosity at shear rate of 25s-1 of mixtures obtained by combination of PVA and XG at different ratio (85:15, 75:25, 65:35) and at different total concentration of polymers in mixtures (0.75%, 1.5%, 3%).

The mixtures at 3% of concentration were chosen as pilot mixtures to obtain film via solvent casting. Lower concentrations of polymers affect the thickness and mechanical properties of prepared films that result too thin and fragile.

Measurement of pH of mixtures

The different pH of mixtures resulted weak acidic, as reported in Tab. 18. However, pH values are compatible with probiotics survival and chemical stability of chitosan. Glycine and glycerol addition does not affect significantly pH of mixtures.

	pH without glycerol	**pH with glycerol 1%**
mixture 3% PVA:XG 65:35	5.62	5.63
mixture 5% PVA:GG 85:15	5.55	5.53
	pH without glycine	**pH with glycine 1%**
mixture 3% PVA:XG 75:25	5.68	5.54

Tab. 18 Different pH values of mixtures either with or without glycerol or glycine.

4.3.3.2 Characterization of lyophilized dressings loaded with probiotics

In a preliminary phase, the mixtures 1-6 reported in Tab. 12 and 13 of the Methods (corresponding to PVA and XG mixtures obtained by blending the solutions at different concentrations of xanthan gum (0.25% and 0.5%) with different volumes of solution of PVA at 5%) were freeze-dried in different amounts (2.5ml or 5ml), in 19.62 cm^2 plastic holders.

Formulations made with 2.5 ml of polymer mixture (in 19.62 cm^2 holders) resulted too thin, breakable and not easy to handle. Consequently, 5 ml of polymer mixture were placed in the holders and freeze-dried to obtain thicker and stronger formulations. The detachment from the plastic holders was good for preliminary lyophilized dressing 4 and 6 (PVA 5% and XG 0.5% mixtures at ratios (volumes) 50:50 and 30:70, respectively), while the others were only partially detached. The mechanical resistance of these formulations was tested with TA.XT Plus, which allows to measure the breaking strength of the formulations. Breaking forces are between 0.040 and 0.170 N, as illustrated in Tab. 19.

Lyophilized dressings	**Breaking Force (mN) ±sd**
1	54.70 (±7)
2	163.40 (±21)
3	101.90 (±13)
4	79.25 (±9)
5	129.20 (±17)
6	45.40 (±6)

Tab. 19 Breaking force (mN) of the different formulations described in Table 12 and 13 of the methods obtained from 2.5ml of mixture in a 19.62cm^2 holder.

The concentration of xanthan gum appeared to play a key role in the mechanical properties of resulting lyophilized. Thus, different ratios of PVA and XG, at different total concentrations and added with glycine 1%w/v as cryoprotectant, in according with Tab. 14 of Methods, were subjected to freeze-drying. As for the detachment from the holder, the only formulations that could be detached from the support without breaking them were β, e and η (3% of PVA:XG ratio 75:25 + gly 1% and 0.75% of PVA:XG ratio 85:15 + gly 1%, respectively). The lyophilized α and δ (3% of PVA:XG ratio 85:15 + gly 1% and 1,5% of PVA:XG ratio 85:15 + gly 1%, respectively) were extremely exfoliated, and it was not possible to measure their thickness. Data are reported in Tab. 20.

Formulation	Thickness (mm)	Breaking force (mN) (±sd)
α	Not measurable	690 (±90)
β	1.75	1680 (±200)
γ	1.85	1030 (±10)
δ	Not measurable	1230 (±150)
ε	1.85	510 (±60)
ζ	1.55	720 (±90)
η	2.10	230 (±30)
θ	2.07	1170 (±140)
ι	1.30	220 (±30)

Tab. 20 Breaking force (mN) of the different formulations described in Table 15b of the methods section.

In this preliminary phase, the higher polymer concentration and a high ratio of PVA in mixtures appeared crucial for obtaining suitable lyophilized dressings.

Thus, the mixtures reported in Tab. 15b were subjected to freeze-dried. Only the sample obtained from mixture at 3% of PVA:XG ratio 75:25 + gly 1% was completely detachable from plastic holder, it presented a regular surface and good mechanical properties: 1,95±0,05 mm, Breaking Force 1795±52 mN. This lyophilized was chosen as a prototype to incorporate *L. plantarum*. Mixtures were prepared twice as concentrated as reported and submitted to UV radiation to break down residual microorganisms and then diluted 1:1 with a probiotic suspension at concentration of $4*10^7$ CFU/ml. These mixtures were subjected to rheological evaluation by rotational rheometer.

The viscosity of the mixtures after the addition of lactobacilli, as could be expected, has a slight decrease (Fig. 46). A statistical significant difference can be appreciated between the viscosity at shear rate $50s^{-1}$ of samples in presence or absence of probiotics (student t-test, p value 0.05, n=3). This was not however considered relevant for the production of lyophilized dressings.

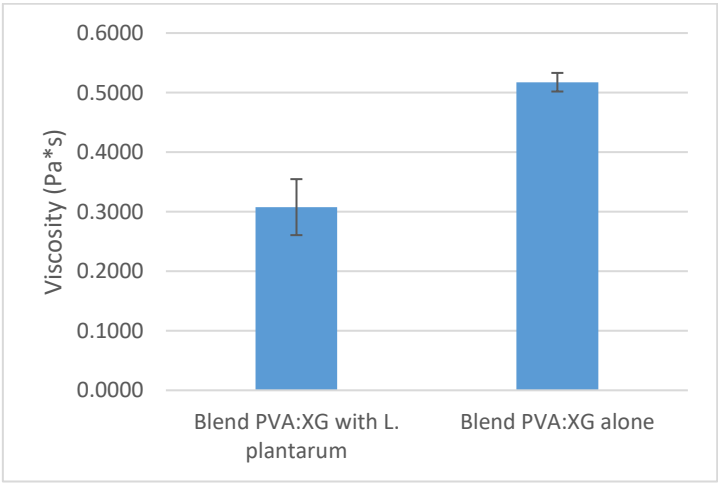

Fig. 46 Comparison between the viscosity at shear rate 50s-1 of two samples (3% of PVA:XG ratio 75:25 added with 1% glycine) chosen as pilot mixture to freeze-dried, both loaded and unloaded with L. Plantarum at 10^7 CFU/ml.

Probiotics concentration in lyophilized

Starting from a suspension of $4*10^7$ CFU/ml and diluting 1:1 with the polymer mixtures, we obtain a concentration of $2x10^7$. During the drying process, the mean bacterial abatement in Log_{10} is 0.46 with a mean percentage of survival of 32.7%.

The lyophilized, obtained starting from 5ml of mixture will contain $5 * 2x10^7 x\frac{32}{100} = 3.2x * 10^7$ CFU.

The lyophilized dressing weight about 0.2g (± 2%) after drying, thus the probiotic concentration is about $1.6x10^8$ CFU/g.

4.3.3.3 Characterization of films loaded with probiotics

To realize the films with PVA and XG mixtures, the polymers mixtures reported in Tab. 14 of the Methods were evaluated. These mixtures were subjected to solvent casting to obtain films. However, only films with the higher ratio of PVA and XG and the higher PVA concentration can be detached from the glass support (Samples θ PVA:XG 87:13 and ι – PVA:XG 94:6), although they are still too thin and friable. This phase helped to clarify the importance of using suitably high polymer concentrations to obtain films that could be handled.

In a further phase of the work, films by solvent casting were obtained (using the glass support), pouring the mixtures corresponding to different concentrations of total polymers in mixture (3%, 1.5%, 0.75%) and combinations in different ratios of PVA and XG (85:15, 75:25, 65:35) in according to Tab. 15a of the Methods, previously tested for rheological characteristics. In this case, the only films that could be detached from the glass support are G, H and I, that is the three films obtained from the mixtures at 0.75% w/v of PVA:XG in ratios 85:15, 75:25 and 65:35, respectively. It was decided to change the casting support and PTFE support was employed to improve film detachment. In spite of this, the films B, C, E, and F, while detaching from the media, resulted too fragile and were easily broken (samples B and C were obtained from mixtures at 3% of PVA:XG in ratios 75:25 and 65:35, respectively; samples E and F were obtained from mixtures at 1.5% of PVA:XG in ratios 75:25 and 65:35, respectively. The remaining films have been characterized for thickness, and mechanical properties (breaking force). The results of this characterization are reported in Tab. 21 and 22.

Mixtures	**Obtained films - ↕ µm** (mean±sd)
A (3% PVA:XG 85:15)	57.50 (±3.42)
D (1.5% PVA:XG 85:15)	31.00 (±1.83)
G (0.75% PVA:XG 85:1)	7.75 (±1.50)
H (0.75% PVA:XG 75:25)	6.50 (±1.73)
I (0.75% PVA:XG 65:35)	9.00 (±1.41)

Tab. 21 film thicknesses (µm) obtained from mixtures reported in Table 15a of the Methods.

Mixtures	**Obtained films - F (N)** (mean±sd)
A (3% PVA:XG 85:15)	-
D (1.5% PVA:XG 85:15)	-
G (0.75% PVA:XG 85:1)	1.239 (±0.069)
H (0.75% PVA:XG 75:25)	1.293 (±0.217)
I (0.75% PVA:XG 65:35)	4.109 (±0.601)

Tab. 22 film breaking force (N) obtained from mixtures reported in Table 15a of the Methods.

The employment of a PTFE support resulted of critical importance for a good detachment. The breaking force of the films increased as the total polymer in mixtures increased. Formulations A and D were not characterized as the maximum force exceeded the measuring limits of the apparatus. Nevertheless, the films were too rigid to be handled, and probably difficult to apply in vivo on a wounded irregular surface of the body, i.e. on a knee.

Glycerol 1% w/v was therefore added as a plasticizer to promote detachment from the support and to improve elasticity of the film. Plasticizers, improve the elasticity and flexibility of the films making them less fragile. The plasticizers are commonly small molecules miscible with the film-forming polymers, in this case the glycerol, one of the most used plasticizers in the pharmaceutical formulations. Between the plasticizer and the polymer occur molecular interaction resulting in a higher mobility of polymer chains. (Krull S.M. et al., 2016).

In this preliminary phase, the crucial role of the total polymer concentrations, PVA:XG ratios and viscosity of mixtures was investigated and led to the development of three mixtures added with glycerol as plasticizer, with a high ratio of PVA and a total concentration of 4% (Tab. 16 of Methods).

A rheological test was performed using a rotational rheometer to verify the influence of glycerol on the viscosity of the mixtures. Statistically significant difference can be observed between the viscosity of mixtures at 3% of PVA:XG 85:15 both with and without addition of glycerol 1% w/v and between the viscosity of mixtures at 3% of PVA:XG 75:25 both with and without addition of glycerol 1% w/v; but no statistically significant difference can be observed between mixtures at 3% of PVA:XG 65:35 both with and without addition of glycerol 1% w/v (student t-test, p value 0.05, n=3), as illustrated in Fig. 47.

These mixtures, containing the plasticizer, were employed to obtain the pilot films. Resistant, elastic and easy to handle films were obtained, that could be easily detached from the PTFE support.

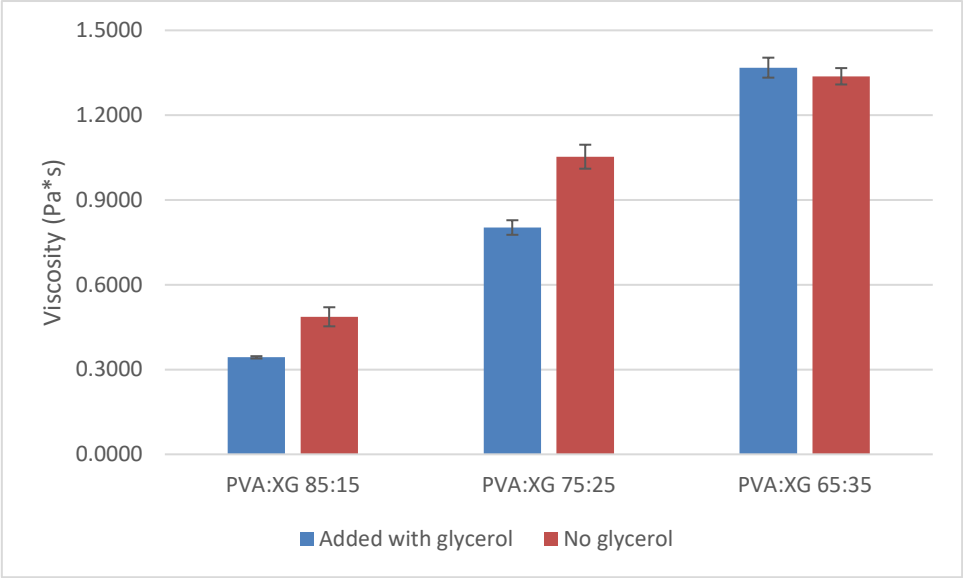

Fig. 47 Comparison among viscosity at 25^{s-1} of different mixtures at 3% of PVA and XG either in presence or in absence of glycerol 1% w/v.

Mechanical properties of films

The PVA:XG films added with glycerol (in according with Tab. 16 of Methods) were tested for thickness and breaking force, and the results are reported in Tab. 23 and 24.

FILM	Mean ↕ (μm) ±sd
PVA:XG 85:15	95.8 (±21.5)
PVA:XG 75:25	98.4 (±11.4)
PVA:XG 65:35	147.7 (±18.3)

Tab. 23 thicknesses of film at 3% of PVA:XG added with glycerol.

FILM	Mean F (N) ±sd
PVA:XG 85:15	7.158 (±1.126)
PVA:XG 75:25	2.002 (±0.238)
PVA:XG 65:35	8.878 (±1.095)

Tab. 24 breaking force of film at 3% of PVA:XG added with glycerol.

Bending test

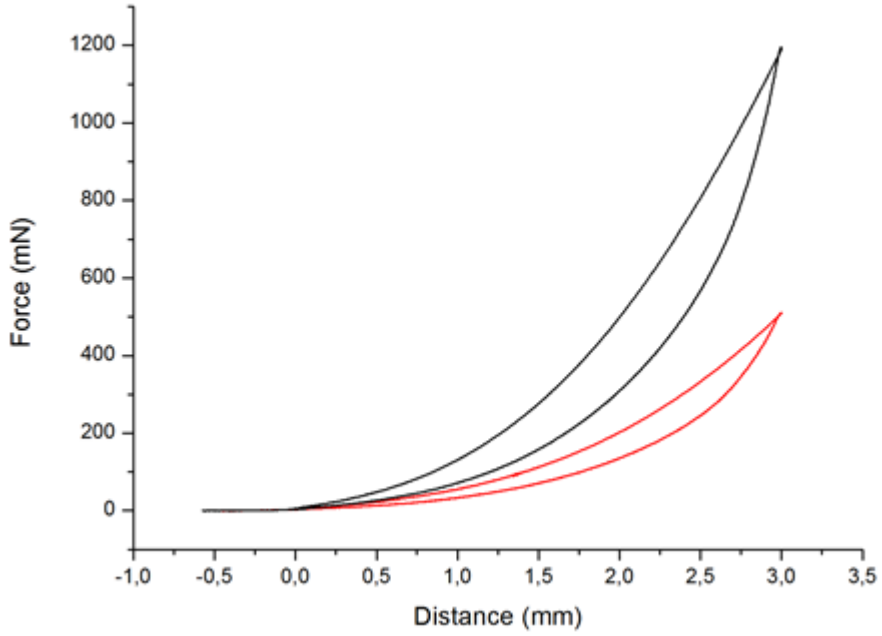

Fig. 48 Force/distance graph of bending test on films at 3% of PVA:XG 65:35 with and without glycerol (red line= film with glycerol, black line=film without glycerol)

The graph in Fig n. 48 shows the force necessary to obtain the bending deformation for a distance of 3mm of films of PVA:XG 65:35 with and without glycerol. The force needed to bend the film without glycerol is always higher than the force necessary to bend the film added with glycerol confirming its better mechanical properties, suitable for handling and application in wounds. There is a statistical significant difference between the two mean values (student t-test unpaired, p value 0,05, n=3) as shown below (Fig. 49).

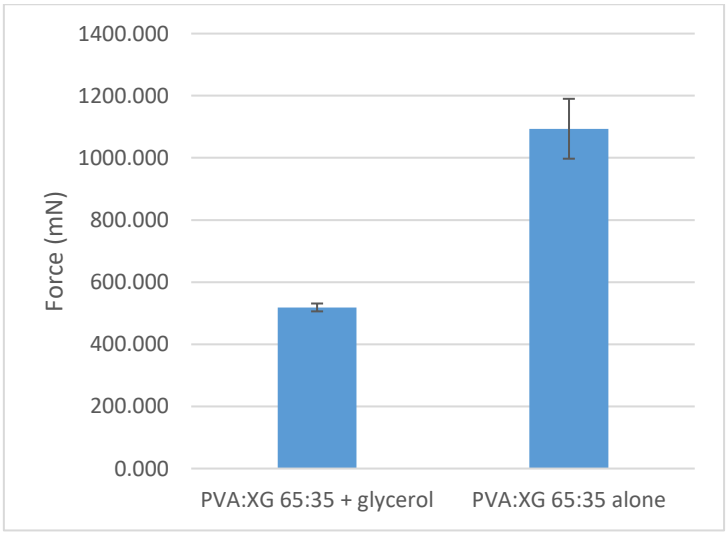

Fig. 49 Maximum force measured at 3mm of bending (mean±sd; n=3) for films of PVA:XG 65:35 with and without glycerol.

Elasticity of films

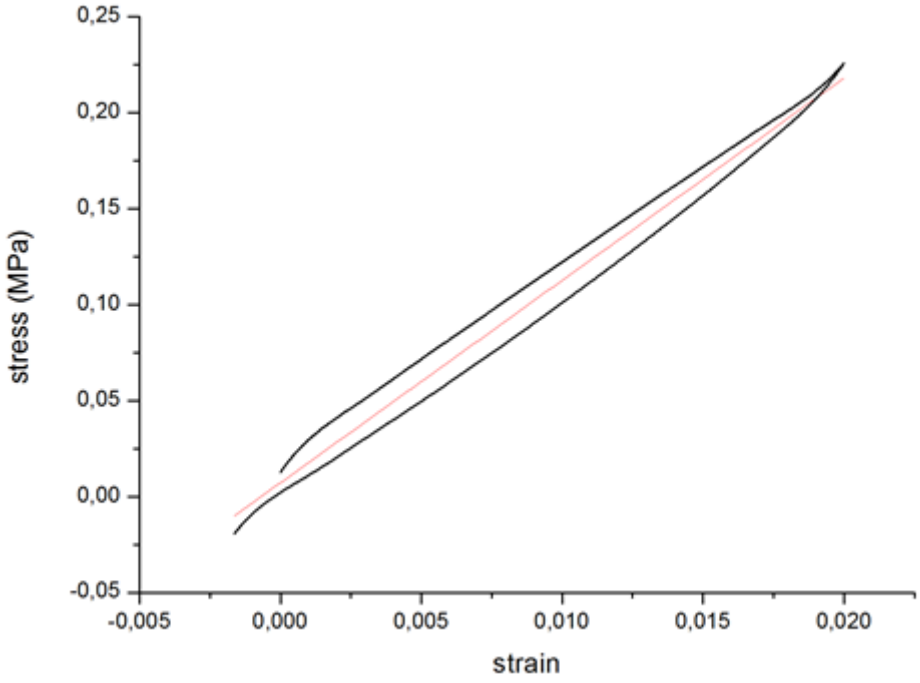

Fig. 50 Stress/strain curve of film PVA:XG 85:15 (without glycerol). The linear fit (in red) represent the slope of the curve.

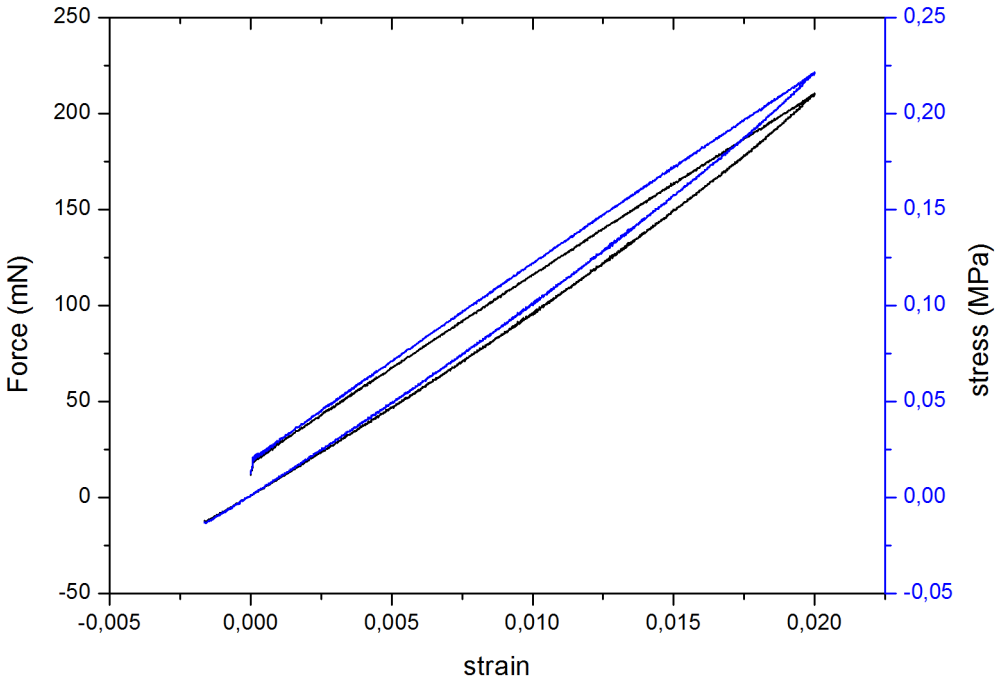

Fig. 51 The graph plots Force and Stress as function of applied Strain for film PVA:XG 85:15 (without glycerol).

The graph in Fig. 50 shows the force and the relative stress needed to extend the film of PVA:XG 85:15 (without glycerol). The return curve shows the presence of a small hysteresis cycle caused by a loss of elasticity during the elongation that was recovered after few seconds of force application. This indicates the elastic properties of the film.

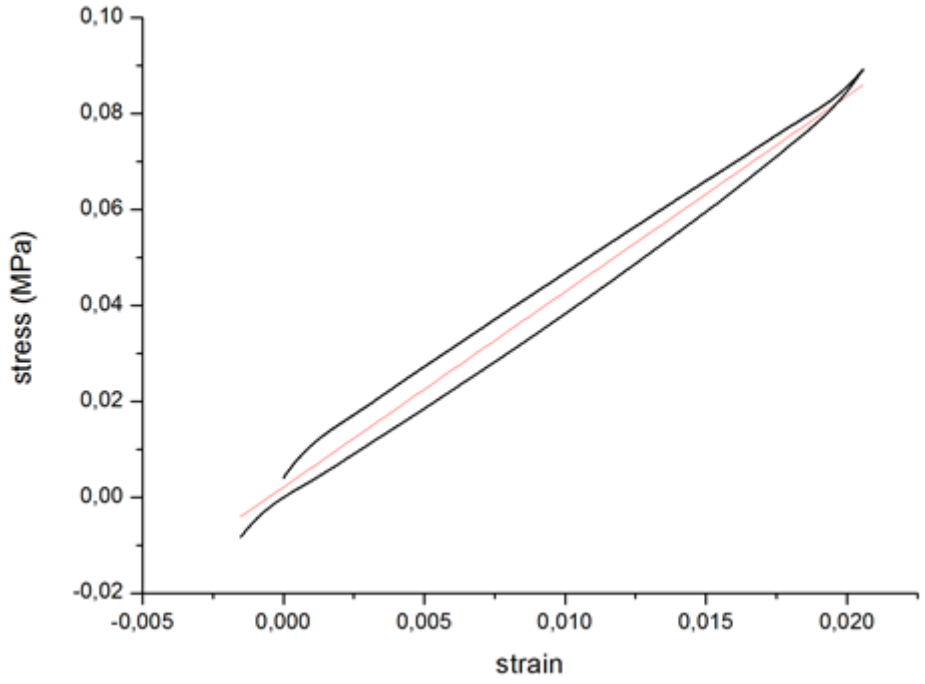

Fig. 52 Stress/strain curve of film sample PVA:XG 65:35 added with glycerol. The linear fit represents the slope of the curve.

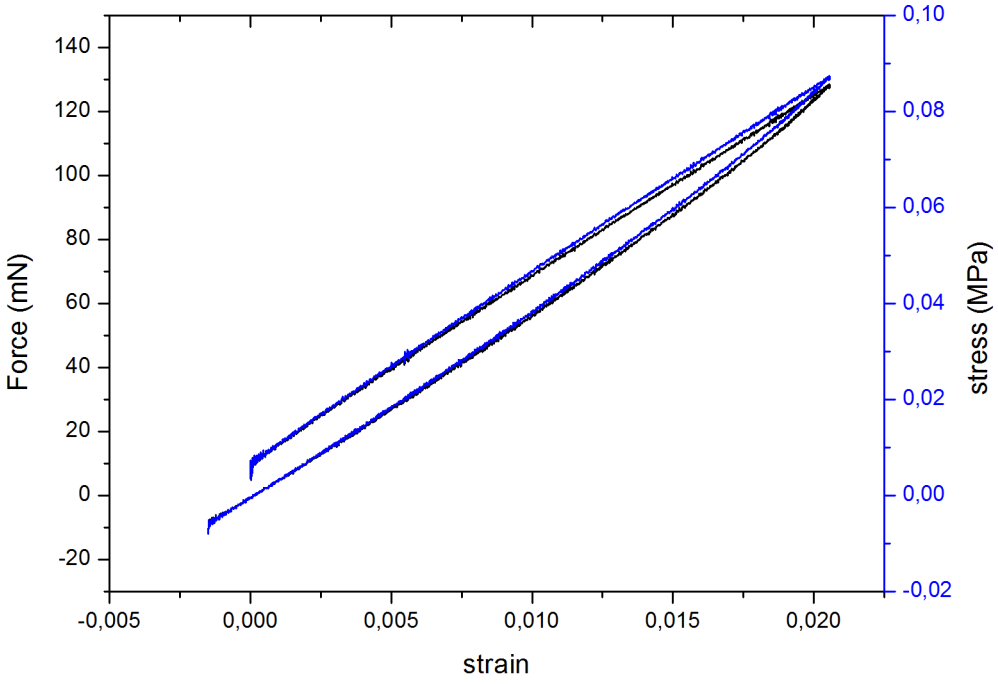

Fig. 53 Graph Force and Stress as function of Applied Strain for film PVA:XG 65:35 added with glycerol.

The graph in Fig 52 shows the force and the relative stress needed to extend the film of PVA:XG 65:35 added with glycerol. The return curve shows the presence of a hysteresis cycle caused by a loss of elasticity during the elongation that was recovered after few seconds of force application. This indicate the elastic properties of the film. The elasticity of this sample results significant higher compare with the elasticity of previous sample (film without glycerol).

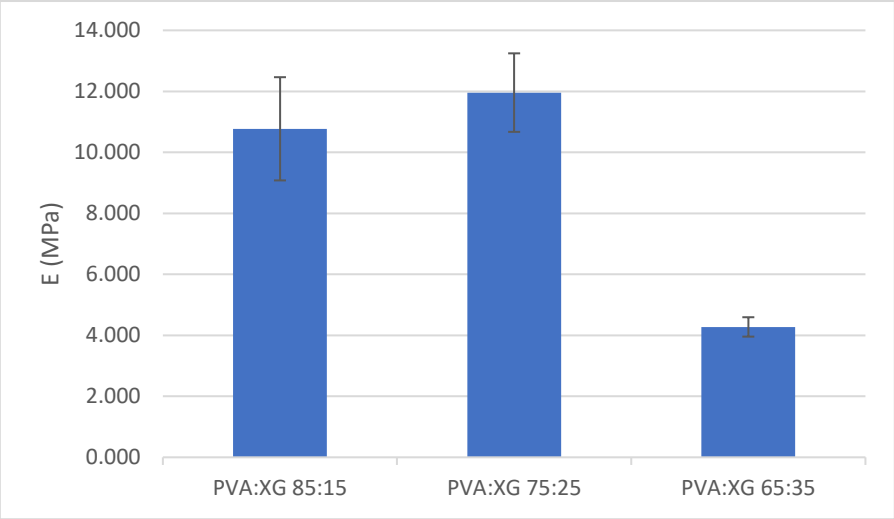

Fig. 54 Comparison between Young's modulus for films of PVA:XG at different ratios added with glycerol. Film PVA:XG 65:35 results the most promising and a statistically significant difference can be observed between this sample and the others (student t-test, p value 0.05, n=3)

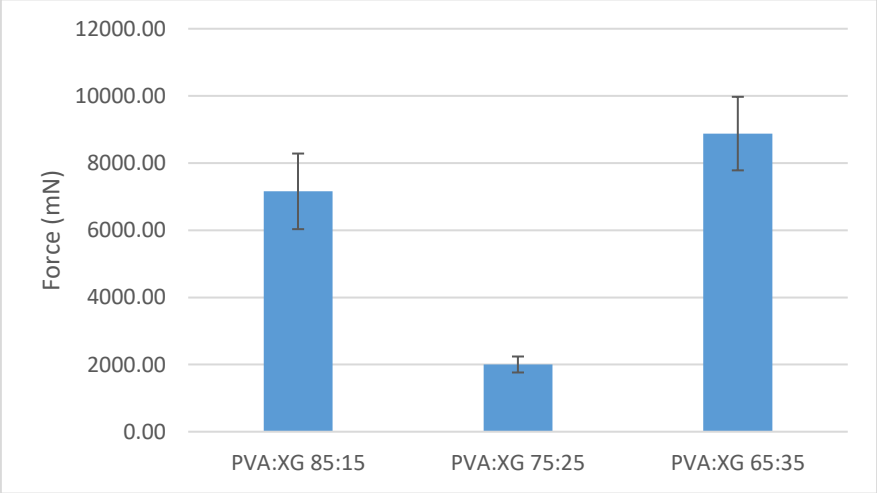

Fig. 55 Fig. 55: Comparison among Force (mN) until sample breaking of films of PVA:XG in different ratios added with glycerol. Film PVA:XG 65:35 with glycerol results the most promising.

The results of Young's modulus study (Fig. 54) show that the film obtained from mixture at 3% of PVA:XG 65:35 added with 1% of glycerol, compared to the other two films (from mixtures at 3% of PVA:XG 85:15 and 75:25, added with glycerol), is the less stiff and the better adaptable to the anatomic shape of the wound area. Nevertheless, the Force needed to break the sample by elongation is higher for film of PVA:XG 65:35 added with glycerol (Fig. 55). Thus, this sample resulted the most promising and was chosen as conclusive formulation to load probiotics.

Probiotics concentration in film

Starting from a suspension of $4*10^7$ CFU/ml and diluting 1:1 with the polymer mixtures, we obtain a concentration of $2x10^7$. During the casting process, the mean bacterial abatement in Log_{10} is 0.61 with a mean percentage of survival of 25.6%. The film, obtained starting from 20ml of mixture will contain $20 * 2x10^7 x \frac{25}{100} = 10^8$ CFU.

The film weighs about 0.8g (± 3.5%) after casting, thus the probiotic concentration in the polymer network is about $1.25x10^8$ CFU/g.

4.3.3.4 Characterization of film loaded with nanoemulsion

Guar Gum is completely soluble in water, especially in hot water, but blended together with XG a difficult in solubilization occurs, thus GG was used only to prepare film loaded with nanoemulsion. A precipitation occurs blending PVA, XG and NE probably due to interaction among the carboxylic group of XG and the amino groups of chitosan.

Polymer mixtures of PVA and guar gum (GG) at various total polymers concentrations (4%, 4.5%, 5%, 10% w/v) were tested. A total concentration lower than 5% results in an inadequate viscosity to obtain films with a thickness about 100µm, considered a target by comparison with commercial film. A total concentration of 10% results in films that entrapped air bubbles during the solvent casting.

Mixtures of PVA and guar gum (GG) at 5% and in different ratios of PVA:GG (85:15, 75:25 and 65:35) were prepared. Glycerol 1% was added as plasticizer to improve the elasticity of the resulted film, in according with Tab. 17 of Methods.

Thickness of films at different ratios of PVA:GG added with glycerol both unloaded and loaded with NE was measured and data are reported in Tab. 25 and 26.

FILM	↕ **µm** (mean±sd)
PVA:GG 85:15	103.50 (±14.82)
PVA:GG 75:25	89.00 (±5.60)
PVA:GG 65:35	117.25 (±73.83)

Tab. 25 Thickness of PVA:GG film added with glycerol.

FILM WITH NE	↕ **µm** (mean±sd)
PVA:GG 85:15	156.25 (±12.28)
PVA:GG 75:25	130.25 (±17.06)
PVA:GG 65:35	144.25 (±6.08)

Tab. 26 Thickness of PVA:GG film added with glycerol and NE.

Only the sample at 5% of PVA:GG ratio 85:15 was employed because the polymers in the starting mixture was completely dissolved and the resulting film presented a regular structure and surface compare to the others.

Elasticity of films

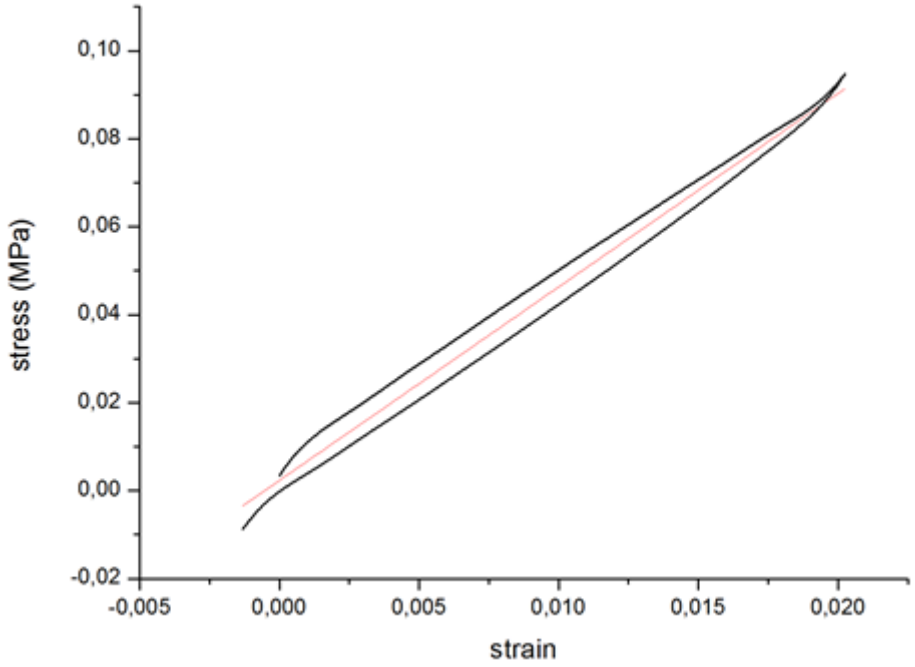

Fig. 56 Stress/strain curve of film sample of PVA:GG 85:15 with glycerol. The linear fit (red) represent the slope of the curve.

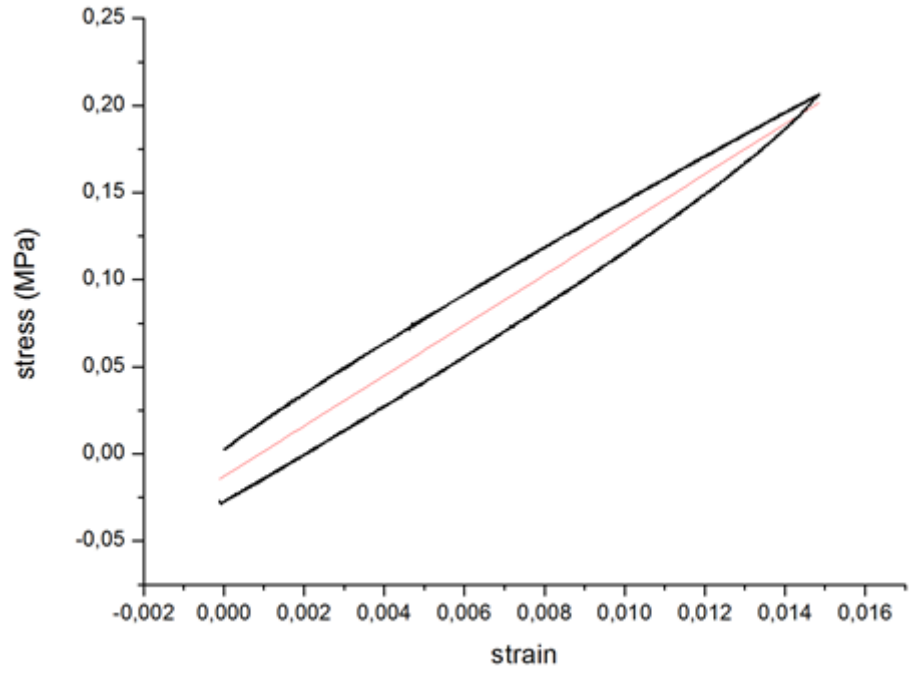

Fig. 57 Stress/strain curve of film sample of PVA:GG 85:15 with glycerol and loaded with NE. The linear fit (red) represents the slope of the curve.

The graphs in Fig. 56 and 57 show the force and the relative stress needed to extend the film of PVA:GG 85:15 added with glycerol and the film of PVA:GG 85:15 added with glycerol an NE, respectively. The return curve shows the presence of a hysteresis cycle caused by a loss of elasticity during the elongation that was recovered after few seconds of force application. This indicate the elastic properties of the film.

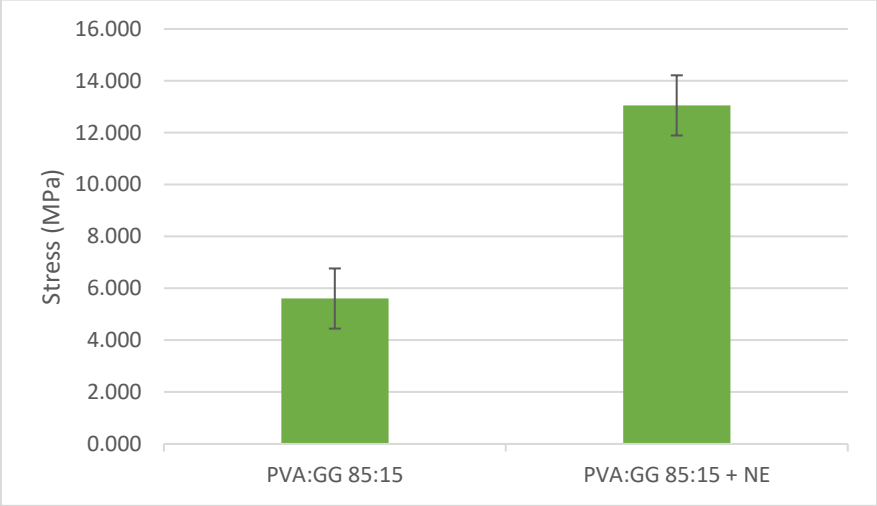

Fig. 58 Comparison between Young's modulus for films of PVA:XG 85:15 added with glycerol both with or without NE . Film loaded with NE results more strength and a statistically significant difference can be observed between this sample and the unloaded one (student t-test, p value 0.05, n=3)

The film of PVA:GG ratio 85:15 added with glycerol results elastic with a Young's modulus similar to that of the probiotic pilot film (PVA:XG 65:35 added with glycerol). At solid state, a significant increase of stiffness in films after addition of NE was observed (Fig. 58) (student t-test, p value 0.05, n=3), probably due to the strength effect of nanoparticles in the polymer network. Thus, NE affects the stiffness like any other included filler in polymer composite.

Antioxidant concentration in film

The concentration of α-tocopherol in the colloidal system is about 300µg/ml. After addition of polymers and glycerol, the obtained mixture was subjected to solvent casting and a homogeneous distribution of the nanodroplets in film is expect, in according to the CLSM analysis. A film obtained from 20ml of mixture will contains about 1.2g of polymers and glycerol and about 1.16mg/ml of organic molecules related to the nanoemulsion compounds. Thus, the theoretical weight of obtained film is 1.223g. By weighing the films, our samples diverge from the theoretical weight ±6.5%. The calculated theoretical concentration of α-tocopherol in film is 5µg/mg.

Franz cell release study on NE loaded film

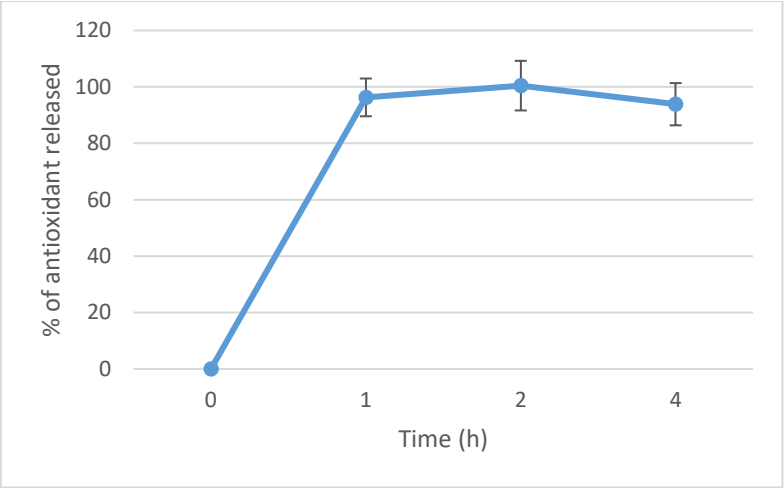

Fig. 59 Percentage of antioxidant released from film (PVA:GG 85:15 + glycerol and NE) during time (mean±sd, n=3).

The antioxidant was completely released from the formulation in 1 hours (Fig. 59). Then a slight decrease in concentration occurs probably due to oxidation of α-tocopherol. The formulation in the donor chamber results completely dissolved at the end of the test. In conclusion, the hydration of the film leads to the occurrence of a semisolid capable of protecting wounds and delivering antioxidant in damaged tissue.

Laser Scanning Confocal Microscope analysis (CLSM)

By means of CLSM analysis a regular distribution of NE in the polymer matrix of the film can be observed (Fig. 60). This confirms the good ability of the chitosan oleate nanoemulsions to be homogeneously dispersed in aqueous environment. This property is important to prepare homogeneous samples, but also, as previously demonstrated, to improve α-tocopherol release in finely dispersed form. This in turn can positively affect the interaction with the biological substrates like the humid environment of wounds.

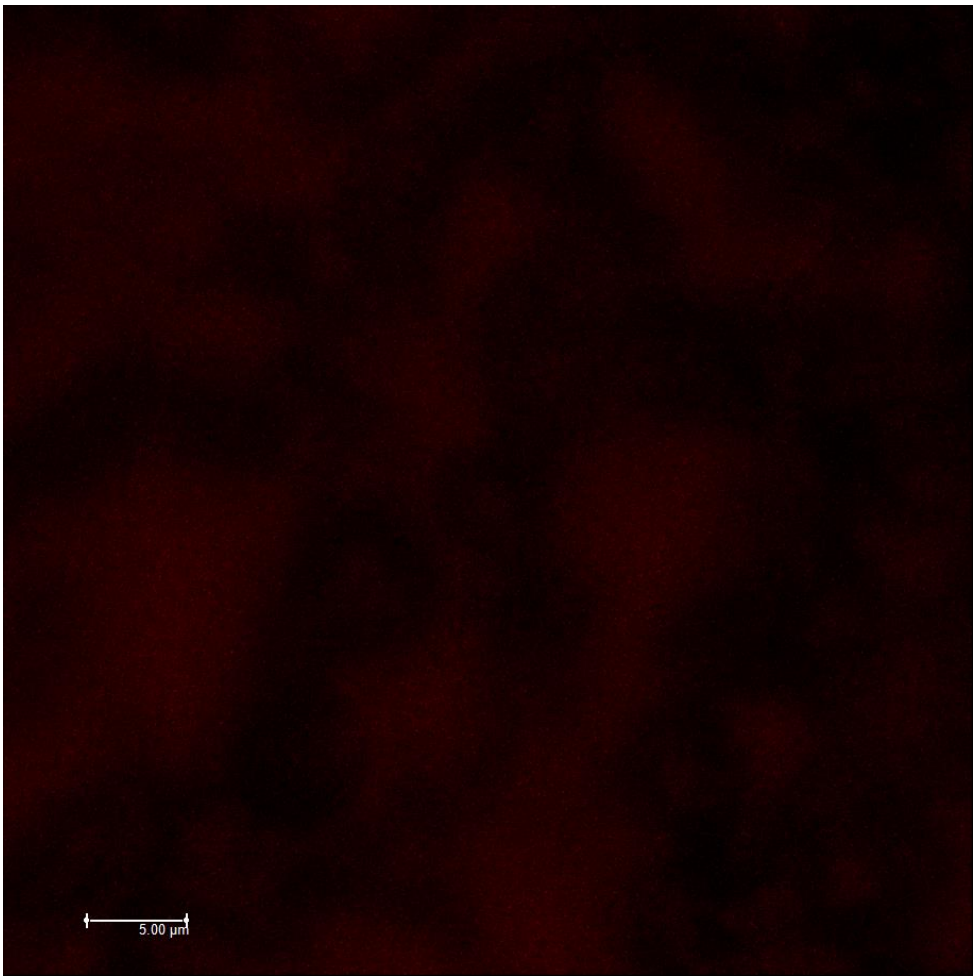

Fig. 60 CLSM micrograph of a film (PVA:GG 85:15 with glycerol) embedding NE loaded with a fluorescent dye (Nile Red).

4.3.3.5 Hydration properties, bioadhesion properties, SEM and DSC of lyophilized dressings and films

Evaluation of the hydration properties of lyophilized dressing and films

The water uptake characterization shows a weight gain of 96.17±10%, after 60 seconds of contact with the saline solution for lyophilized of PVA:XG 75:25 added with glycine and loaded with *L. plantarum*. Film of PVA:XG 65:35 added with glycerol and loaded with *L. plantarum* shows a weight gain of 57.35±10,40 after 60 seconds of contact with the saline solution, indicating a good absorption capacity. The same profile was observed for the film of PVA:GG 85:15 added with glycerol and loaded with NE that show a weight gain of 63.99±1,2%. The higher absorption capacity of lyophilized dressing, with values statically significant different from the other formulations (student t-test, p value 0.05, n=3) starting from 1 minute of contact (Fig. 61), can be attributed to the peculiar porous structure of this kind of dressings.

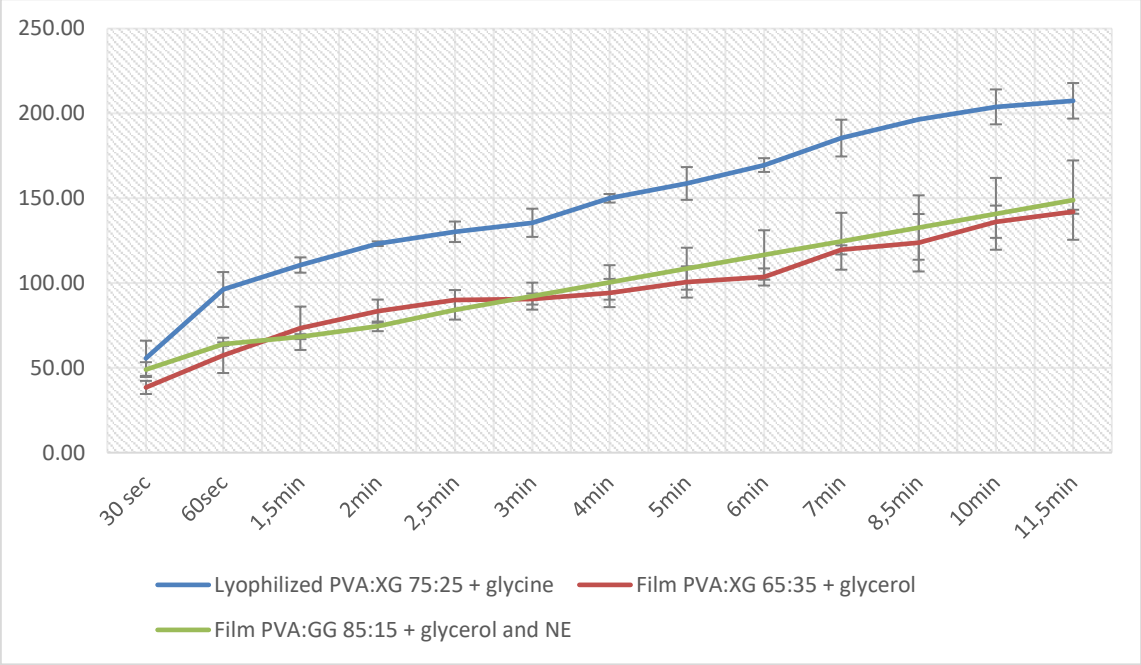

Fig. 61 percentage of weight gain by means of water uptake test for different formulations: lyophilized PVA:XG 75:25 + Gly, film PVA:XG 35:65 + glycerol, film PVA:GG +glycerol and NE (mean±sd).

Bioadhesion properties of lyophilized dressing and films

Lyophilized of PVA:XG 65:35 added with glycine, film of PVA:XG 65:35 added with glycerol and loaded with *L. plantarum*, film of PVA:GG 85:15 added with glycerol and NE, show a positive bioadhesion behavior, with detachment force values in the range of 150-250mN (Fig. 62). Positive bioadhesion/mucoadhesion, less relevant for the application on skin wounds, is however a useful property in case of application to wounded mucosae such as for example buccal lesions due to radio-chemotherapy, or aftae. This makes the developed formulations a flexible and versatile instrument to treat different kind of lesions.

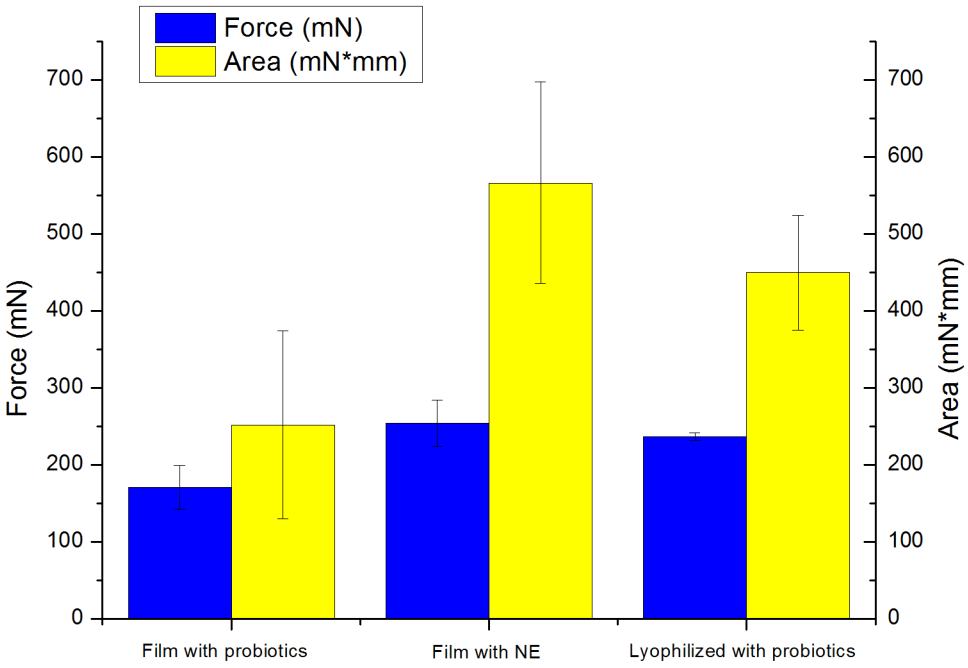

Fig. 62 Bioadhesion properties (Force, Area) of different formulations (from left: film PVA:XG 65:35 + glycerol, film PVA:GG 85:15 + Glycerol and NE, lyophilized PVA:XG 75:25 + Gly) (mean±sd, n=3).

Electronic Scanning Microscopy (SEM) of lyophilized dressings and films

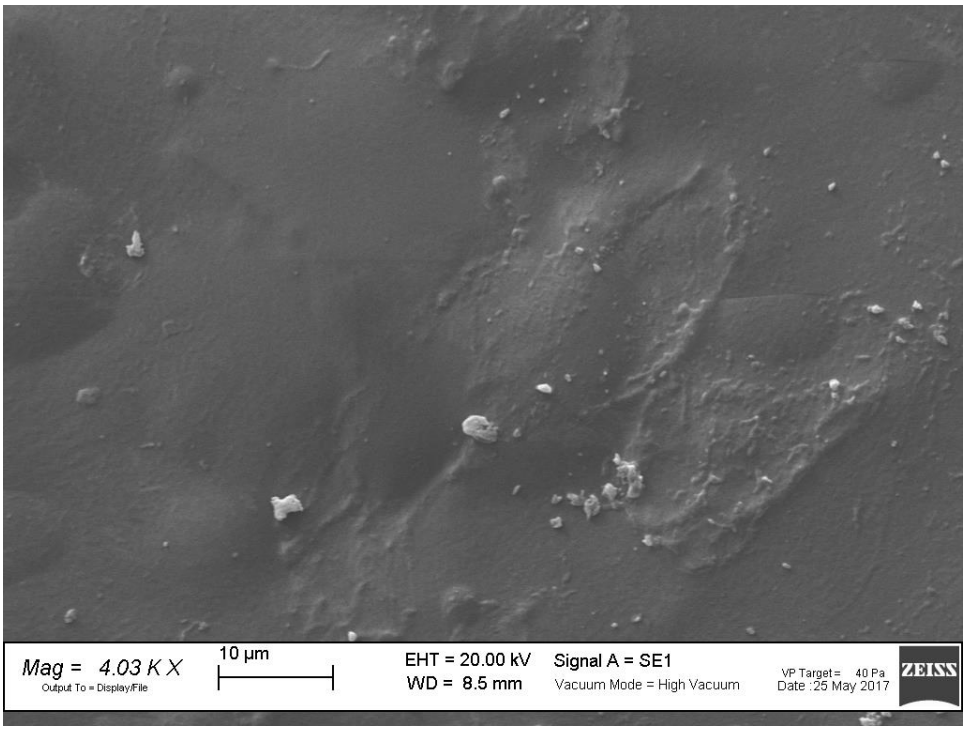

Fig. 63 SEM Micrograph of the film surface (3% of PVA:XG 65:35 added with glycerol).

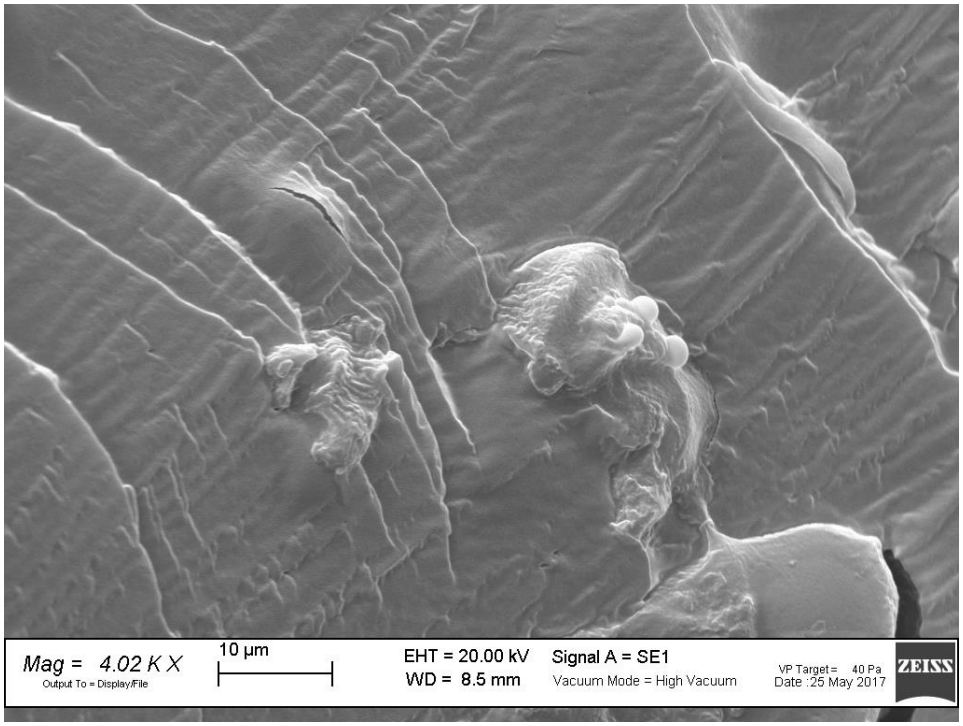

Fig. 64 SEM Micrograph of the film section (3% of PVA:XG 65:35 added with glycerol).

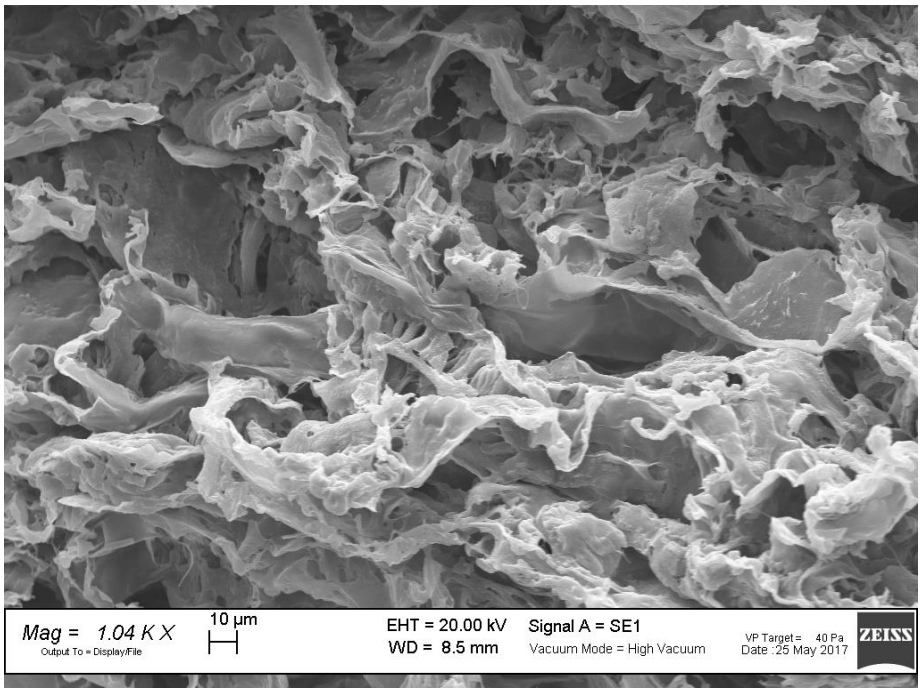

Fig. 65 SEM Micrograph of the surface of lyophilized (3% PVA:XG 75:25 + gly) loaded with probiotic 1.6x10^8 CFU/g.

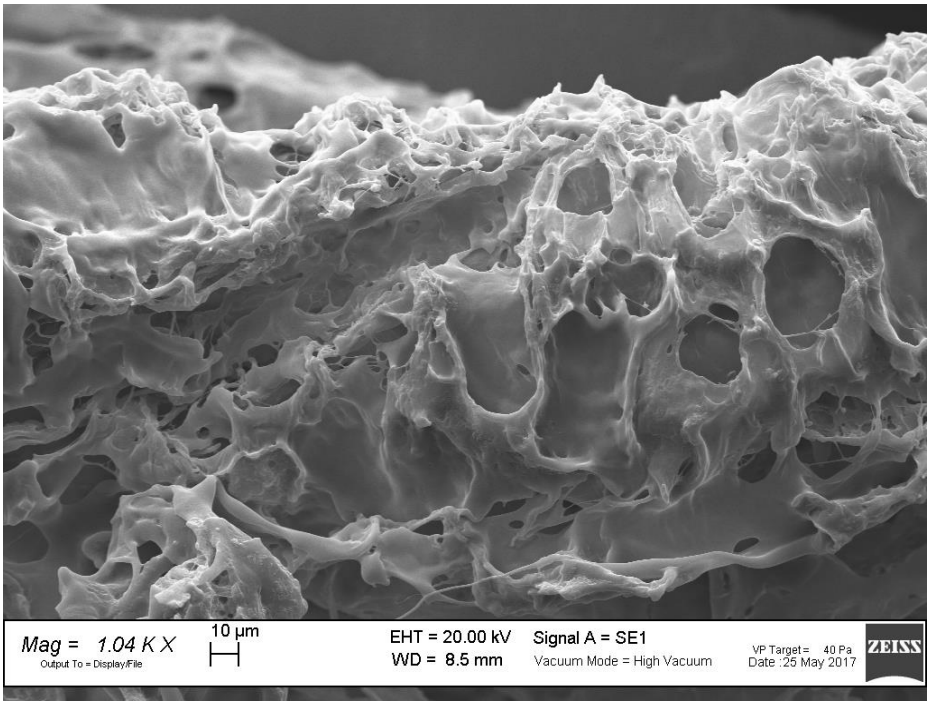

Fig. 66 SEM Micrograph of the section of lyophilized (3% PVA:XG 75:25 + gly) loaded with probiotic 1.6x10^8 CFU/g.

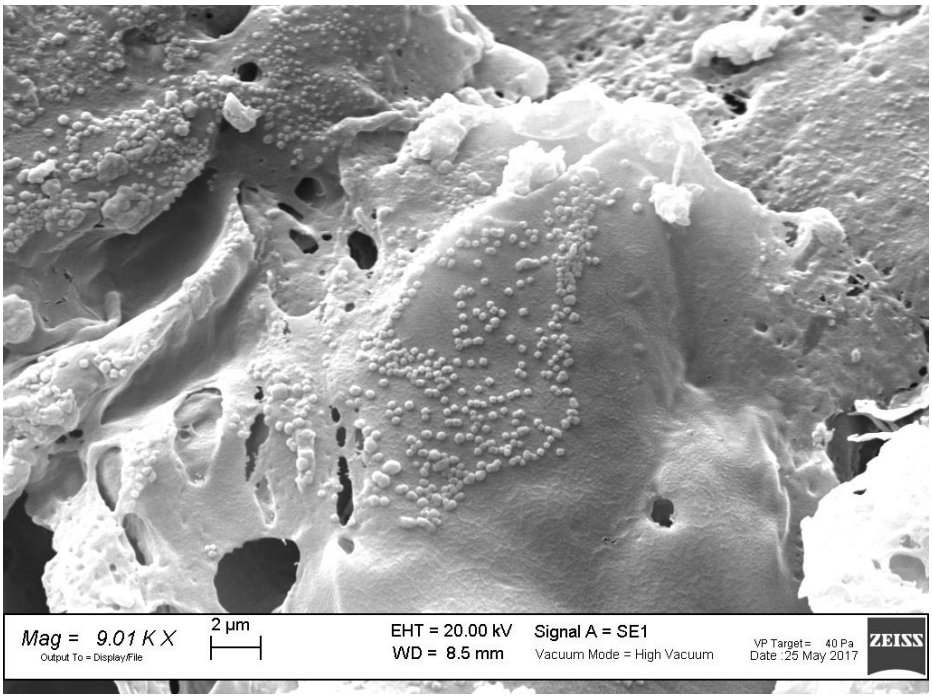

Fig. 67 SEM Micrograph of a details of the probiotic loaded film surface (3% of PVA:XG 65:35 added with glycerol and loaded with $1.25x10^8$ CFU/g of L. plantarum).

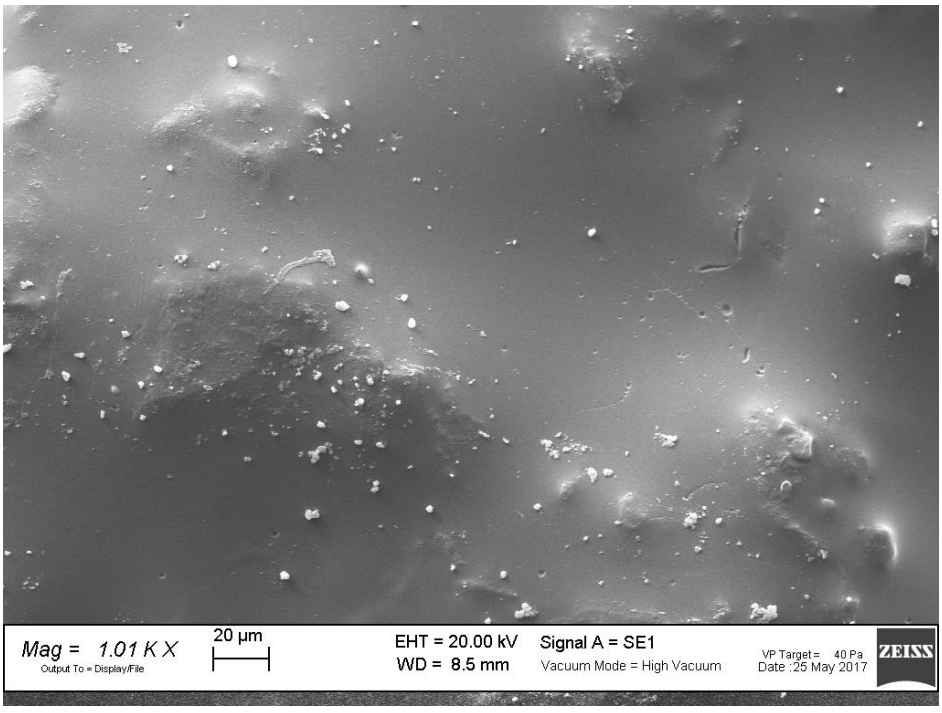

Fig. 68 SEM Micrograph of the film surface (5% of PVA:GG 85:15 added with glycerol and loaded with NE)

SEM images show the surface of films (PVA:XG 65:35 + Glycerol) both unloaded (Fig. 63) and loaded (Fig. 67) with *L. plantarum*. It can be noted, in the film loaded, the presence of a surface roughness and rounded shapes that could be caused by presence of microorganisms.

Fig. 65 shows a SEM image of the surface of lyophilized (PVA:XG 75:25 + Glycine) loaded with *L. plantarum*. The porosity characterizing the lyophilized is clearly visible compared to the compact structure of the film. Fig. 66 shows a SEM image of the section of lyophilized loaded with *L. plantarum.*

Fig. 68 shows a SEM image of the surface of film (PVA:GG 85:15 + Glycerol) loaded with nanoemulsion that appear smooth and particularly compact.

Differential Scanning Calorimetry (DSC) of lyophilized dressings and films

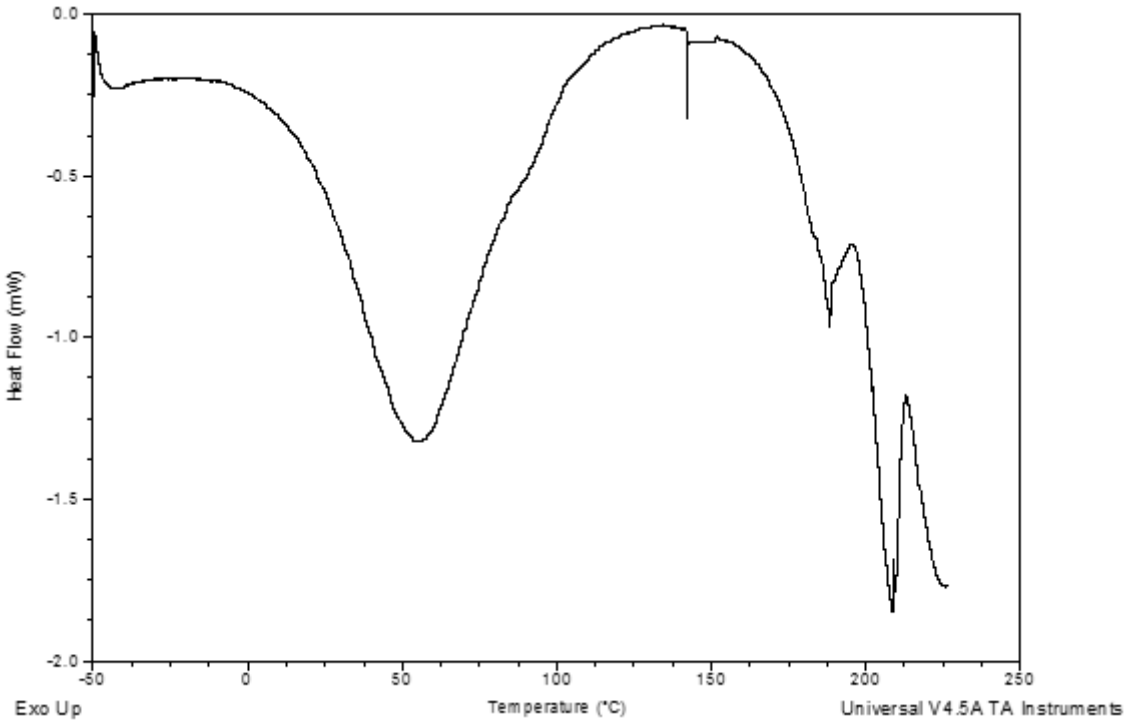

Fig. 69 DSC of lyophilized (PVA:XG 75:25) with glycine.

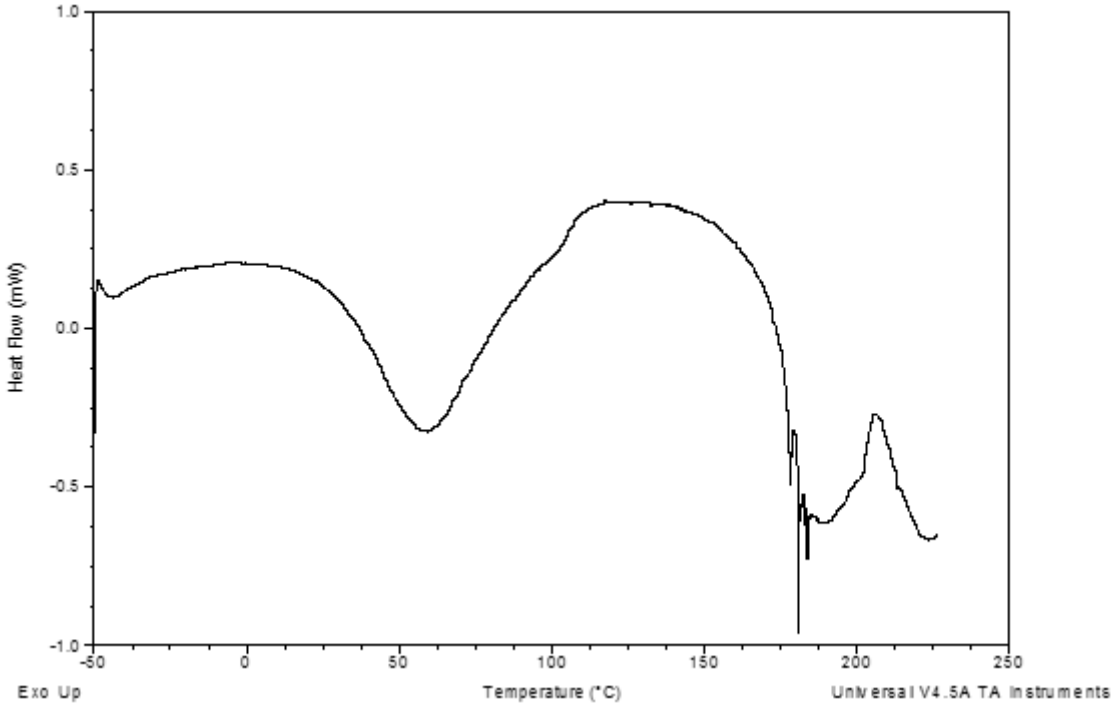

Fig. 70 DSC of lyophilized (PVA:XG 75:25) with glycine and loaded with L. plantarum at $8x10^6$ CFU/g.

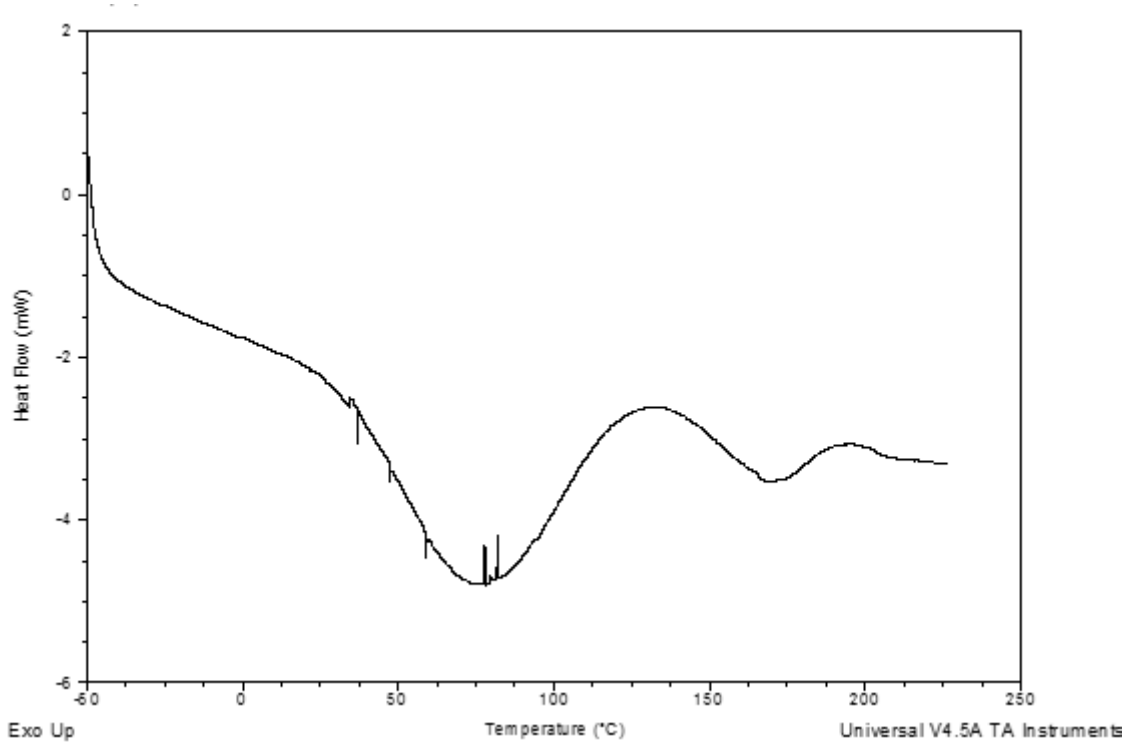

Fig. 71 DSC of film (PVA:XG 65:35) with glycerol.

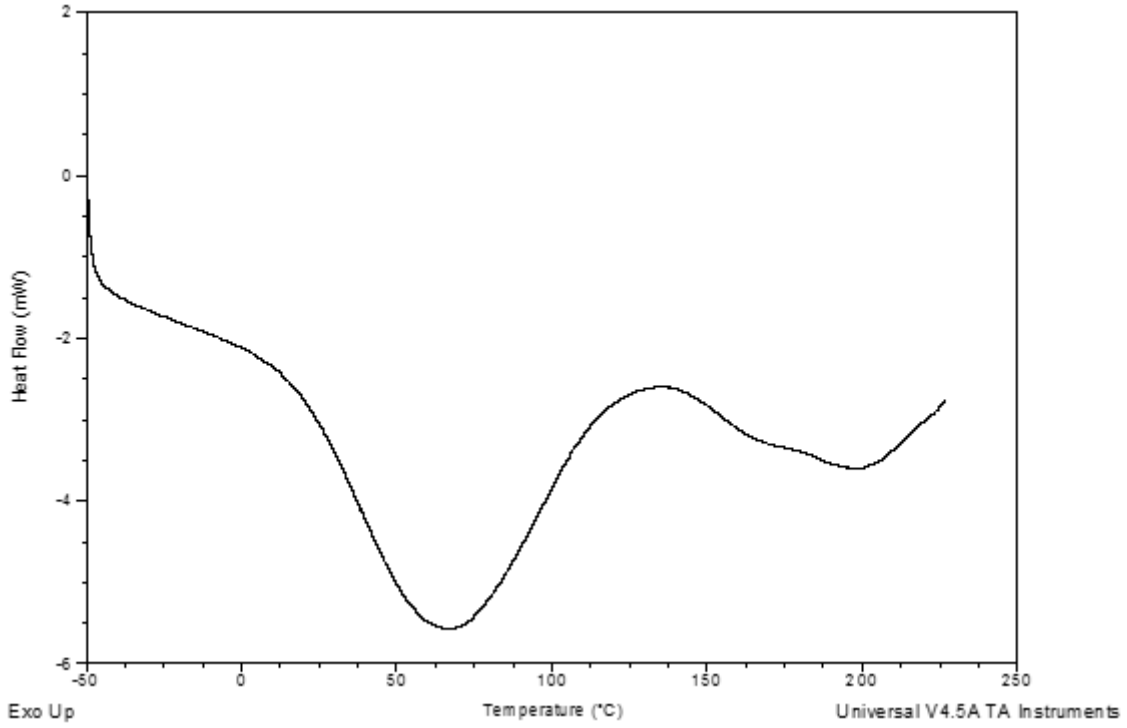

Fig. 72 DSC of film (PVA:XG 65:35) with glycerol and loaded with L. plantarum at 1.6x10^8 CFU/g.

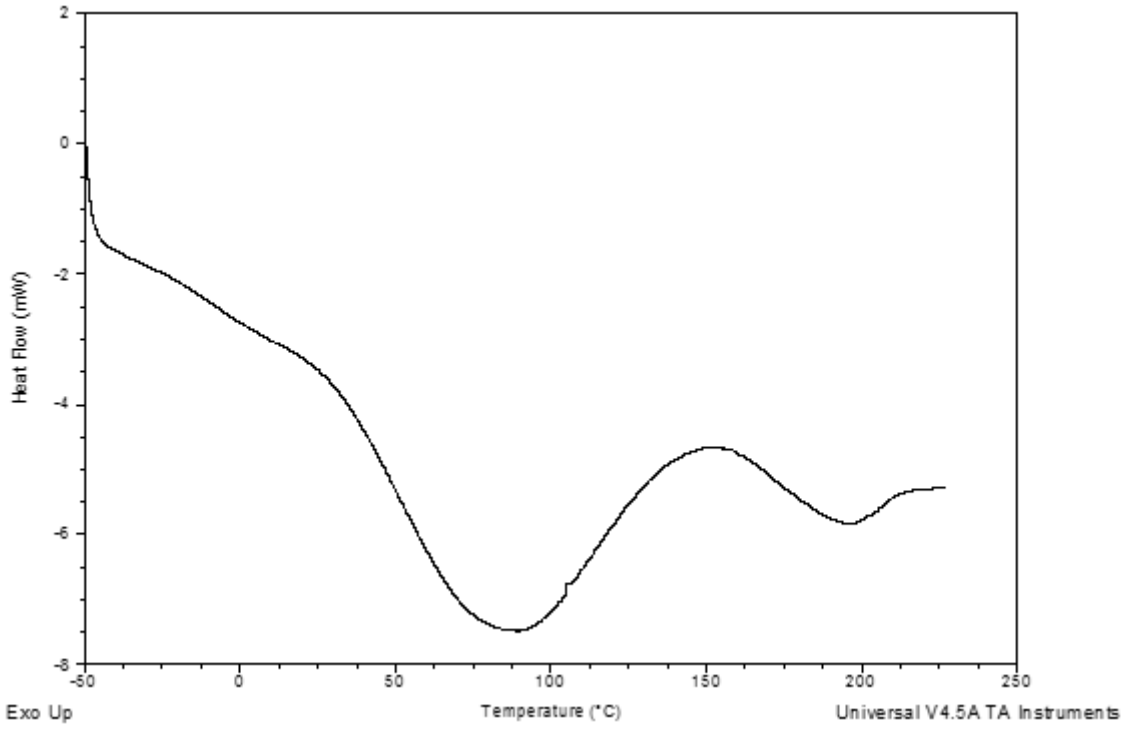

Fig. 73 DSC of film (PVA:GG 85:15) with glycerol 1% and loaded with NE.

DSC curves show a first peak (70°C) indicating the loss of water. The second relaxation between 170°C and 220°C is due to melting of crystalline domains of PVA. (Campos, A. et al., 2011) In our samples, the glass transition of PVA at 85°C cannot be observed because of the overlapping with the broad signal at 90-95°C caused by the water loss from PVA, XG and GG.

The peaks related to the water loss in the lyophilized dressings seem different from those observed in the films. This could be ascribed to the different drying process, freeze-drying or solvent evaporation, as a lower percentage of water residue is obtained in lyophilized dressings. On the other hand, the DSC curves of the lyophilized dressings differ probably for the different surface area of the samples, which lead to a different amount of residue water (Fig. 69 and 70).

About the films, an additional peak (170°C) was observed in the film loaded with probiotics (Fig. 72) compared to the unloaded one (Fig. 71). Furthermore, a shift of the peak of melting of PVA is observed in the sample loaded with probiotics (Fig. 72).

In the film loaded with nanoemulsions (Fig. 73), a shift in the PVA melting could be observed. In literature is reported a shift of the melting peak of PVA due to interaction with glycerol in mixtures. (Allam M. et al., 2013)

The presence of water in films is confirmed by SEM micrograph illustrated in Fig. 74 that shows fractures on the surface when the electron beam hits the sample causing a sudden water evaporation.

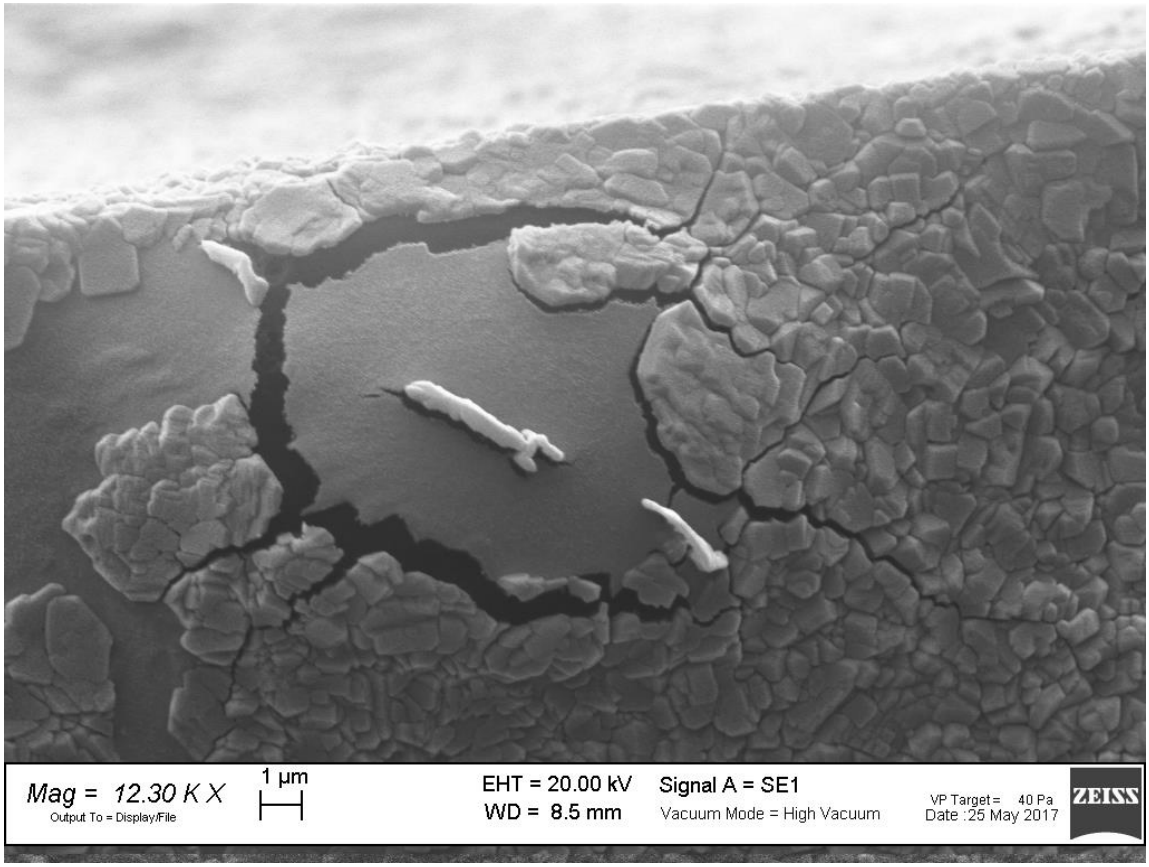

Fig. 74 Sample details of a PVA:XG film fracture during the SEM analysis.

4.3.3.6 Biological evaluation

Probiotics compatibility assessment in polymer mixtures

In Tab. 27 the results of microbiological tests performed on polymer mixtures based on PVA:XG ratios (from 85:15 to 65:35) are given. Polymer mixtures seem to support the probiotics viability. In particular, after several hours of contact, the mixtures seem to promote the probiotics vitality compared to the control, probably due to the prebiotic effect of the xanthan gum.

After 24 hours, the survivals CFU were higher in sample containing the higher concentration of gum 73.8%±10.3, compare to the other sample 34.8%±9.3 and to control in aqueous suspension 12.2%±1.6 (n=2).

Time of contact	Sample	% of survival CFU
T0	A	112.4±7.4
T3h	A	154.7±33.0
T6h	A	73.8±10.3
T24h	A	95.2±1.6
T0	B	87.2±13.4
T3h	B	34.8±9.3
T6h	B	118.7±5.4
T24h	B	63.6±2.8

Tab. 27 Mean (n=3) viability of probiotics in sample A (mixture PVA:XG 85:15) and in sample B (mixture PVA:XG 75:25).

Viability and stability of probiotics in lyophilized dressing and films

The method of preparation of the formulations, solvent casting or lyophilization, seems to affect in a different manner the probiotics survival, as it was expected.

Immediately after preparation, the survival L*. plantarum* in films of PVA:XG 65:35 added with glycerol is 25.6%±8.8 (n=3), respect to the control, the survival in the lyophilized dressing of PVA:XG 75:25 added with glycine, was 35.0%±2.3 (n=3). The increase of survival in lyophilized formulation is significantly higher compared to the film.

Time (days)	% of survival CFU
Samples at 7 days (n=2)	
Film PVA:XG 65:35+glycerol	12.2%±0.3
Lyophilized PVA:XG 75:25+gly	26.9%±6.7
Samples at 14 days (n=2)	
Film PVA:XG 65:35+glycerol	11.2%±1.2
Lyophilized PVA:XG 75:25+gly	18.7%±0.7

Tab. 28 Viability of L. Plantarum after 7 and 14 days of storage at 4-6°C (mean±sd, n=2).

Stability evaluation at 7 and 14 days, respect to the control in aqueous suspension, (at 4-6°C) shows a significant reduction in the vitality of probiotics with a higher survival capability in lyophilized formulations (Tab. 28).

Release of probiotic from formulation to simulant wound fluid

Lyophilized dressings and films were assessed for their probiotics release profile. The large amount of probiotics were released in the simulant wound fluid in about 1 h, as illustrated in fig. 75a.

In fig. 75b the concentrations are represented in Log_{10} scale. The lyophilized seems to release *L. plantarum* slightly faster, at 30 minutes, compared to films. At 6 h, a marginal decrease in concentration of live microorganisms can be observed probably due to the abatement of probiotics.

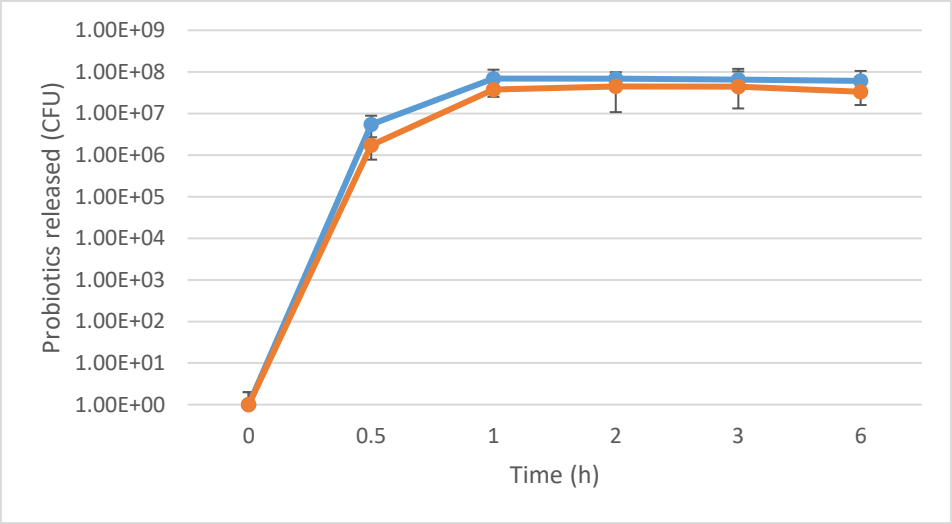

Fig. 75 a Concentration of L. plantarum released from lyophilized and film at different times. (mean±sd, n=3)

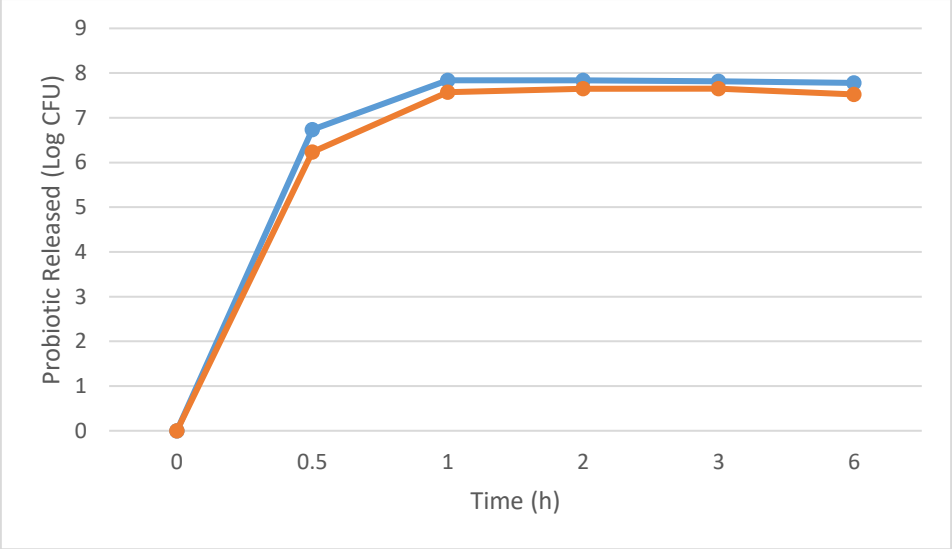

Fig. 75 b Concentration of L. plantarum released from lyophilized and film at different times in Log scale. (mean, n=3)

In vitro test on fibroblasts

Fig. 76 shows the viability of the fibroblast cells after exposure for 24h to the developed formulations (film loaded with probiotics, film loaded with NE and lyophilized dressing loaded with probiotics), compared with the viability in complete medium. A percentage of viability higher than 50% is considered a good target to evaluate the sample biocompatibility. All the tested formulations result biocompatible based on this test, although a certain decrease in fibroblast viability is probably due to the effect of gums that after dissolution come in contact with cells by passing through Transwell pores and are likely to affect gas/water cell exchange.

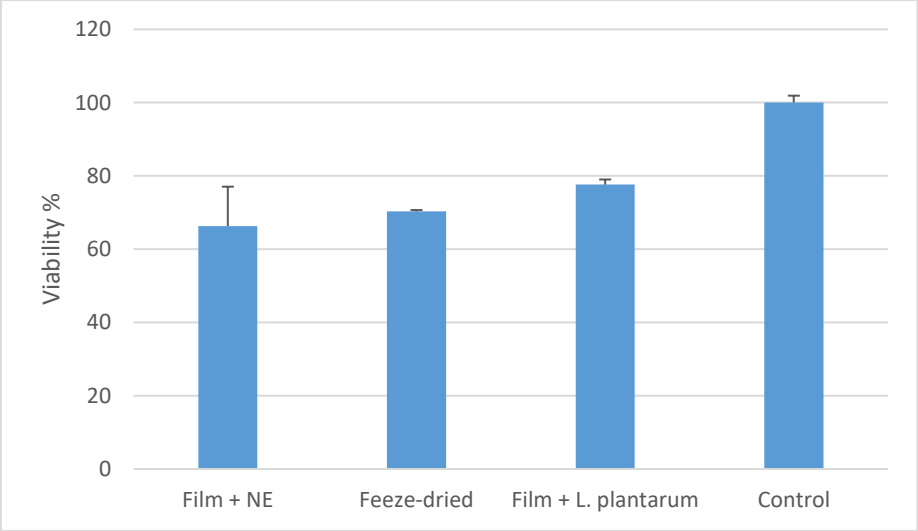

Fig. 76 Results of viability (%) test on fibroblast culture exposed to different formulations (mean±sem).

4.3.3.7 Composite films with polyurethane backing

To further improve the mechanical resistance properties of the films and the application to skin wounds, a polyurethane backing was used as support.

The high porosity of the polyurethane support, well visible from the SEM microphotographs (Fig. 77 and 78), allows gas/liquid exchange, essential to a non-occlusive medication. The mixtures can be poured directly on this support and can be submitted to solvent casting. Preliminary experiments confirmed the possibility to obtain a film compenetrated in the polyurethane backing.

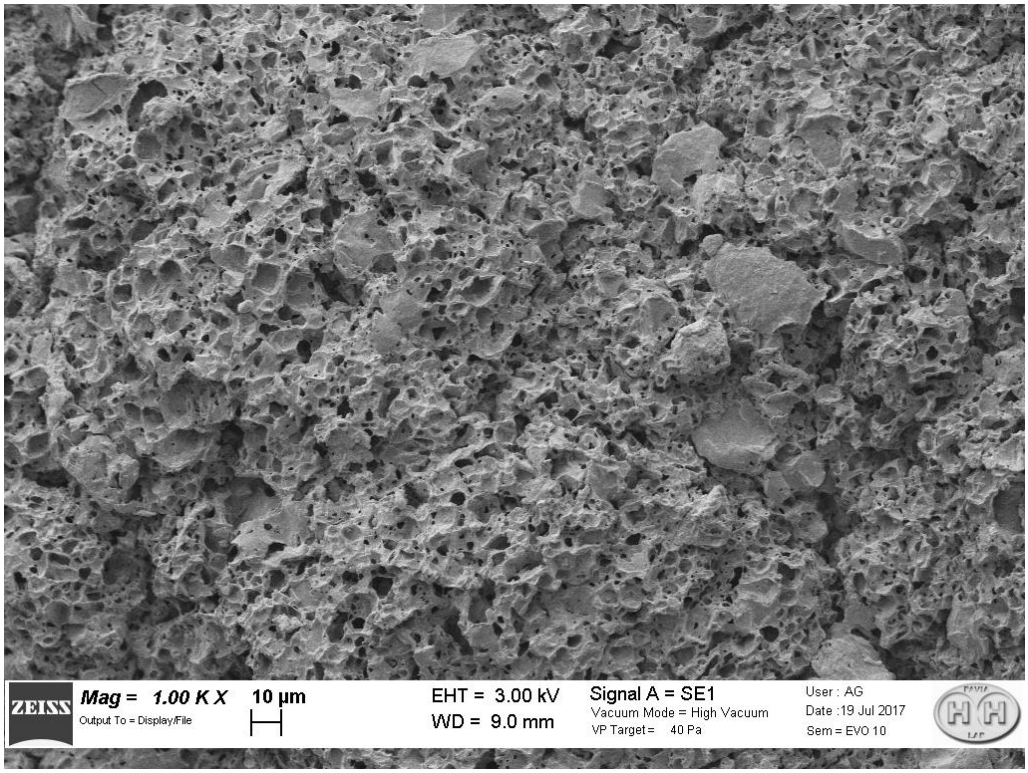

Fig. 77 SEM micrograph of the polyurethanes backing for films.

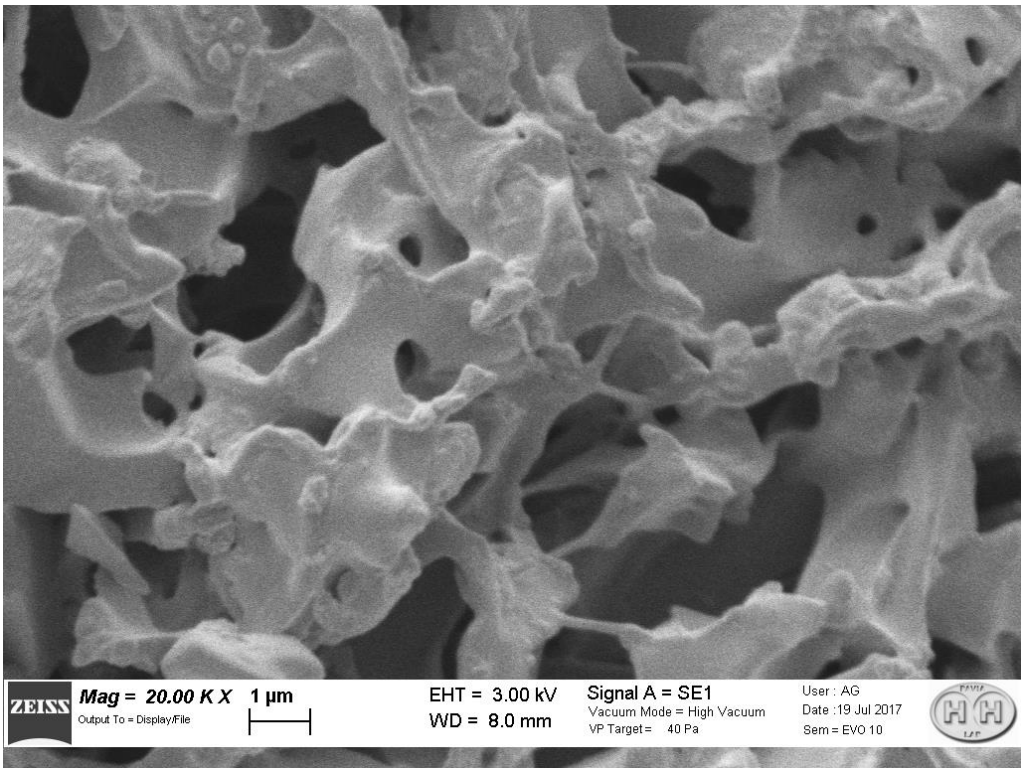

Fig. 78 SEM micrograph detail of the polyurethanes backing for films.

4.3.4 CONCLUSIONS - SECTION TWO

Film properties

Films, loaded with either nanoemulsion or probiotics, and lyophilized dressings loaded with probiotics have been prepared. Polymers (PVA, XG and GG) and glycerol, employed to prepare the formulations, proved biocompatible with *L. plantarum*.

Films made of blends of PVA xanthan gum or guar gum were able to embed both nanoemulsions and probiotics. The addition of glycerol as a plasticizer increased the elasticity of both types. Gums are effective as prebiotics and further improved film elasticity. Films resulted suitable for application to skin wounds as for elasticity, tensile strength and anatomic adaptability.

Lyophilized dressing properties

The lyophilized dressings showed good mechanical strength and high porosity and therefore a high surface area. The viability and growth of probiotics in lyophilized dressing was significantly improved with respect to films and the hydration capacity significantly faster due to their highly porous structure.

Common features

In vitro release profile of probiotics was satisfactory and this should facilitate wound healing, due their foreseen antibacterial effect by competition with any possible pathogens present in the injured tissue (Ramos A. N. et al., 2012; Ramos A. N., et al. 2015). Release studies on films suggest that the antioxidant could be made available the wound fluids already within one hour. Stability studies suggest that formulations can be stored at 4-8 ° C for 14 days, while maintaining a significant amount of viable probiotics.

S.E.M. microphotographs show that both films and dressings possess a regular polymeric structure. CLSM microphotographs indicate a fine and regular distribution of nanoemulsions inside the polymeric network. *In vitro* evaluation on human fibroblasts indicate a good biocompatibility of the formulations.

Both formulations exhibit positive bioadhesion properties which is compatible with possible topical application even on wounded mucosa. Due to the hydration properties, they are also promising for effective moisturizing medication, of absorbing exudates and forming a semi-solid barrier on the wound. Furthermore, the medications should be easily removed, thus reducing pain.

Unfortunately, *L. Plantarum* was found to be incompatible with the simultaneous presence of nanoemulsions, likely due to the antibacterial effect of chitosan, which resulted in a significant microbial abatement.

Poster presentation related to Section Two:

“Lyophilized dressings and films loaded with lactobacillus plantarum intended for skin treatment.” Accepted for presentation (registration number 72H3H-MMFUI-W44G8-8W747-S4CG7) at the PBP World Meeting, Granada (Spain), March 19-22, 2018.

5. GENERAL CONCLUSIONS

According to the aim of the work, the following results were reached.

- medicated dressings containing an antioxidant able to release the drug timely and efficiently in order to restore the oxidative balance thus improving the wound healing process;
- films and dressings capable of maintaining the viability of probiotics and assure their release to wounded tissues.

Future perspectives

An advanced medication prototype was obtained by casting the semi-solid blends, loaded with either nanoemulsions or probiotics, on a highly porous polyurethane support, acting as a backing.

This advanced formulation will be tested in vivo on animals. It is believed that the films incorporating probiotics could represent an innovative, user friendly and low-cost medication tool for *infected wounds.*

On the other hand, given the encountered incompatibility between nanoemulsions and probiotics, a composite medication, separately embedding antioxidant-containing nanoemulsions and probiotics, will be developed as an innovative multifunctional medication for skin lesions complicated by oxidative stress.

Acknowledgments

Firstly, I would like to express my sincere gratitude to my tutor Prof. Carla Marcella Caramella for the continuous support of my PhD study and related research, for her cordiality and immense knowledge. Her guidance helped me all the time in research and writing of this thesis. I could not have imagined having a better advisor and mentor for my PhD study.

Besides my advisor, I would like to express distinct thanks to Prof. Maria Cristina Bonferoni[1] for giving her precious scientific input to my research project and continuously tutoring my lab work. I'd also thank Prof. Cinzia Boselli for supporting of my PhD related research, in particular in vivo studies on animals.

My special thanks also go to Prof. Rita Palmeira de Oliveira[3] for providing the opportunity to join her team as PhD visiting student, and generously giving access to her laboratory and research facilities.

My sincere thanks also go to Dr. Giorgio Marrubini[1], Dr. Federica Riva[2], Dr. Antonia Icaro Cornaglia[2], Prof. Piercarlo Mustarelli[4], Prof. Giovanna Bruni[4], Prof. Vittorio Berbenni[4], Prof. Pietro Grisoli[1], Dr. Silvia Malacrida[1], Prof. Daniele Dondi[5] and Dr. Simone Lazzaroni[5] for their significant support to the experimental part.

I thank my fellow labmates for helping me in the lab work. In particular, I am grateful to Dr. Fabio Invernizzi[4] for the effective and valuable collaboration.

Last but not least, I would like to thank my parents for generously supporting me in all circumstances.

1 - Department of Drug Science, University of Pavia, Pavia, Italy.

2 - Department of Public Health, Experimental and Forensic Medicine, Histology and Embryology Unit, University of Pavia, Pavia, Italy.

3 - Centro de Investigação em Ciências da Saúde, University of Beira Interior, Covilha, Portugal.

4 - Department of Physical Chemistry, University of Pavia, Pavia, Italy.

5 - Department of Chemistry, University of Pavia, Pavia, Italy.

6. BIBLIOGRAPHY

Abdelwahed W. et al. ***Freeze-drying of nanoparticles: Formulation, process and storage considerations.*** Advanced Drug Delivery Reviews 58 1688-1713 (2006)

Allam M et al. ***Physical Properties of PVA Doped with Algal Glycerol.*** J. Appl. Polym. Sci. 130: 4482–4489 (2013)

Andrews K.L. et al. ***Wound management of chronic diabetic foot ulcers: From the basics to regenerative medicine.*** Prosthetics and Orthotics International 39(1) 29-39 (2014)

Arda O. et al. ***Basic histological structure and functions of facial skin.*** Clinics in Dermatology 32 3–13 (2014)

Ashcroft G.S. et al. ***The effects of ageing on cutaneous wound healing in mammals.*** J. Anat. 187 1-26 (1995)

Baquerizo Nole K.L. et al. ***Probiotics and prebiotics in dermatology.*** J Am Acad Dermatol 71 814-21 (2014)

Baumbusch L.O. et al. ***Interactive effects of ozone and low UV-B radiation on antioxidants in spruce (Picea abies) and pine (Pinus sylvestris) needles.*** Physiol Plant. 104(2) 248-254 (1998)

Bele C. et al. ***Tocopherol Content in Vegetable Oils Using a Rapid HPLC Fluorescence Detection Method.*** Not Bot Horti Agrobo 41(1) 93-96 (2013)

Boateng J.S. et al. ***Wound Healing Dressings and Drug Delivery Systems: A Review.*** Journal of Pharmaceutical Sciences 97 2892–2923 (2008)

Bondet V. et al. ***Kinetics and Mechanisms of Antioxidant Activity using the DPPH• Free Radical Method.*** LWT - Food Science and Technology 30(6) 609-615 (1997)

Bonferoni M.C. et al. ***A novel ionic amphiphilic chitosan derivative as a stabilizer of nanoemulsions: Improvement of antimicrobial activity of Cymbopogon citratus essential oil.*** Colloids and Surfaces B: Biointerfaces 152 385–392 (2017)

Bonferoni M.C. et al. ***Ionic polymeric micelles based on chitosan and fatty acids and intended for wound healing. Comparison of linoleic and oleic acid.*** Eur J Pharm Biopharm. 87(1) 101-106 (2014)

Bouchemal K. et al. ***Nano-emulsion formulation using spontaneous emulsification: solvent, oil and surfactant optimization.*** International Journal of Pharmaceutics 280 241–251 (2004)

Brachkova M.I. et al. ***Alginate Films Containing Viable Lactobacillus Plantarum: Preparation and In Vitro Evaluation.*** AAPS PharmSciTech 13(2) 357-363 (2012)

Cabral M.E.S. et al. ***Formulation and quality control of semi-solid containing harmless bacteria by-products: chronic wounds pro-healing activity.*** Pharmaceutical Development and Technology 20:8 911-918 (2015)

Campos A. et al. ***Biodegradation of Blend Films PVA/PVC, PVA/PCL in Soil and Soil with Landfill Leachate.*** Braz. Arch. Biol. Technol. 54(6) 1367-1378 (2011)

Cardoso C.R. et al. ***Oleic acid modulation of the immune response in wound healing: A new approach for skin repair.*** Immunobiology 216 409–415 (2011)

Cardoso, C.R. et al. ***Oleic acid modulation of the immune response in wound healing: a new approach for skin repair.*** Immunobiology 216 409-15 (2011)

Carocho M. and Ferreira I.C.F.R. ***A review on antioxidants, prooxidants and related controversy: Natural and synthetic compounds, screening and analysis methodologies and future perspectives.*** Food and Chemical Toxicology 51 15–25 (2013)

Carocho M. et al. Castanea sativa Mill. ***Flowers amongst the Most Powerful Antioxidant Matrices: A Phytochemical Approach in Decoctions and Infusions.*** BioMed Research International pp.1-7 (2014)

Castana S. et al., ***A fast, sensitive method for the simultaneous determination of α-tocopherol and α-tocopheryl acetate in mixed micelles.*** Journal of Chromatography B 822 339–346 (2005)

Demidova-Rice T.N. et al. ***Acute and Impaired Wound Healing: Pathophysiology and Current Methods for Drug Delivery, Part 1: Normal and Chronic Wounds: Biology, Causes, and Approaches to Care.*** Adv Skin Wound Care. 25(7) 304–314 (2012)

Deshmukh A.S. et al. ***Polymeric micelles: Basic research to clinical practice.*** International Journal of Pharmaceutics 532 249–268 (2017)

Dikalov S.I. and Harrison D.G. ***Methods for Detection of Mitochondrial and Cellular Reactive Oxygen Species.*** Antioxid. Redox Signal. 20 372–382 (2014)

Drago H. et al. ***The Next Generation of Burns Treatment: Intelligent Films and Matrix, Controlled Enzymatic Debridement, and Adult Stem Cells.*** Transplantation Proceedings, 42 345–349 (2010)

Eming S.A. et al. ***Inflammation in Wound Repair: Molecular and Cellular Mechanisms.*** Journal of Investigative Dermatology 127 514–525 (2007)

Falanga V. and Eaglstein W.H. ***The "trap" hypothesis of venous ulceration.*** The Lancet; 341 1006-1008 (1993)

Fan K. et al. ***State of the Art in Topical Wound-Healing Products.*** Plast. Reconstr. Surg. 127 (Suppl.): 44S-59S (2011)

Farrar D. ***Advanced wound repair therapies.*** Chap. 1 (Stephens P.), Chap. 2 (Thomas J. G., Motlagh H., Povey S. B. and Percival S. L.), Chap. 3 (Larson B. J., Nauta A., Kawai K., Longaker M. T. and Lorenz H. P.), Woodhead Publishing Ed. (2011)

Felton L.A. ***Mechanisms of polymeric film formation.*** Int J Pharm. 457(2) 423-7 (2013)

Fraisl P. et al. ***Regulation of Angiogenesis by Oxygen and Metabolism.*** Developmental Cell 16 167-179 (2009)

Fryd M. M. and Mason T.G. ***Time-Dependent Nanoemulsion Droplet Size Reduction By Evaporative Ripening.*** J. Phys. Chem. Lett. 1 3349–3353 (2010)

Garcıa P. et al. ***Alpha-tocopherol microspheres with cross-linked and acetylated inulin and their release profile in a hydrophilic model.*** Eur. J. Lipid Sci. Technol., 115 811–819 (2013)

George Han and Roger Ceilley. ***Chronic Wound Healing: A Review of Current Management and Treatments.*** Adv Ther 34 599–610 (2017)

Gibson G.R. et al. ***Dietary modulation of the human colonic microbiota: updating the concept of prebiotics.*** Nutr Res Rev. 17(2) 259-75 (2004)

Gourbeyre P. ***Probiotics, prebiotics, and synbiotics: impact on the gut immune system and allergic reactions.*** Journal of Leukocyte Biology Volume 89 685-695 (2011)

Greenhalgh D.G. ***The role of apoptosis in wound healing.*** The International Journal of Biochemistry & Cell Biology 30 1019-1030 (1998)

Gupta A. et al. ***Nanoemulsions: formation, properties and applications.*** Soft Matter 12 2826-2841 (2016)

Gutteridge J.M. ***Lipid peroxidation and antioxidants as biomarkers of tissue damage.*** Clin Chem. 41(12 Pt 2) 1819-28 (1995)

Häkkinen L. et al. ***An improved method for culture of epidermal keratinocytes from newborn mouse skin.*** Methods Cell Sci. 23 189-96 (2001)

Halpner A.D. et al. ***Protection by vitamin C of oxidant-induced loss of vitamin E in rat hepatocytes.*** J. Nutr. Biochem. 9 355-359 (1998)

Hickson M. ***Examining the evidence for the use of probiotics in clinical practice.*** Nursing Standard 27 29 35-41 (2013)

Higley H.R. et al. ***Extravasation of macromolecules and possible trapping of transforming growth factor-β in venous ulceration.*** British journal of Dermatology 132 79-85 (1995)

Hobson R. ***Vitamin E and wound healing: an evidence-based review.*** Int Wound J 13 331–335 (2016)

Hobson R. ***Vitamin E and wound healing: an evidence-based review.*** Int Wound J 13 331–335 (2016)

Hoobin P. et al. ***Water sorption properties, molecular mobility and probiotic survival in freeze dried protein-carbohydrate matrices.*** Food & Function 4 1376-1386 (2013)

IUPAC. ***Compendium of Chemical Terminology***, 2nd ed. (the "Gold Book"). Compiled by A. D. McNaught and A. Wilkinson. Blackwell Scientific Publications, Oxford (1997). XML on-line corrected version: http://goldbook.iupac.org (2006-) created by M. Nic, J. Jirat, B. Kosata; updates compiled by A. Jenkins. ISBN 0-9678550-9-8. https://doi.org/10.1351/goldbook.

Janke J.J. et al. ***Oleic Acid Phase Behavior from Molecular Dynamics Simulations.*** Langmuir 30 10661-10667 (2014)

Järbrink K. et al. ***The humanistic and economic burden of chronic wounds: a protocol for a systematic review.*** Syst Rev. 6:15 (2017)

Karatan E. and Watnick P. ***Signals, Regulatory Networks, and Materials That Build and Break Bacterial Biofilms***. Microbiology And Molecular Biology Reviews 73(2)310–347 (2009)

Karatepe O. et al. ***The Impact of Valvular Oxidative Stress on the Development of Venous Stasis Ulcer.*** Angiology 61(3) 283-288 (2010)

Karlton-Senaye B.D. and Ibrahim S.A. ***Impact of gums on the growth of probiotics.*** Agro FOOD Industry Hi Tech 24(4) 10-14 (2013)

Kim H.H. et al. ***Laser scanning confocal microscope (LSCM)-fluorescence spectral properties of Nile Red embedded in polystyrene film of different thickness.*** Chemical Physics Letters 432 200–204 (2006)

Krull S.M. et al. ***Critical material attributes (CMAs) of strip films loaded with poorly water-soluble drug nanoparticles: I. Impact of plasticizer on film properties and dissolution.*** Eur J Pharm Sci. 92 146–155 (2016)

Kunkemoeller B. and Kyriakides T.R. ***Redox signaling in diabetic wound healing regulates extracellular matrix deposition.*** Antioxid Redox Signal. 27(12) 823-838 (2017)

Leaper D. et al. ***Approach to chronic wound infections.*** British Journal of Dermatology 173 351–358 (2015)

Li X. et al. ***Microencapsulation of nanoemulsions: novel Trojan particles for bioactive lipid molecule delivery.*** International Journal of Nanomedicine 6 1313–1325 (2011)

Liakos I.L. et al. ***All natural cellulose acetate—Lemongrass essential oil antimicrobial nanocapsules.*** *International Journal of Pharmaceutics 510(2) 508-515 (2016)*

Liang L et. Al. ***Characterization of the b-lactoglobulin/a-tocopherol complex and its impact on a-tocopherol stability.*** Food Chemistry 126 821–826 (2011)

Maiti N.C. et al. ***Fluorescence Dynamics of Dye Probes in Micelles.*** J. Phys. Chem. B 101 11051-11060 (1997)

Mariotto S. et al. ***Protective effect of Arbutus unedo aqueous extract in carrageenan-induced lung inflammation in mice.*** Pharmacol Res. 57(2) 110-24 (2008)

Mason T.G. et al. ***Nanoemulsions: formation, structure, and physical properties.*** J. Phys.: Condens. Matter 18 R635–R666 (2006)

Mast B.A. and Schultz G.S. ***Interactions of cytokines, growth factors, and proteases in acute and chronic wounds.*** Wound Rep Reg 4 411-20 (1996)

Mayet et al. ***A Comprehensive Review of Advanced Biopolymeric Wound Healing Systems.*** Journal Of Pharmaceutical Sciences 103 2211–2230 (2014)

McLennan SV et al. ***Matrix metalloproteinases and their roles in poor wound healing in diabetes.*** Wound Practice and Research 16:3 116-121 (2008)

Menke N.B. et al. ***Impaired wound healing.*** Clinics in Dermatology 25 19–25 (2007)

Mohammad A. et al. ***Physical Properties of PVA Doped with Algal Glycerol.*** J. Appl. Polym. Sci. 130 4482–4489 (2013)

Muller-Goymann C.C. ***Physicochemical characterization of colloidal drug delivery systems such as reverse micelles, vesicles, liquid crystals and nanoparticles for topical administration.*** European Journal of Pharmaceutics and Biopharmaceutics 58 343–356 (2004)

Musalmah M. et al. ***Comparative Effects of Palm Vitamin E and α-Tocopherol on Healing and Wound Tissue Antioxidant Enzyme Levels in Diabetic Rats.*** Lipids 40(6) 575-580 (2005)

Muxika A. et al. ***Chitosan as a bioactive polymer: Processing, properties and applications.*** Int. J. Biol. Macromol. (2017) http://dx.doi.org/10.1016/j.ijbiomac.2017.07.087

Muzzarelli R.A.A., ***Chitin and chitosans for the repair of wounded skin, nerve, cartilage and bone.*** Carbohydr. Polym. 76, 167-182 (2009)

Naoi S. et al. ***Phase transition of locust bean gum–,tara gum– and guar gum–water systems.*** Journal of Thermal Analysis and Calorimetry. 70 841-852 (2002)

O'Meara S et al. ***Systematic reviews of wound care management: (3) antimicrobial agents for chronic wounds; (4) diabetic foot ulceration.*** Health Technol Assess 4(21) (2000)

Oelschlaeger T.A. ***Mechanisms of probiotic actions – A review.*** International Journal of Medical Microbiology 300 57–62 (2010)

Palace V. P. et al. ***Antioxidant potentials of vitamin A and carotenoids and their relevance to heart disease.*** Free Radical Biology & Medicine 26 746–761 (1999)

Palanisamy et al. ***Antibiofilm properties of chemically synthesized silver nanoparticles found against Pseudomonas aeruginosa.*** Journal of Nanobiotechnology 12:2 (2014)

Panchatcharam M. et al. ***Curcumin improves wound healing by modulating collagen and decreasing reactive oxygen species.*** Molecular and Cellular Biochemistry 290 87–96 (2006)

Pandey S. et al. ***Natural gum modified emulsion gel as single carrier for the oral delivery of probiotic-drug combination.*** International Journal of Biological Macromolecules 92 504–514 (2016)

Patrulea V. ***Chitosan as a starting material for wound healing applications.*** European Journal of Pharmaceutics and Biopharmaceutics 97 417–426 (2015)

Pavelescu L.A. ***On reactive oxygen species measurement in living systems.*** Journal of Medicine and Life Vol. 8, Special Issue, 38-42 (2015)

Peral M.C. et al. ***Bacteriotherapy with Lactobacillus plantarum in burns.*** Int Wound J. 6 73–81 (2009)

Pereira G.G. et al. ***Polymeric Films Loaded with Vitamin E and Aloe vera for Topical Application in the Treatment of Burn Wounds.*** BioMed Research International pp. 1-9 (2014)

Pereira L. M. et al. ***Effect of oleic and linoleic acids on the inflammatory phase of wound healing in rats.*** Cell Biochem Funct 26 197–204 (2008)

Persoon A et al., ***Leg ulcers: a review of their impact on daily life.*** J Clin Nurs. 13(3) 341-54 (2004)

Polk D.B. and Yan F. ***Probiotics and immune health.*** Curr Opin Gastroenterol. October 27(6) 496-501 (2011)

Proniuk S. et al. ***A Simplified and Rapid High-Performance Liquid Chromatographic Assay for Ketoprofen in Isopropyl Myristate.*** Journal of Chromatographic Science 36 (1998)

Qing C. ***The molecular biology in wound healing & non-healing wound.*** Chinese Journal of Traumatology xxx 1-5 (2017)

Rael L.T. et al. ***Lipid Peroxidation and the Thiobarbituric Acid Assay: Standardization of the Assay When Using Saturated and Unsaturated Fatty Acids.*** Journal of Biochemistry and Molecular Biology 37(6) 749-752 (2004)

Ramos A.N. et al. ***Antipathogenic properties of Lactobacillus plantarum on Pseudomonas aeruginosa: The potential use of its supernatants in the treatment of infected chronic wounds.*** Wound Rep Reg 20 552–562 (2012)

Ramos A.N. et al. ***Compounds from Lactobacillus plantarum culture supernatants with potential pro-healing and anti-pathogenic properties in skin chronic wounds.*** Journal of Pharmaceutical Biology 53 350-358 (2015)

Rice-Evans C.A. et al. ***Structure-antioxidant activity relationships of Flavonoids and phenolic acids.*** Free Radical Biology & Medicine 20(7) 933-956 (1996)

Rittie´ L. and Fisher G.J. ***Natural and Sun-Induced Aging of Human Skin.*** Cold Spring Harb Perspect Med 2015;5:a015370 (2015)

Riva F. et al. ***Generation of human epidermal constructs on a collagen layer alone.*** Tissue Eng. 13 2769-2777 (2007)

Roy S. et al. ***Dermal wound healing is subject to redox control.*** Mol Ther. 13(1) 211–220 (2006)

Rozman B. et al. ***Temperature-Sensitive Microemulsion Gel: An Effective Topical Delivery System for Simultaneous Delivery of Vitamins C and E.*** AAPS PharmSciTech 10(1) 54–61 (2009)

Saarialho-Kere U. K. ***Patterns of matrix metalloproteinase and TIMP expression in chronic ulcers.*** Arch Dermatol Res 290 (Suppl):S47–S54 (1998)

Schäfer M. and Werner S. ***Oxidative stress in normal and impaired wound repair.*** Pharmacological Research 58 165–171 (2008)

Schultz G.S. et al. **Wound bed preparation: a systematic approach to wound management.** Wound Repair and Regeneration 11 Suppl. 1:S1-28 (2003)

Shami S.K. et al. ***Leg ulceration in venous disease.*** Postgrad Med J. 68(804) 779-85 (1992)

Singer A.J. et al. ***Cutaneous wound healing***. The New England Journal of Medicine 341:738-746 (1999)

Siti H.N. et al. ***The role of oxidative stress, antioxidants and vascular inflammation in cardiovascular disease (a review).*** Vascular Pharmacology 71 40–56 (2015)

Sodium chloride and calcium chloride solution. ***British Pharmacopoeia*** Addendum. London: HMSO, 1995

Sosnik A. and Seremeta K.P. ***Advantages and challenges of the spray-drying technology for the production of pure drug particles and drug-loaded polymeric carriers.*** Advances in Colloid and Interface Science 223 40–54 (2015)

Stojadinovic A. et al. ***Topical advances in wound care.*** Gynecologic Oncology 111 S70–S80 (2008)

Tadros T. et al. ***Formation and stability of nano-emulsions.*** Advances in Colloid and Interface Science 108-109 pp.303–318 (2004)

Tadros T. ***Polymeric surfactants in disperse systems.*** Advances in Colloid and Interface Science 147–148 pp.281–299 (2009)

Takahashi M. et al. ***Thermal and viscoelastic properties of xanthan gum/chitosan complexes in aqueous solutions.*** Journal of Thermal Analysis and Calorimetry 85(3) 669–674 (2006)

Thomas S. and Fram, P., ***The development of a novel technique for predicting the exudate handling properties of modern wound dressings.*** World Wide Wounds (2001)

Thomas S. ***Assessment and management of wound exudates.*** J Wound Care 6:327–330 (1997)

Torchilin V. P. ***Micellar Nanocarriers: Pharmaceutical Perspectives.*** Pharmaceutical Research 24(1) 1-16 (2007)

Turunen M. et al. ***Metabolism and function of coenzyme Q***. Biochimica et Biophysica Acta 1660 171-199 (2004)

Ushio-Fukai M, Nakamura Y. ***Reactive oxygen species and angiogenesis: NADPH oxidase as target for cancer therapy.*** Cancer Lett. 266(1) 37-52 (2008)

Vishwakarma P. et al. ***Orally Disintegrating Strips (ODS) Convenience of Liquid Dosage Form and Dose Accuracy of Solid Dosage Form.*** American Journal of Pharmacy & Health Research 3(5) (2015)

Wainwright C.L. ***Matrix metalloproteinases, oxidative stress and the acute response to acute myocardial ischaemia and reperfusion.*** Current Opinion in Pharmacology 4 132–138 (2004)

Wang W. et al. ***Peroxynitrite-induced myocardial injury is mediated through matrix metalloproteinase-2.*** Cardiovascular Research 53 165-174 (2002)

Wang Y et al. ***Plasma and Dietary Antioxidant Status as Cardiovascular Disease Risk Factors: A Review of Human Studies.*** Nutrients 5 2969-3004 (2013)

Wlaschek M. and Scharffetter-Kochanek K. ***Oxidative stress in chronic venous leg ulcers.*** Wound Repair and Regeneration 13 452-461 (2005)

Xiang Li et al. ***Microencapsulation of nanoemulsions: novel Trojan particles for bioactive lipid molecule delivery.*** International Journal of Nanomedicine 6 1313–1325 (2011)

Xie J. and Schaich K.M. ***Re-evaluation of the 2,2-Diphenyl-1-picrylhydrazyl Free Radical (DPPH) Assay for Antioxidant Activity.*** J. Agric. Food Chem. 62 4251-4260 (2014)

Y. Singh et al. ***Nanoemulsion: Concepts, development and applications in drug delivery.*** Journal of Controlled Release 252 28–49 (2017)

Zhong S. P. et al. ***Tissue scaffolds for skin wound healing and dermal reconstruction.*** Tissue scaffolds for skin wound healing 2 510-525 (2010)

Zingg J.M. ***Vitamin E: A Role in Signal Transduction.*** Annu. Rev. Nutr. 35 135-173 (2015)